CHALMERS

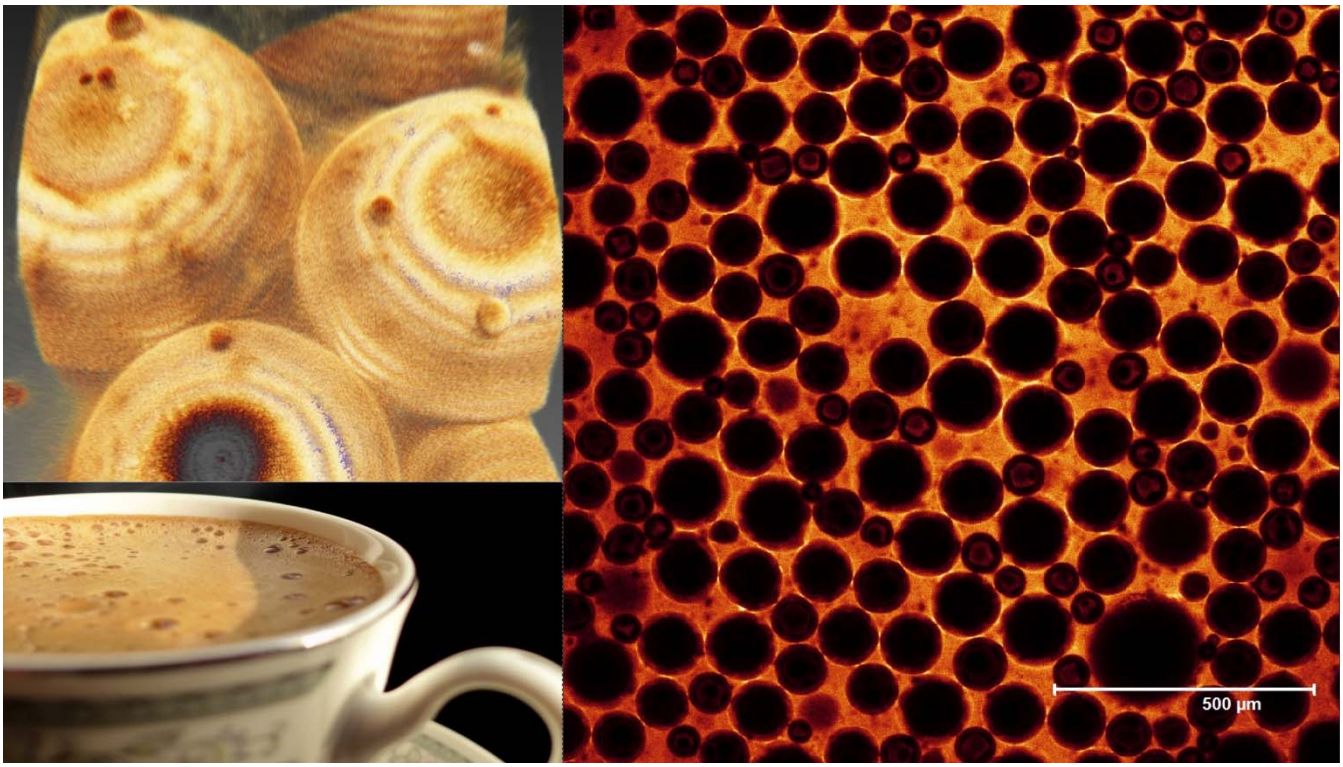

Microstructure of Instant Coffee Foam

Confocal Microscopy Method Development and Production Related Parameters Affecting Foam Kinetics

Master of Science Thesis in the Master Degree Programme Biotechnology

Gustav Nilsson

Department of Biology and Biological Engineering
Division of Food and Nutrition Science
CHALMERS UNIVERSITY OF TECHNOLOGY
Gothenburg, Sweden 2015

Microstructure of Instant Coffee Foam

Confocal Microscopy Method Development and Production Related Parameters Affecting Foam Kinetics

GUSTAV NILSSON

Department of Biology and Biological Engineering
Division of Food and Nutrition Science
CHALMERS UNIVERSITY OF TECHNOLOGY
Gothenburg, Sweden 2015

Microstructure of Instant Coffee Foam
Confocal Microscopy Method Development and Production Related Parameters Affecting Foam Kinetics
GUSTAV NILSSON

Department of Biology and Biological Engineering
Division of Food and Nutrition Science
Chalmers University of Technology
SE-412 96 Göteborg
Sweden
Telephone + 46 (0)31-772 1000

Cover:
Top left, 3D model of a small section of coffee foam, made in Avizo from CLSM images. Bottom left, image of a cup of coffee taken from http://www.free-picture.net/albums/Drinks/coffee/black-coffee_1388253627.jpg. Right, CLSM 2D image of coffee foam stained with Texas red.

Gothenburg, Sweden 2015

Microstructure of Instant Coffee Foam
Confocal Microscopy Method Development and Production Related Parameters Affecting Foam Kinetics
GUSTAV NILSSON
Department of Biology and Biological Engineering
Division of Food and Nutrition Science
Chalmers University of Technology

Abstract

Coffee foam is despite being an important parameter for the sensory impressions a cup of coffee provides perhaps the least studied part of this enormous commercial product consumed worldwide. In terms of microstructure and rheology the field is considerably lacking in data. This project aimed to develop a method to study coffee foam from instant coffee, by confocal laser scanning microscopy (CLSM) with the intention of providing data that may be used for production purposes.

The instrument setup and operation of the method were defined, efficient dyes identified and common artefacts explained. The average bubble area was measured as a function of time by image analysis, the distribution and movement of particles in the lamellae could be observed and in particular surface active lipids and proteins could be stained and detected. A significant advantage of the method compared to e.g. rheological measurements in a rheometer turned out to be the small sample volumes needed. In addition, a simple method for measuring drainage using a USB-microscope was developed and applied to the foam.

The analyzed parameters were filtering (pore sizes of 0.20-0.80 μm), pH adjustment (pH 4.0-6.3), hydrophobic particle addition (~1 μm) as well as the combined effects of filtering and particle addition to the coffee pre-foaming.

Growth rate of average bubble area in coffee foam was shown to be virtually linear for at least the first 25 minutes, as oppose to what was described in literature for dynamic liquid foams in general, where growth was described as logarithmic. Extrapolating the growth of average bubble area to minute zero as a measure of foamability proved viable.

Previously reported data of increased foamability in the pH range of 5.7-6.3 was confirmed. The results showed that higher pH values (>pH 5.0) had a negative impact on foam stability, and a lower pH increased foam stability. Filtering and particle addition showed that the interaction between various particles in the coffee play an important role for both foamability and foam stability.

Keywords: Instant coffee, Coffee foam, Crema, Confocal laser scanning microscopy, CLSM, Foam microstructure, Average bubble area, Drainage, Foamability, Foam stability

Acknowledgements

First and foremost I would like to thank Niklas Lorén, Associate Professor, Structure and Material Design and Marco Berta, PhD, Structure and Material Design, for giving the opportunity to do my Master's thesis here at SP Food and Bioscience and for guiding me throughout this project. I would also like to thank all the great people working in the Structure and Material Design department for making me feel welcome and helping me whenever I had questions or problems. Special thanks to Annika Altskär for teaching me how to use the confocal microscope and for all her support and valuable input along the way.

Gustav Nilsson, Gothenburg, May 2015

Table of Contents

Chapter 1 – The Project

1.1 Introduction

Being the second largest traded product as well as one of the most consumed beverages worldwide [1], coffee does indeed pose for an interesting area of research. However, from a chemical and process-technological standpoint, coffee and the various methods of making coffee are relatively well studied. Foaming on the other hand, despite being recognized as a significant parameter of quality and the experience of drinking e.g. espresso, is surprisingly sparsely studied.

Crema, the layer of dense brown foam on top of a freshly brewed cup of espresso, has been the main focus of the few studies performed thus far. In addition to being a major factor for mouthfeel, it has been shown to positively impact the release of high volatiles such as methyl furans both in the cup headspace and in the mouth during consumption, increasing the "roasted" characteristic of the coffee [2]. The quality of instant coffee, which is naturally foaming due to gas released from the granules during dissolution, is therefore most definitely impacted in a similar way. Instant coffee, dating back to the late 19th century, is essentially the result of freeze- or spray drying strong brewed coffee. The final product consists of a powder, or more commonly small granules, that can rapidly be redissolved in hot water to reform the coffee.

Even though fresh coffee is the overall most consumed type of coffee in the world by volume, instant coffee has over the last few years continuously gained market share. Almost half of the world actually prefers instant coffee, with the divide being very closely aligned to the tea versus coffee preferences. Relatively new markets in countries that are mostly tea-drinking e.g. China, Russia and Turkey tend to prefer instant over home brewed coffee [3]. The United Kingdom being the largest instant coffee consumer in Europe is also a good example of this. General convenience, lower price and the fact that households used to only boil water for tea do not need to buy any new equipment i.e. a coffeemaker, are believed to be contributing reasons for this global increase in consumption.

Improving the knowledge of instant coffee foam, how to influence it and how it relates to the perception of the coffee is undoubtedly one of the major aspects of providing better quality for the current consumers, as well as increasing the acceptance of instant coffee in countries generally preferring the fresh kind.

1.2 Objectives

Little is known about the microstructure of coffee foam, how it changes over time and how the structure correlates to rheology and composition. This project intends to examine the microstructure of the foam in 2D and 3D by confocal laser scanning microscopy (CLSM), various sample stains, image analysis- and 3D modeling software. As to gain a better understanding of which properties impact the structure and how they relate to the rheology and subsequently to quality. The ultimate goal being to provide data that in the future can be used to improve the quality of the coffee foam and thereby better the experience of drinking instant coffee. This is very much relevant due to the inherent simplicity and convenience of preparing a cup of instant coffee. Improving its quality will not only make good coffee more accessible to people in developing countries and people in other low income households not able or willing to buy the more expensive coffee for home brewing or the equipment needed to make it. But even people used to, and able to afford, fresh homebrewed coffee can, and do, find themselves in situations where instant coffee might be the only option.

1.3 Aim

This project is a follow-up of an initial MSc study on coffee foam rheology performed by Gmoser [4],under the supervision and by initiative of PhD Marco Berta and Associate Professor Niklas Lorén, both at SP Food and Bioscience, department of Structure and Material Design.

The initial aim is to develop methods that can be used to reliably study the coffee foam microstructure using CLSM and possibly other microscopy techniques. Important characteristics of the methods should include the capability to follow the time dependent evolution of the foam and ability to characterize potential particles and compounds found in the lamellae. Sample staining, creation and handling as well as instrument setup and operation are steps that will have to be defined.

The secondary aim is to study production related parameters affecting the foam and relate these to structural and quality changes as well as changes in time, using the developed methods and image analysis software. However, as the project is very much explorative it is dependent on the limitations of the methods to be developed.

The main points of the project are:

- Perform a literature study on microstructure of coffee foam and other relevant food foams.
- Develop methods to study the structure of coffee foam with CLSM.
- Develop methods to be able to follow the time dependent evolution of the foam micro structure.
- Use the developed CLSM methods and image to characterize foam structure in relation to production relevant parameters such as pH, filtering and particle addition.

1.4 Hypothesis

The main assumption is that quantitative and qualitative measurements and observations on coffee foam microstructure by CLSM can be used to assess foam quality relevant properties which can be beneficial in the coffee industry.

Hypotheses include:

- Particles in the coffee are expected to influence foam stability and structure, possibly as a Pickering emulsion.

- The pH of the coffee is known to impact foamability; it will thus affect the foam stability in a similar way.

Chapter 2 – Background

2.1 Coffee

All types of coffee are produced from one, or a blend of both, beans from two specific species of coffee plant, *Coffea arabica* and *Coffea canephora*. *Coffea arabica* being the most commonly used due to its superior flavor, owing to the lower content of chlorogenic acid compared to the cheaper coffee from the *Coffea canephora* bean, commonly referred to as "Robusta coffee" [5, 6].

In 1996, Arabica coffee accounted for about 90 % of the world's coffee production, in 2004 this had dropped to about 70 % and in 2013 it was almost down to 60 % [5, 7, 8]. This relative decrease is however mostly due to the continuously increasing cultivation of Robusta. Robusta coffee does indeed have an inferior taste due to the chlorogenic acid content, but there are other compositional differences as well. Such as a lower total fat content, higher fraction of polar lipids, higher caffeine content as well as higher content of carbohydrates and other soluble solids [7, 9]. The plant itself is also more robust than the Arabica species, hence the common name. It is easier to grow and capable of producing higher yields, making it overall much more inexpensive. Therefore it is often the bean of choice in the emerging markets. It is also the bean which has traditionally been used for the production of instant coffee, mostly due to it containing more solids and thus providing a better yield of coffee granules [10]. Nowadays instant coffee from pure Arabica or blended is however readily available, even though Robusta still dominates the market.

Coffee is, as many other beverages, a multiphase and multicomponent system with constituents continuously interacting with each other. Carbohydrates, proteins, lipids, chlorogenic acid, caffeine and minerals were identified by Briandet et al [5]. to be the most important molecules in coffee, but far from the only ones. Coffee is extremely complex and also contains various organic acids, melanoidins, peptides, amino acids, polyphenols, carotenoids, lactones etc. [6, 7, 11]. In fact, only the volatile fraction is estimated to be comprised of around 800 different compounds, many of which are formed during the roasting of the beans through e.g. the Maillard reaction or through thermal breakdown [11].

Roasting is, together with type of bean, probably the major factors impacting the composition of the ready coffee. Nunes et al [12] showed that lipid content was decreased with increased degree of roasting, protein content was increased with degree of roasting and carbohydrate was content increased up to a point, after which it started to drop off again. These same trends were seen for both types of coffee bean but the extreme points of carbohydrate content were different, correlated to roasting degrees of 9.7 % and 7.6 % for Arabica and Robusta respectively. Roasting degree was defined as the percentage of weight lost during the roasting process.

2.2 Instant Coffee

Instant, or soluble, coffee was developed in the end of the 19th century, the process has since been improved upon several times but the very basic principle remains the same. Essentially, brew strong coffee and remove the water, forming granules that can later be redissolved in hot water to reform the coffee.

The initial processing steps are the same independent of the intended coffee product. Coffee cherries are harvested and the beans are separated from the fruit by one of two methods, the dry- or the wet method. The wet method is more dependent on processing equipment and is also demanding a lot of water, while the dry method is more traditional and manual labor intensive. The wet method generally results in a

higher quality bean. The beans are then roasted, ground and packaged for home brewing or used for instant coffee production [13].

Compared to home brewing the instant coffee production process is more energetic due to the need for efficiency and high yields. Temperatures of 140-180 °C and above-atmospheric pressures are used in a series of extraction columns, followed by a few slightly less harsh extraction steps at ~100 °C before the extract, now containing 20-30 % solids, is cooled down. After which the brew is put through various filters and concentration steps such as centrifugation and/or evaporation before the desired quality is reached. The granules are then obtained by either freeze drying or spray drying the now highly concentrated coffee extract, freeze drying providing higher quality granules but being the more expensive process [13].

The high temperature extraction and the various filter- and concentration operations does indeed impact the quality and taste of the coffee [14]. Thermally unstable components breaks down further compared to home brewed coffee and loss of some desired aroma compounds in the removed water- or steam streams are unavoidable [10]. Measures to counteract this are however taken, it is common to recover aroma compounds by e.g. distilling the exiting water streams and spraying the compounds back onto the ready coffee granules during the packaging [13]. Pressing oil out of the spent coffee grounds and adding it back into the process can also be done. The exact same characteristic and chemical composition as home brewed ground roast coffee has however not yet been achieved.

2.3 Coffee Foam

Coffee foam, also referred to as crema, is the foam found on the surface of certain coffee beverages, probably most notably espresso. It is consisting of a liquid phase of coffee and a gas phase of water vapor, carbon dioxide formed during the roasting (Millard reaction) and volatile aroma compounds [15]. As the foam continuously breaks down during the consumption, both on its own in the cup and in the mouth of the consumer during each sip, it is “dosing” out the aroma compounds trapped in the bubbles. This improves the experience of drinking coffee by making the sensory impressions more constant during the consumption as well as extending the potential consumption time itself. The foam also provides a certain mouthfeel, a creamy texture, perceived as pleasant and to indicate quality. To a minor extent the foam is also providing an insulting effect, keeping the coffee warm for a bit longer. A relatively thin layer of small monodispersed bubbles is generally what is strived for.

2.3.1 Coffee Constituents Impacting Foam Stability and Foamability

A study on coffee foam stability by Nunes et al [12] showed that the stability is correlated to the carbohydrate content. High molecular weight polysaccharides, mostly galactomannan and arabinogalactan, the two main extractable carbohydrates in coffee, provide a more stable foam by increasing the liquid viscosity. Carbohydrate content is, as mentioned above in section 2.1, dependent on type of bean as well as the roasting process. The structure and size of the carbohydrates are also very much dependent on the roasting process. Galactomannan branching does e.g. decrease with increased degree of roasting, giving it a higher tendency to associate with other molecules [12].

In a following study, again by Nunes et al [16] high molecular weight complexes (~2000 kDa) consisting of these previously mentioned polysaccharides as well as proteins and phenolic compounds were identified and correlated to foam stability. Even though their relative abundance (0.3-0.9 % of total solids) was very low they were shown to strongly impact the foam. If this was due to them being surfactants or thickeners was however not discussed, Piazza et al [17] assume them to be surface active though. There was also a clear correlation between the formation of these large complexes and degree

of roasting, with increasing concentrations up to 7.6 % roasting, after which the concentration started to drop off again. Galactomannan branching i.e. willingness to associate with other molecules might play an important role in the formation. Linkages formed during the Maillard reaction are thought to be responsible for holding these complexes together, but electrostatic and hydrophobic interactions do in all likelihood significantly contribute to this as well [16, 17]. Both debranching and Maillard linkage are theoretically increasing with degree of roasting but the fact that there is a max point after which the content decreases again disputes this. It is however most likely due to thermal breakdown of the complex constituents or the complex itself during too extreme roasting.

Foamability was also investigated by Nunes et al [12] in their first study. It was shown to be dependent on protein content as well as on pH, as proteins have the highest capability for foaming near their isoelectric point. Which is roughly pH 5.7-6.3 for a majority of the ones found in green coffee beans, green coffee beans being what the coffee beans are generally called before roasting [12, 18]. The pH was shown to increase linearly with degree of roasting in both types of coffees, reaching pH ~5.7 at around 12 % and 8 % of roasting for Arabica and Robusta respectively. The increase in pH was theorized to be the result of the destruction of chlorogenic acid during the roasting, this was later confirmed to be the major factor by Fujioka et al [6].

Lipid content is a known contributor to the characteristic creamy sensation of espresso foam. The high pressure in the machine emulsifies the oil from the coffee ground [17]. Instant coffees and most other kinds of coffee are however prepared in much less energetic ways and it is not unlikely that the lipid fraction behaves differently in these. However, what is known for coffee foams, and foams dependent on proteins in general, is that lipid content is associated with decreased surface tension and reduced foamability and foam stability [9, 19].

Destabilization of beer foams by lipids was studied by Wilde et al [20] and they showed that free fatty acids in general were foam-negative but also that chain length and degree of saturation significantly influenced the degree of impact on the structure. Chain lengths below C12 were not surface active and were therefore not affecting the foam, C12-C14 and unsaturated acids up to C18 disrupted the film of adsorbed proteins and saturated C16-C18 acids were theorized to form hydrophobic aggregates inducing film-bridging. Unsaturated C16-C18 acids were shown to be the most effective anti-foaming agents.

2.3.2 Evolution of Foam Microstructure with Time

Coffee foam is as previously mentioned a very dynamic system, impacted by many physical and chemical parameters of the coffee itself, the brewing method and the surrounding environment. Its transient nature makes it inherently hard to study and little is actually known about its time-dependent microstructure. The information below applies to dynamic foams in general and even though coffee foam is expected to behave in a similar fashion it has thus far not been extensively studied.

2.3.2.1 Coarsening

Coarsening, or Ostwald ripening, is one of the two main destructive processes taking place inside dynamic foam [21-23]. Driven by the pressure difference between bubbles of different sizes it is responsible for large bubbles growing even larger and small bubbles shrinking, overall resulting in an increase in average bubble size [23]. Smaller bubbles have higher internal pressures compared to larger ones, thus gas will dissolve in the lamellae and diffuse towards the bigger bubbles. As bubbles grow, the liquid film is stretched, becoming thinner and weaker. The chance of bubbles bursting or coalescing is therefore continuously increasing.

The dynamics of coarsening have been rather well defined in two-dimensions, said to follow von Neumann's law, *Equation 1* [22]. The growth rate of a domain (bubble) is dependent, not on size and shape, but on the number of sides it has i.e. how many other bubbles it is in contact with. Average growth rate has also been shown to follow the simple formula, *Equation 2*, quite accurately [22].

$$\frac{dA}{dt} = -M\gamma\kappa\left(2\pi - \sum_{i=1}^{n}\alpha_i\right) = -2\pi M\gamma\kappa\left(1 - \frac{1}{6}n\right)$$

Equation 1. *Von Neumann´s law, dA/dt=rate of change of the area of the domain, -γκ=pressure difference between adjacent bubbles, M=diffusivity, α_i=angle at a triple junction on the domain, n=number of such triple junctions.*

$$G \sim t^{2/3}$$

Equation 2. *Average growth rate of domains in a two-dimensional foam model, G=growth rate, t=time.*

Furthermore, the pressure driving the diffusion can be described as Laplace pressure by *Equation 3*, assuming bubbles as spheres.

$$\Delta P = 2\sigma_T/r$$

Equation 3. *Laplace pressure of a spherical object, P=pressure, $\boldsymbol{\sigma_T}$=interfacial tension, r=radius*

Coarsening in three dimensions is however not as simple as in two dimensional systems, von Neumann´s law does not apply here in its current form. However, Lambert et al [24] showed that while growth rate of a bubble does not depend on the number of faces alone (compare sides in 2D), for bubbles with many faces the average growth rate followed *Equation 4* fairly well. Foam in its later stages of deterioration did however not have enough bubbles for this relationship to function, as the number of faces was too low.

$$G_f \sim f - f_0$$

Equation 4. *Average growth rate of bubbles with many faces, G=growth rate, f=faces*

As it stands right now, deriving a formula for growth rate in 3D requires too many assumptions for accurate predictions, thus results are only approximate [22, 24]. MacPherson et al [25] have however postulated a modification to von Neumann´s law said to make it relatively precise in 3D, *Equation 5*.

$$\frac{dV}{dt} = -2\pi M\gamma\kappa\left(\mathcal{L}(D) - \frac{1}{6}\sum_{i=1}^{n} e_i\,(D)\right)$$

Equation 5. *Proposed three-dimensional von Neumann relation, dV/dt=rate of change of the volume of the domain, $\mathcal{L}(D)$=natural measure of the linear size of domain D, e_i=length of the triple line (edge) i, summation of all triple lines (n) of domain D.*

2.3.2.2 Drainage

Drainage is the other of the two main processes of foam destabilization. Driven by gravity alone, the liquid in the lamellae is continuously flowing down towards the liquid phase, reducing the bulk volume and stability of the foam [19, 23, 26, 27].

Drainage results in a very heterogeneous foam as the top part drains faster and to a greater extent than the bottom part in contact with the liquid. As the top part dries out it becomes characterized by larger bubbles with more polyhedral shapes, compared to the smaller and more spherical bubbles of the lower and wetter part, which is initially supplied by liquid from the foam above [23]. The top part of the foam, now built up with thin and weak lamellae, consequently also has increased concentrations of compounds not able to follow the draining liquid. Destabilization of the foam by liquid stretching around the large bubbles is increased due to these compounds tendencies to concentrate unevenly in the lamellae, resulting in even more tension. Depicted in *Figure 1* below is a characteristic "old" foam, the top part being heavily drained.

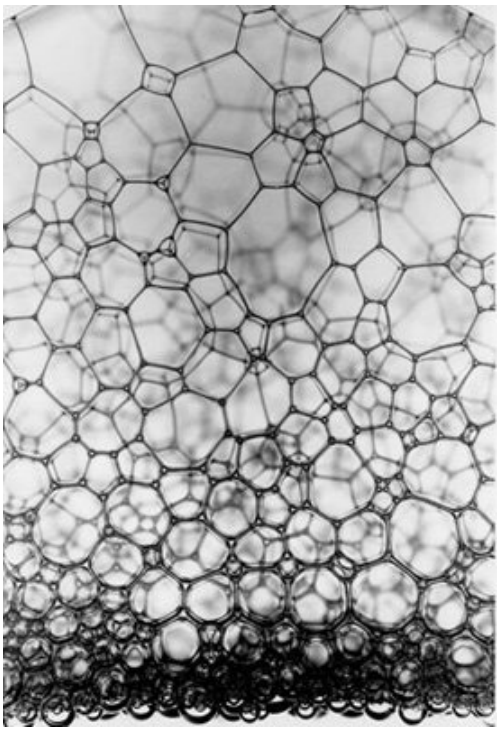

Figure 1. *Picture of a characteristic "old" foam, large polyhedral bubbles with thin lamellae at the top and small spherical bubbles with larger lamellae in the wet bottom part [28]***.**

The two main factors affecting the drainage rate are liquid viscosity and bubble size, smaller bubbles and higher viscosity reduces drainage and thus stabilizes the foam. In a study on egg white- and whey protein foams by Yang et al [27] addition of sucrose was shown to both increase the viscosity of the liquid and decrease the bubble size, however as these properties are closely related it is not very surprising that both were simultaneously affected. It is nevertheless interesting and potentially relevant to coffee foam as well, as sugar is one of the most common things to add to coffee. Time of addition is however in all likelihood heavily affecting the result i.e. adding sugar before or after the initial foam formation. In instant coffee, adding sugar at the beginning when the majority coffee granules are not dissolved versus adding sugar on top of the ready foam and stirring the cup again.

Initially the characteristic time of foam drainage can be estimated by *Equation 6* [27, 29, 30], this equation does however only produce an approximate value and should therefore be used for relative comparisons between foams and not to generate absolute time values [27].

$$t_{DR} = \frac{H_F}{\left(\frac{K_m \rho g A_{0min}}{\pi \eta}\right) \Phi_L}$$

Equation 6. *Estimation of characteristic foam drainage time (t_{DR}), H_F=foam height, K_m=dimensionless permeability coefficient for liquid drainage ($6*10^{-3}$ for channel dominated drainage or $2*10^{-3}$ for node-dominated drainage), ρ=density, η=viscosity, g=gravity, A_{0min}=initial mean bubble area, Φ_L=liquid phase fraction.*

The surfactants in the foam also play a significant role in the drainage process. Depending on the type of surfactant, the liquid flow can be characterized in one of two ways. For a rigid, typically large and relatively nonmobile surfactant the liquid behaves as though it is flowing down any type of fixed surface i.e. by Poiseuille flow. That is, the flow is slower close to the bubble surfaces and faster deep inside the lamella. This is typically described as "Channel-dominated flow" as the resistance from the bubble surfaces is the main impacting factor. In contrast, when the surfactants are small and mobile the flow is not significantly impeded even when in contact with the bubble surfaces, here the nodes are the main contributor to the resistance, thus it is labeled "Node-dominated flow" [31]. Nodes being the junctions in the foam, each comprised of four lamellae meeting in a tetrahedral formation with angles of 109,47 ° between the axes, as described by Plateau [32]. If the flow is channel-dominated the draining process is slower and the foam more stable compared to node-dominated flow. However, in reality the foam draining typically proceeds through a mixture of both flow types and the relative contribution of each change with time as e.g. the thickness of the lamellae decrease, making it hard to characterize a foam simply as one or the other.

2.3.2.3 Evaporation

As coffee is typically hot, brewed just a few degrees below boiling and served straight away, evaporation is certainly a factor initially affecting the foam, perhaps in later stages as well depending on the rate of cooling. This phenomenon is however not very well studied at all and the relative impact compared to e.g. drainage is not known. It does however affect the foam in the same way as drainage i.e. by removing water from the lamellae and thereby weakening the structure [9, 15]. As with drainage the top part of the foam is again the most affected region.

The increased concentration of particles in the lamellae due to water loss is as mentioned above a major factor contributing to the weakening the foam structure. Volatile compounds do in all likelihood follow the evaporating water to varying extents, but if the relative amount of compounds leaving the shrinking lamellae through vapor is significant or negligible compared to drainage is not known.

2.4 Particle Stabilized Foams

A particle stabilized emulsion, also known as a Pickering emulsion, is an emulsion, e.g. a foam, stabilized by solid particles absorbed at the air/water interface. The adsorption is essentially irreversible as removing the particles requires very large amounts of energy. Thus foams stabilized in this manner can stay stable many times longer than foams with protein or viscosity stabilizers, in some cases even indefinitely [33, 34].

The initial formation of the Pickering foam can however be a bit difficult, with particle size, concentration, shape, hydrophobicity and foaming process all impacting the result. The particles need to be hydrophobic enough to absorb at the interface, but too hydrophobic particles tend to aggregate with each other and form gels or precipitate [33]. Size of particles needed for optimal stability appears to be heavily dependent on the system, as foams stabilized by particles of widely different sizes have been reported, e.g. 70 nm and 226.8 μm respectively for the two previously cited articles, Gonzenbach et al [34] and Wege et al [33]. High shear mixing tends to be the preferred way of creating a foam, a food blender running at 15 000 rpm was able to form a stable Pickering foam in the study by Wege et al. Also shown in the same study was an interesting correlation between concentration, size, foamability and foam stability. For the foam to be stable the surfaces of the bubbles needs to be covered by the particles, these high concentrations of particles were however shown to reduce the foamability. Low concentrations of smaller particles, while not enough to fully cover the bubbles and stabilize the foam, did increase the foamability [33].

2.5 Confocal Laser Scanning Microscopy

The confocal laser scanning microscope, abbreviated CLSM, is a versatile instrument used to observe structures and structural changes in a wide range of samples in several different fields of research. It can be used either in a traditional upright setup or inverted. Its key feature is the ability to noninvasively view structures at select depths in a sample i.e. it having the capability to see inside bulk materials. Scanning a specific volume of a sample by compiling images of an area (x, y) at different depth (z) also allows for the reconstruction of structures as three dimensional models. Time-lapse imaging is another strong suit of the CLSM, the ability to monitor changes in a single plane over time or in a volume (4D-imaging) have in many cases proven uniquely useful [35].

Most commonly a CLSM is run as a fluorescence microscope, although it can be run in reflection mode as well. Reflection mode being when the light returning from the sample hit by the laser is picked up at essentially the same wavelength as the light the laser in question emits, the reflected light, as the name implies. Fluorescence on the hand relies on exciting fluorescent molecules and picking up the light that is emitted when they return to their ground state i.e. light of longer wavelengths. Some samples have the ability to autofluoresce but often sample staining is required. Staining also opens up the possibility of specifically staining certain parts of sample with dyes (fluorophores) having affinity for different classes of compounds. Providing the capability to characterize potentially unidentified compounds, define their location in the sample as well as potentially determine their relative abundance if image analysis can be efficiently employed.

2.5.1 The Confocal Laser Scanning Microscope Principle

The main piece of engineering setting the CLSM apart from the traditional widefield fluorescence microscope is the use of a pinhole before the photodetector. The pinhole is what allows for optical sectioning as opposed to physical sectioning which is often employed when using the widefield microscope. It works by blocking fluorescence originating from molecules outside (below and above) the focal plane.

Figure 2 below shows the basics of a CLSM setup. The laser(s), first passing through an acousto-optical tunable filter (AOTF) allowing for adjustment of wavelength and intensity [36], is directed towards the beam splitter. The beam splitter, most commonly a dichroic mirror, points the laser towards the objective, first passing computer controlled mirrors allowing for scanning along the x- and y-axes. The objective, providing magnification and being important for image quality and resolution, focuses the light into the sample. Light emitted from the excited fluorophores in the sample is focused in the same

objective, passed straight through the beam splitter and is then refocused in a second lens towards the photomultiplier. Before hitting the photomultiplier tube (PMT) and being translated into an electrical signal and later to a digital color intensity, the laser passes through the pinhole, where the out of focus light is blocked.

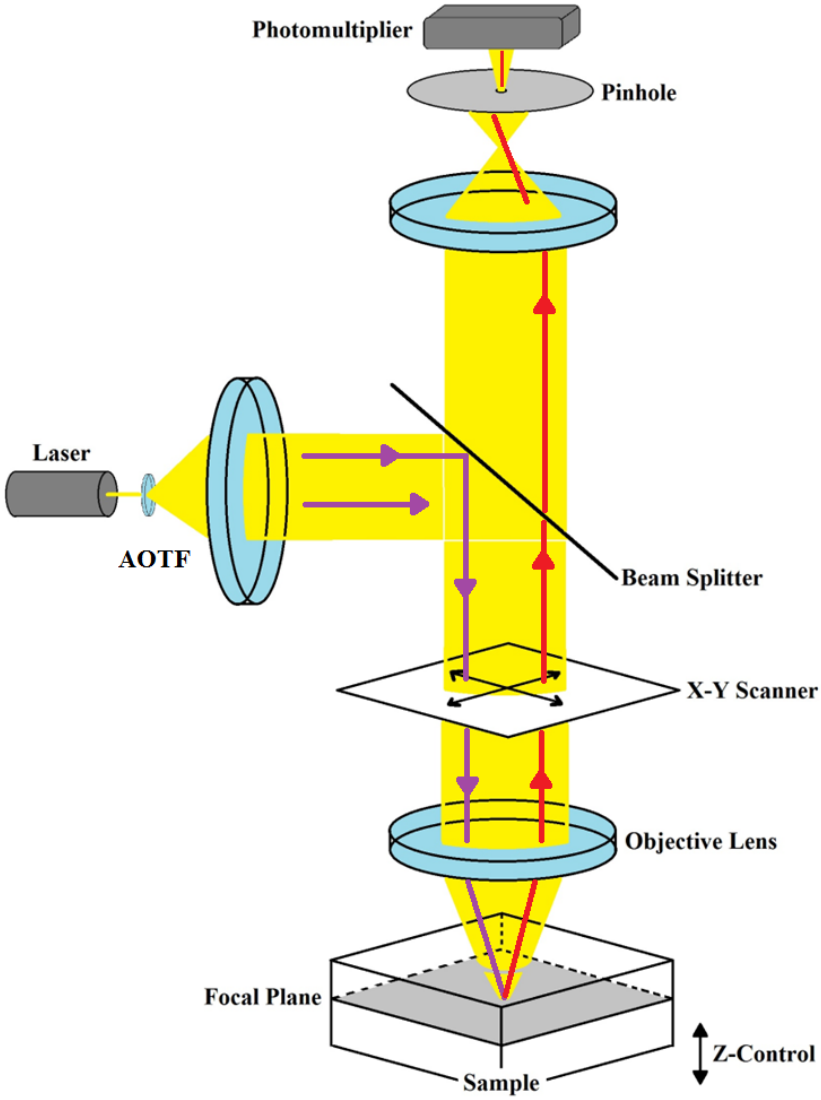

Figure 2. *Schematic depicting the main components and principle of a confocal laser scanning microscope.*

To create an image, an area (x,y) of the sample is scanned point by point. Each point digitally represented as a fluorescence intensity readout translated to greyscale i.e. a pixel. The greyscale can then digitally be set to a color of choice in the image appearing on the monitor. By using different colors for different dyes better contrast can be produced in the image and compounds of different classes can be differentiated between. However, in reality even when only a 2D image is created, there is a third dimension that should be taken into account, namely the thickness of the focal plane. Every pixel is in actuality a voxel (portmanteau of "volume" and "pixel"). The thickness of the focal plane i.e. height of a voxel is determined by *Equation 7.* A thicker plane, allowing for light from a larger volume to enter the PMT, decreases the contrast but might sometimes be necessary for detection.

$$Thickness\ of\ Focal\ plane\ (nm)\ =\ \sqrt{\left(\left(\frac{\lambda * n}{NA^2}\right)^2 + \left(\frac{AU * n * \sqrt{2} * 1{,}22 * \lambda}{NA^2}\right)^2\right)}$$

Equation 7. *Equation for focal plane thickness in nm, AU=pinhole diameter in airy units, λ=highest emitted wavelength, n=refractive index, NA=numerical aperture.*

The main limitation of the CLSM is however still the data acquisition speed, seeing as the laser has to scan each point of an area (typically between 512x512 and 2048x2048). And furthermore if 3D models are to be created this needs to be repeated several times at different depths. Consequently the creation of a high definition 3D model can take everything from a minute and up to an hour. This causes problems for highly dynamic systems, such as coffee foam, and thus image quality may have to be sacrificed for the sake of greater image acquisition speed.

Chapter 3 – Method Development

3.1 The Foam Creation Process

Figure 3 below shows coffee pre- and post-foaming, (1) and (2) respectively. The coffee foam creation process was standardized and implemented throughout the project as follows. The coffee foam was created by letting instant coffee (Gevalia Mellanrost) granules (0.20 g) dissolve in room temperate tap water (10 ml) in a 50 ml plastic centrifuge tube for 2-3 minutes, gently mixing the coffee by swirling the tube by hand before foaming by mixing the coffee with an IKA yellow line Dl25 basic Disperser/homogenizer/Ultra-Turrax at 20 500 rpm for 15 sec.

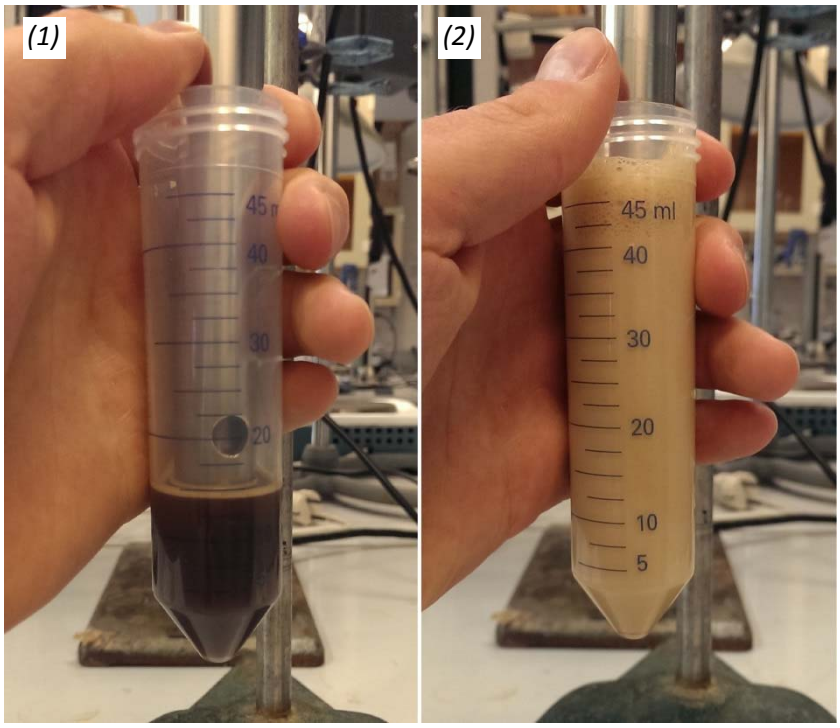

Figure 3. *Instant Coffee dissolved in a 50 ml centrifuge tube pre- and post-foaming with an IKA yellow line Ultra-Turrax at 20 500 rpm, (1) and (2) respectively.*

3.2 CLSM Setup and Sample Handling

The best method for studying the foam with CLSM was determined to be through an inverted microscope setup with the foam placed on a cover glass. As coffee foam is very dynamic and the focal plane very thin, looking at the foam through the cover glass to ensure a flat steady surface was crucial. Menzel-Gläser, 24x60 mm Cover slips #1.5 were used. A small well, confining the foam on the glass, was created by using a SecureSeal™ adhesive spacer (9 mm diameter, 0.12 mm depth) from Life Technologies, see *Figure 4* below.

After foaming with the Ultra-Turrax the foam was left in the tube for two minutes before a sample was extracted and placed on the cover glass. This was done to allow for the heavy initial drainage to pass, as immediately extracting a sample resulted in the then very wet foam quickly draining and forming a liquid film on the cover glass surface, greatly reducing the observable depth and the image quality.

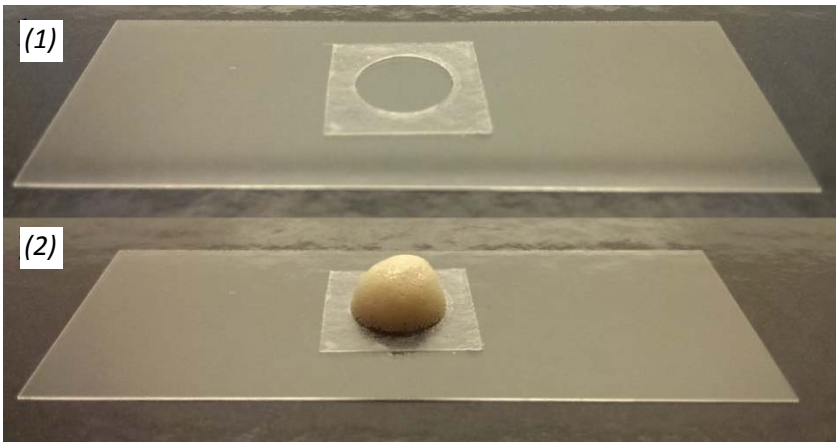

Figure 4. *Cover slip with a SecureSeal™ adhesive spacer attached, without (1) and with (2) foam.*

When trying to look at the foam from above three major problems were identified. The uneven surface of the foam made it hard to get clear pictures as parts became either under- or overexposed due them being at different relative heights paralleled to the lens. Secondly, the foam breakdown along the z-axis meant that the focus of microscope constantly had to be adjusted to follow the foam down. This movement made it essentially impossible to capture any 3D-stacks as the adjustments made along the z-axis pre-scan quickly became irrelevant and the foam would often completely leave the focal plane mid scan. Trying to compensate for this by increasing the depths the focal plane was set to move to during the scan also proved too difficult as predicting the foam movement on a µm-scale could not be done accurately enough. Placing the foam in a cup with a cover glass on top, in contact with the foam, also impacted the behavior and structure of the foam too much. As this meant that foam was encapsulated and in contact with solid surfaces on all sides, being exposed to different capillary and wetting forced compared to when on a liquid surface in an open cup. The third problem encountered was the staining, as will be discussed in more detail in *Section 3.3*. For reasons such as, large amounts of dye being required and water solubility issues, mixing dyes into the coffee pre-foaming could only be done with a few select dyes, others had to be pre-dried on the cover glass before placing the foam on top. This pre-drying method did however prove very efficient for the inverted microscope setup but due to it relying on the dyes diffusing into the sample it was not very effective for an upright setup as the top part of the foam would often remain unstained. Even in the cases the dye managed to reach the uppermost parts of the foam, the time it took would mean that early, possibly very valuable, information could not be obtained. The continuous draining of liquid down toward the glass in the lamellae was in all likelihood significantly contributing to counter the diffusion of the stains, as it acted in the opposite direction to the capillary force. The possibility of applying stains on top of the foam was not further investigated as it was believed to impact the structure too much and even if successful would not solve the previously mentioned problem of the foams uneven surface and deterioration along the z-axis.

To asses if any components of the coffee foam autofluoresced, five lambda scans, or wavelength scans, were performed. The sample was excited at 488, 496, 514, 543 and 594 nm and autofluorescence was scanned for between the exciting wavelength and 700 nm. Minor autofluorescence was detected in all wavelengths, with the most intense being between 530-540 nm when exciting with 488 nm. However, compared to the fluorescence intensity of stained foam this was very much negligible. Sample staining was thus deemed necessary. The graphs from the lambda scans can be found in *Appendix 1*.

3.3 Sample Staining

Two ways of staining were tested, mixing the dye into the coffee before foaming as well as drying the dye on a cover glass before placing ready foam on top, letting the stain redissolve and diffuse up into

the foam. With pre-drying the dye turning out to be the better option, allowing for a wider range of stains to be used, providing equal or often better image quality as well as significantly lowering dye consumption.

Mixing the dye into the coffee could only be done efficiently for dyes with high water solubility. Even though the homogenizer quite efficiently dispersed most dyes throughout the entire sample during foam formation, dyes with low water solubility would aggregate in the liquid/bubble interphases independent of their potential to stain compounds in the coffee, as is expected for undissolved compounds. On the other hand, when dried on a cover glass and left to diffuse into foam, even dyes with low water solubility would relatively efficiently stain the foam. Both particles and entire foam structures could be stained this way. Even when using water soluble dyes, particle staining was equally if not more pronounced when dyes were dried onto the cover glass compared to when mixed into the coffee pre-foaming. This was not expected as dissolving the stains in the coffee should ensure a lot of contact between the particles and the stain. However, this might simply be due to the concentration gradient that develops when a stain diffuses into foam. The concentrations of dye to total volume of foam were the same in both cases, but since the unstained foam is initially placed on top of the glass the dye becomes more concentrated close to the cover glass, in the observable plane. The volume of foam put onto the cover glass could not be efficiently measured but was approximated as 0.19ml, which is half the volume of 9mm sphere i.e. the diameter of the secure seal well.

Another point in favor of drying the dyes on the cover glass is that even though no structural differences were actually observed between stained and unstained foam. Mixing the dye into the coffee before foam formation meant that the dye had the opportunity to impact both the foamability and foam stability. While letting the stain diffuse into the already made foam meant that it only could impact the foam stability, theoretically ensuring a comparatively more relevant foam.

The one drawback of pre-drying dye seemed to be the diffusion time before the sample was sufficiently stained. For general stains, i.e. dyes that stain the entire liquid phase, this was not really relevant since the diffusion turned out to be very fast (<1 min). The same could be said for staining of surfaces active compounds. For particles moving freely in the lamellae there was however a significant lag time between the staining and particles becoming visible. In *Figure 5* below, small green specks can be seen in the upper and left regions of the second picture (2), these being small particles eventually becoming stained by the BODIPY™ dye, compare to the first image (1) taken 11.5 minutes earlier.

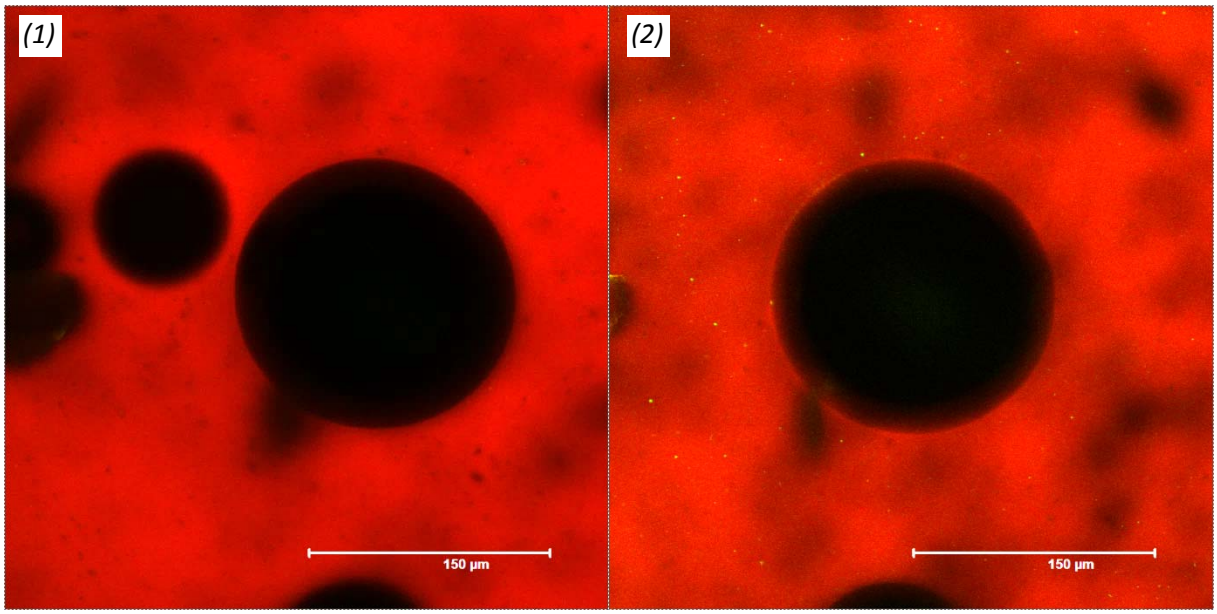

Figure 5. *Foam stained 3µl of Texas Red (Red) and 3µl of BODIPY (Green), dried on a cover glass. (1) Taken 90 seconds after the foam was placed on the cover glass, (2) was taken 13 minutes later.*

3.3.1 The Dyes

Ten different dyes were tested in different combinations in order to identify good ways of staining the foam. Both compound staining, to identify where specific particles aggregate and staining of the entire sample, to observe the foam structure, were evaluated. The combinations were chosen based on which dyes could actually be combined and not interfere with each other's emission spectra as well as which compounds they were expected to stain. The intent being that one dye would stain a specific type of particle and the other dye would stain the background i.e. the structure. Four dyes were also individually tested as to further examine their staining capabilities. *Table 1* below shows the different dyes, their manufacturers and which types of compounds they previously have proven to have affinity. *Table 2* shows the tested dye combinations, the wave lengths used for excitation and the interval used for detection.

Table 1. *Tested dyes, their manufacturers and the types of compounds they have proven to have affinity for.*

Dye	Manufacturer	Affinity for
Acridine Orange - Zinc chloride double salt	Merck Millipore's Certistain®	DNA, RNA, polysaccharides and various other molecules [37-40]
Acriflavine - Acriflavine Hydrochloride	Sigma Aldrich	Carboxylic acids, nitrous acids [41], nucleic acids [42-44]
BODIPY™ FL	Life Technologies	Lipids [45]
Congo red - Direct Red 28	VWR - BDH Chemicals	Cellulose, amyloid fibrils, starch [46]
FITC I - Fluorescein-5-isothyicyanat	Sigma Aldrich	Proteins [45, 47, 48]
Nile blue A - Nile blue sulfate	Chroma-Gesellschaft Schmid & Co	Phospholipids, lecithin and other polar lipids [45, 48-50]
Nile red	Polysciences	Neutral lipids [45, 48-51]
Rhodamine B	Sigma Aldrich	Proteins [45, 47, 48]
Sirius red	VWR - BDH Chemicals	Collagen, proteins [52, 53]
Texas red	Life Technologies - Invitrogen™	Proteins [48, 54, 55]

Table 2. *Combinations of stains tested, the wavelength used to excite and the interval used for detection.*

Dye 1	Excitation/Detection (nm)	Dye 2	Excitation/Detection (nm)
Acridine Orange	488/500-583	-	-
Acridine Orange	488/500-583	Congo Red	543/550-655
Acridine Orange	488/500-583	FITC I	488/500-535
Acridine Orange	488/500-583	Nile blue	633/640-684
Congo red	543/550-655	-	-
Congo red	543/550-655	BODIPY™	488/494-570
Nile red	488/520-600	Nile blue	633/640-684
Nile red	488/520-600	Texas Red	594/605-695
Rhodamine B	488/540-618	-	-
Texas red	594/605-695	-	-
Texas red	594/605-695	Acriflavine	488/494-568
Texas red	594/605-695	BODIPY™	488/494-548
Texas red	594/605-695	Rhodamine B	488/540-618
Texas red	594/605-695	Sirius red	488/500-578

For staining of the entire sample, Texas red was found to be the most efficient dye. However, due to the high cost of the stain, the large volume needed for it to be mixed into the coffee before foaming could not be justified, hence it was only tested dried on cover glass. Acridine orange produced comparable staining when pre-dried on a cover slip but diffusion was slightly less efficient and thus the observable depth was reduced. However, it should also to be noted that Texas red and Acridine orange have different emission spectra, 605-695 nm and 500-583 nm respectively, still making both useful since a wider range of component stains can employed while still having a dye for the background.

Lipids of varying polarity are as previously mentioned found in coffee. As can be seen in *Figure 4,* section 3.3 above, BODIPY, theoretically having affinity for lipids[47], were able to specifically stain particles moving freely in the lamellae. BODIPY did also have the ability to stain the bubble surfaces,

however this was not as pronounced as the particle staining, indicating that the stain is less selective towards very polar, surface active, lipids. Despite its relatively slow staining it was the most efficient dye for staining the lipid-like particles. Nile red was however also capable of staining these particles but was less specific, dimly staining the entire liquid phase as well. Nile blue, theoretically selective towards polar lipids [45, 49, 50], did indeed stain surface active compounds as excepted and was more selective than both BODIPY and Nile red, not staining any other part of the foam.

Sirius red stained surface active compounds as well as certain particles of very low abundance in the coffee foam. Theoretically having affinity for proteins the staining of surface active compounds was expected. The stained particles may be fragments of coffee bean as they were bigger than all other observed particles, they were also very uncommon, often not being found at all in samples. Their impact on the foam is therefore probably not significant.

Not Acriflavine, Rhodamine B, FITC I nor Congo red did stain the foam in a satisfactory way. Acriflavine and FITC were not able to stain any compounds sufficiently enough for good images to be taken at all. Rhodamine B behaved very unpredictably and to consistently produce good images proved hard. When acceptable images could be taken the stain's selectivity was essentially the same as that of Sirius red, thus it was deemed unnecessary for this study. Congo red interfered with the other dyes' emission spectra too much and was incapable of producing good images on its own.

No dye for specific staining of polysaccharides or other carbohydrate could be identified. However, Acridine orange did manage to stain certain particles brighter than the background and, as mentioned above, Sirius red occasionally stained certain low abundance particles as well. These are in all likelihood not pure carbohydrates but they may be aggregates of polysaccharides and proteins, known to be found in coffee [16] or fragments of coffee bean probably having a carbohydrate fraction.

3.4 Observing Surface Active Compounds

Observing stained surface active compounds directly turned out to be very dependent on the focal plane position along the z-axis i.e. depth in the sample, as well as on the thickness of the plane itself. However, as will be discussed below in *Section 3.5*, there was a reflective effect involving the surface active species that could be seen almost completely independent of these factors as well.

When the focal plane was positioned as such that the top of a bubble was directly in focus, *Figure 6* (1) below, the stained surfaces active compounds were clearly visible. As the focal plane was moved down through the foam the signal decreased, eventually becoming undetectable, see *Figure 6* (2) and *Figure 7* (1-3). This is because the layer around the bubble is very thin, resulting in area facing the lens decreasing with increasing depth, until the bubble's midpoint is reached. With the decrease in signal due to distortion from the sample itself that also contributes to the effect as the focal plane is moved deeper into the foam.

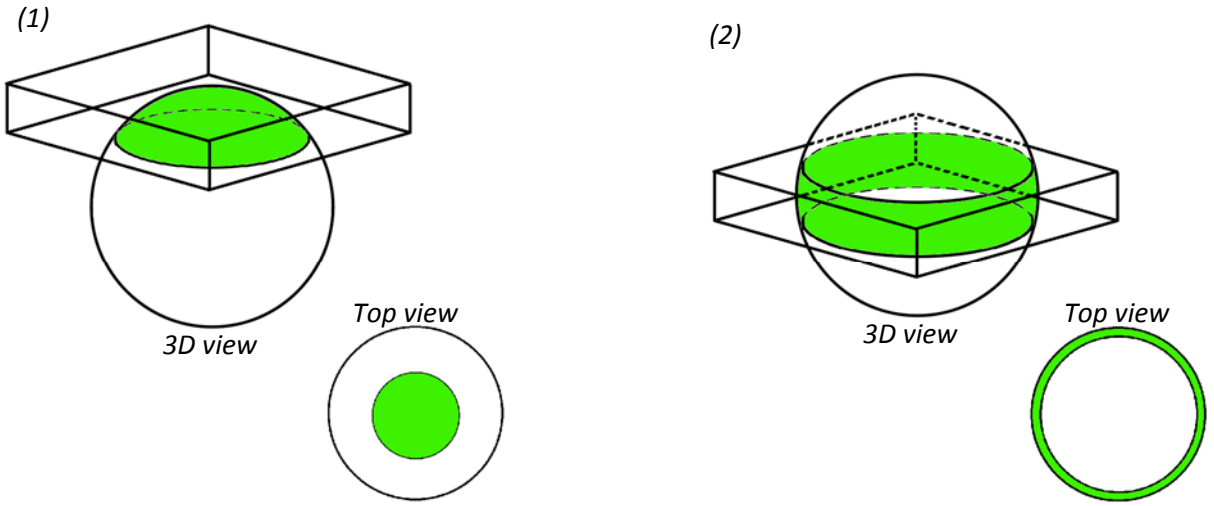

Figure 6. *Illustration of focal plane position relative to a bubble (3D view) and correlating surface of the bubble observed in the in the microscope (Top view).*

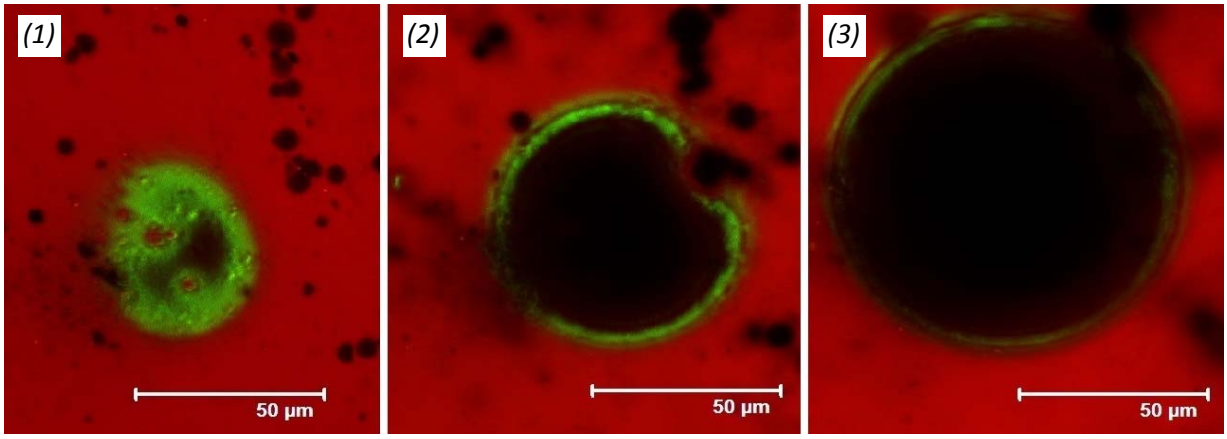

Figure 7. *Foam stained with Nile red (green in the picture) and Texas red (red in the picture). A single bubble viewed at three different depths, increasing from left to right (1-3). Nile red mixed in the coffee pre-foaming to efficiently stain the bubble surface.*

3.5 Reflections in the Foam

When shining a laser into coffee foam, exciting molecules and picking up the returning emitted light, there is as one can imagine going to be a lot of interference from the many air/water interfaces and spherical bubble surfaces found in the sample. What appears as structures or particles in the microscope are sometimes simply the result of light being reflected and refocused. Two instances of these very phenomena are constantly observed. The stained continuous phase appearing as structures inside bubbles at certain depths as well as light from stained surface active compounds being sharply focused into the middle of bubbles, seemingly at all depths.

Figure 8 below shows a series of images taken of a bubble at continuously increasing depths. Once the midpoint of the bubble has been reached (6) a faint ring appears as a structure in the bubble, as the depth is increased this ring becomes sharper and more focused towards the middle of the bubble (7-9). Until finally the distortion from the sample itself becomes too much and the stained structure becomes too indistinct (10). Using the software Avizo, the reflections can also visualized in three dimensions, *Figure 9* below shows foam modeled with and without the reflective structures. Manual pre-processing of the images to separate the reflections from the foam structure has been carried out as no filter or algorithm capable of doing so could be found.

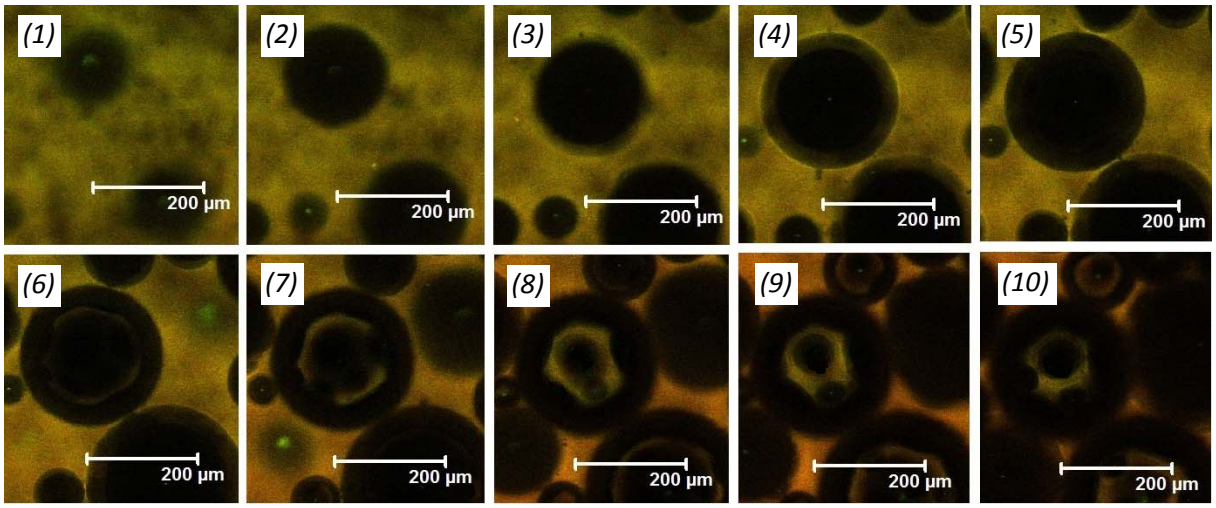

Figure 8. *Foam stained with Acridine Orange, depth of the focal plane increased by 10 µm between each picture (1-10). A reflection appears in the bubble once its midpoint has been reached.*

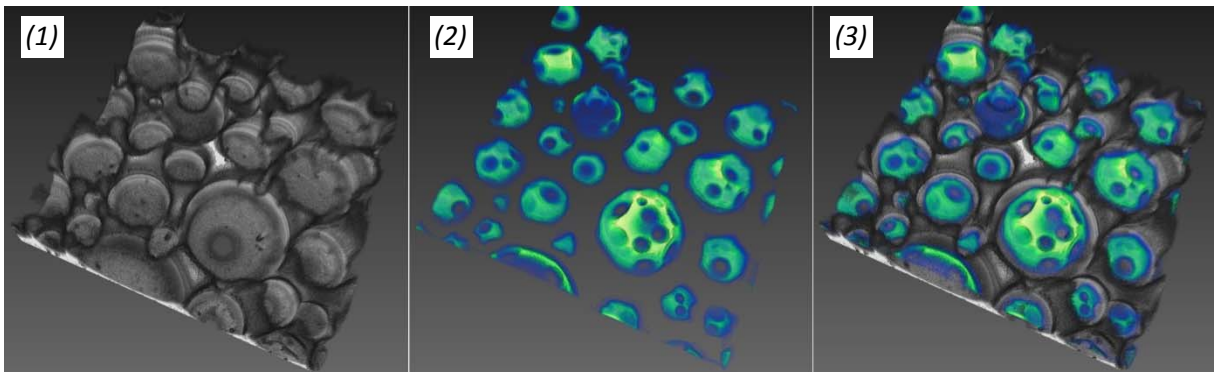

Figure 9. *Foam modeled in Avizo. Reflections removed (1), reflections only (2) and foam with reflections as they appear when images are not edited before 3D-modeling (3).*

However, it should be noted that there is an apparent difference between light emitted from the stained lamellae entering a bubble compared to stained surface active compounds emitting light directly into a bubble. Indicating that the refraction when the light is crossing over from the liquid to the gas phase affects the way the light is then focused towards the lens.

Figure 10 below shows two foam samples stained with different combinations of dyes, Nile red and Texas red (1) as well as Acridine orange and Nile blue (2). In the upper left part of the first picture (1) the previously discussed reflective structures can be observed in two separate bubbles, indicating that these two are positioned closer to the lens compared to the bubbles of similar size around them. The large green spots not surrounded by any black in the left picture (1), red in the right picture (2), are edges of bubbles found deeper into sample, as described in *Section 3.4*. However, in both pictures, every bubble independent on position along the z-axis or size has a relatively well focused dot in the middle of it, in the color representing the surface active compounds. Demonstrating that the bubbles behave essentially as lenses, focusing the light emitted from the surface active compounds.

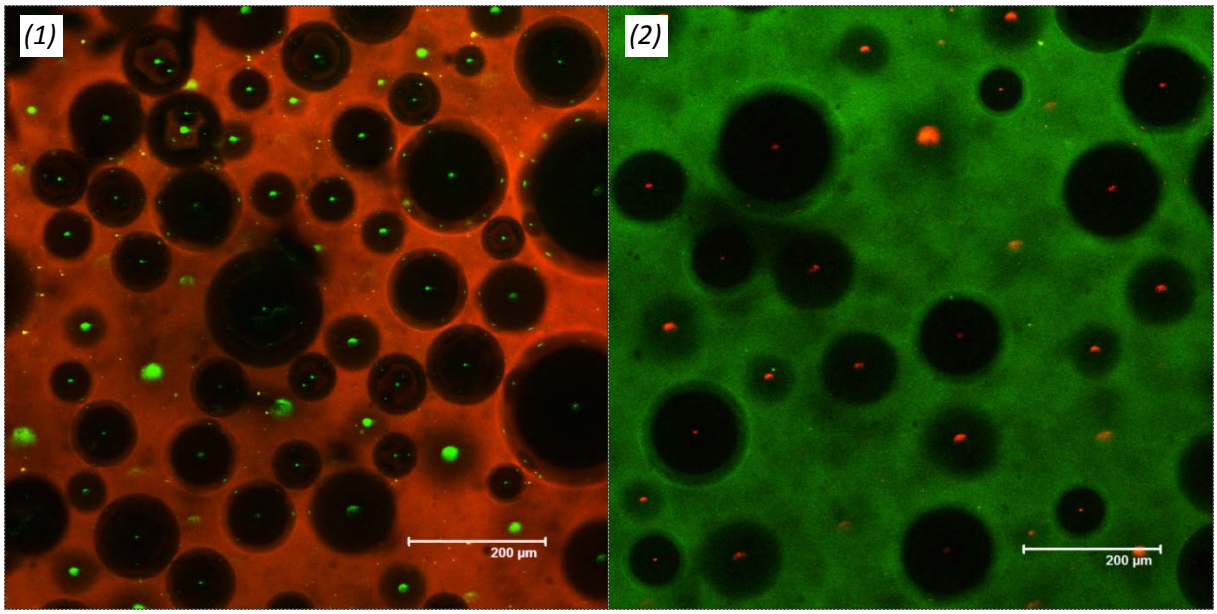

Figure 10. *(1) Foam stained with Nile red (green in the picture) and Texas red (red in the picture). (2) Foam stained Acridine orange (green in the picture) and Nile blue (red in the picture).*

Focal plane thickness does however seem to influence if these reflections are observable or not. Both pictures in *Figure 10* have focal plane thicknesses of 15.5 µm, compare this to e.g. *Figure 7* in *Section 3.4*, where no such reflection was observed despite surface active compounds being stained. There the focal plane thickness was 1.2 µm. The fact that thickness but not z-position of the focal plane affects if the reflections are observed or not suggests that it might be a matter of the thinner focal plane i.e. smaller pinhole not being able to capture enough light for the reflections to be detected. Not that they are only observable at certain depths like the light reflected from the liquid phase.

Also supporting the theory that it is indeed the position of the compounds relative to the bubble that is responsible for the reflective effects is that the two emission spectra are essentially reversed between the pictures in *Figure 10*. The emitted light from the two dyes staining the liquid phase, Texas red and Acridine orange, are detected between 605-695 nm and 500-583 nm respectively. While Nile red and Nile blue, staining the surface active compounds, are detected between 520-600 nm and 640-684 nm respectively. This is demonstrating that the individual wavelength of the dye, in the ~500-700 nm range, is irrelevant for the presence of these reflections.

3.6 Developed Method Summary

A Leica TCS SP2 Spectral confocal & multiphoton system using an inverted DMIRE2 microscope was used to study the foam. The foam was created by dissolving 0.20 g instant coffee in 10 ml tap water and mixing for 15 seconds at 20 500 rpm. The foam was then left in the tube to drain for 2 minutes before being placed on a cover glass with dye pre-dried inside a well created by a SecureSeal™ adhesive spacer. Dye solutions and amounts used per sample are presented in *Table 3* below.

Table 3. *Dyes solutions, their concentrations, solvents, amounts used when pre-dried on a cover slip and observed selectivity of staining.*

Dye	Concentration	Solvent	Amount	Staining
Acridine Orange	2mg/ml	Ethanol	5µl	The entire foam structure and various particles
BODIPY™	1mg/ml	Methanol	3µl	Lipid-like particles in the lamellae and surface active (polar) lipids
Nile Blue	2mg/ml	Ethanol	5µl	Surface active (polar) lipids
Sirius Red	1mg/ml	Water	6µl	Surface active proteins, particles
Texas Red	1mg/ml	Ethanol	3µl	The entire foam structure

Chapter 4 – Experimental Design, Materials and Methods

4.1 Determination of Average Bubble Area in Coffee Foam as a Function of Time

Average bubble size (μm^2) was measured over time. Time-lapses were run in triplicates in the CLSM and average area was defined using ImageJ after pre-processing the pictures in MS paint.

Pre-processing of the images was deemed necessary to ensure reliable data as available software (Leica Las X or ImageJ) could not efficiently identify and separate the bubbles from each other. The previously discussed reflections appearing as structure in the foam also proved very troublesome when only using image analysis software as there was no actual difference in light intensity between the reflections and the genuine lamellae. Only location in the foam reveals if the observed structure is a reflection or not, algorithms able to determine this was not available. Filling in the bubbles was therefore done manually before computing average bubble size. *Figure 11* below shows the progress of the average area determination from original image (1), to filled bubbles (2) and finally after using ImageJ to identify, separate, quantify and measure the bubbles (3). It is recognized that manually drawing circles on bubbles ads a slight subjectivity to analysis, the entire pre-processing being done by the same person did however minimize differences between images as much as possible.

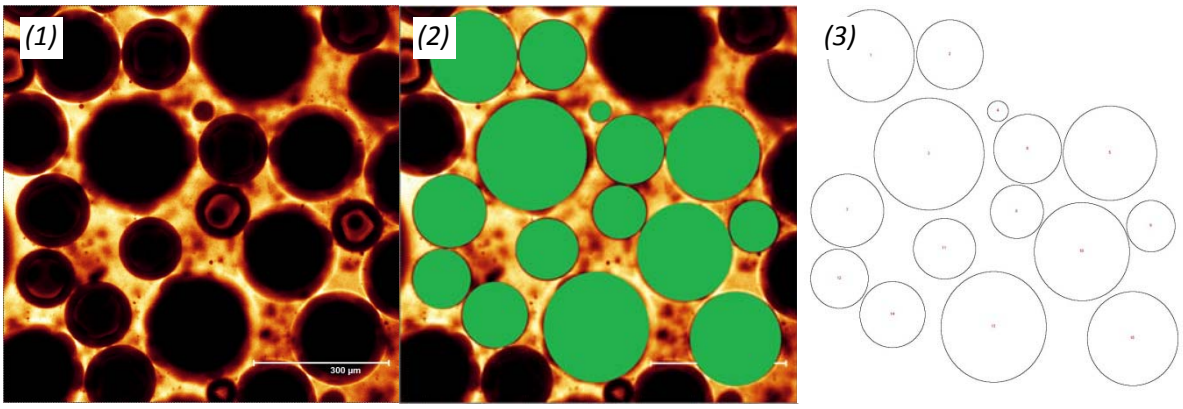

Figure 11. *Images of coffee foam at the three different stages during the average bubble area determination process. (1) raw image, (2) manually edited image, (3) outlines of bubbles measured in ImageJ.*

A Pl Fluotar, 10x, 0.3 NA objective was used for the time-lapses, foam was stained with Texas Red and images were taken >70µm into the sample as to avoid effects from the glass-foam interface to as large extent as possible. The foam was placed on the coverslip 2 minutes after foam formation and the time-lapse was started at minute 4 and ran until minute 25, capturing 8 images in total (Δt=3 min).

The method proved to be reproducible with an average relative standard deviation (%RSD) of 7.17 % (median 6.71 %) across all samples analyzed in the study, ignoring data from two failed test were average %RSD of 18.08 % and 18.11 % were reached due to some undefined complication(s).

4.2 Liquid Drainage in Coffee Foam with Time

Drainage was measured by rigging up a Dino-Lite Pro Digital Microscope AM-413TL to capture time-lapse series of images following the rising liquid surface in a centrifuge tube post-foaming. The time-lapses were run in triplicates using the same parameters as for the average bubble size measurement i.e. 21 minutes in total, one image every 3 minutes, started at minute 4 after foam formation. The cap was left off the tube to mimic the natural deterioration process in a cup and the CLSM analysis, where the foam is exposed to the atmosphere, as much as possible. The distance the surface rose was measured with ImageJ and recalculated to ml using the scale on the tube. *Figure 12* below shows four images taken at minute 4, 10, 16 and 22 during one of the replicates with pH 6.1.

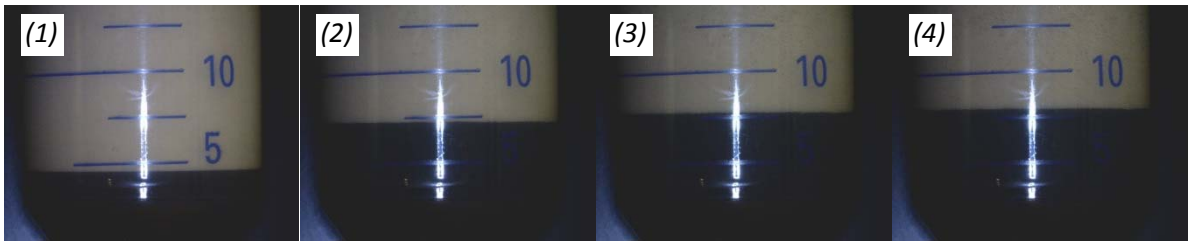

Figure 12. *Images taken from a time-lapse series of a foam drainage measurement of coffee foam with pH 6.1, (1-4) represents 4, 10, 16 and 22 min respectively.*

Distance between each line is 5 mm in reality and the scale was set as such in ImageJ, making 5 mm in the image correlate to 2.5 ml of coffee. The distance between the coffee surface and the 10 ml line was then measured in each picture and amount of drained coffee was calculated according to *Equation 8* below.

$$V = 10 - \left(\frac{L}{2}\right)$$

Equation 8. *Equation for determining ml of drained coffee, V = Amount of coffee drained (ml), L = distance between surface and the 10 ml line in the image (mm).*

Measuring drainage with the Dino-Lite microscope and ImageJ proved reproducible, having an average %RSD of 2.78 % across all samples (median 2.37 %).

4.3 Sample Treatments

Three sample treatments related to processing parameters in coffee production were investigated. pH was investigated since degree of roasting heavily influences acid content in coffee and the pH-range corresponding to the isoelectric points of green coffee proteins (pH 5.7-6.3) can be reached in commercial coffee [12, 18]. Filtration was chosen because instant coffee is put through several filter and concentration steps during production, particles of varying sizes are also, as previously discussed, known to affect foam properties. Lastly, particle addition was chosen as to further investigate the role of particles in coffee foam, allowing for fluorescent and characterized particles (in terms of hydrophobicity and size) to be used.

4.3.1 The Effect of pH Adjustment on Coffee Foam Microstructure

The pH was measured with a HachsenION+ pH3 Laboratory pH meter. Coffee was prepared as described in *Section 3.1* and the pH was adjusted by addition of NaOH (0.5 M) or HCl (0.5 M). Values were initially chosen based on the above mentioned range of isoelectric points of the proteins, two values closer to the standard, one lower and one slightly higher were tested as well. *Table 4* below shows pH values, all samples were run in triplicates.

Table 4. *The different pH values tested.*

Sample	pH (±0.05)
Standard (Non-adjusted coffee)	4.9
1	4.0
2	5.4
3	5.8
4	6.1
5	6.3

4.3.2 The Effect of Filtration on Coffee Foam Microstructure

To remove particles, three different syringe filters were used, presented in *Table 5* below, coffee was prepared as described in *Section 3.1* and slowly pushed by hand through the filters at a constant rate before foaming.

Table 5. *Syringe filters used for removal of particles from the coffee.*

Manufacturer and filter	Pore Size
Life Sciences, Acrodisc® Syringe Filter, Nylon membrane	0.20 µm
Fisher Scientific, Fisherbrand® Syringe Filter, Nylon membrane	0.45 µm
Life Sciences, Acrodisc® Syringe Filter, Versapore®	0.80 µm

4.3.3 The Effect of Particle Addition on Coffee Foam Microstructure

Gmoser [4] concluded that *"the coffee solution is composed of surface active species with high molecular weight since the surface tension decreases over a long time"*. Meaning that large hydrophobic particles are present in the coffee, as the foam ages they migrate at an increasing extent to the bubble interfaces, stabilizing the foam by reducing the surface tension. She also concluded that the concentration of coffee, and thus amount of particles, correlates well to foam stability as increasing the coffee concentration reduces surface tension and increases viscosity. The addition of fluorescent polystyrene (PS) beads was therefore investigated as a means to further study this mechanism, by visually observing the possible aggregation at the bubble surfaces as well as potential migration during foam aging. As just increasing coffee concentration limits the capability of following specific particles since they are not pre-labeled.

Hydrophobic, carboxylate-modified polystyrene latex beads with diameters of ~1 µm were mixed into the coffee pre-foaming, location and behavior of the beads were monitored simultaneously as images for average bubble size were taken. The latex beads were sonicated for 5 min at 45 kHz before being mixed into the coffee.

The sample volume was reduced from 10 ml to 2.5 ml during these tests to minimize the volume of latex beads used. New samples of standard coffee was run in triplicates at this lower volume and the average bubble size was measured at three points in time, 4, 13 and 25 minutes, and compared to the previously established standard. T-tests (*Appendix 4*) confirm that statistically there is no difference in bubble area (using a p-value of 0.05).

The latex beads were also mixed into coffee and studied pre-foaming in the CLSM to see if the Ultra-Turrax damaged the beads or otherwise affected their appearance. No difference between pre- and post-foaming could be noted.

The amount of beads in the coffee was started out low, a total concentration of 0.1 % (w/w) was initially used. Fluorescently labeled beads were used in the coffee studied in the CLSM and unlabeled beads for the drainage measurements. *Table 6* below shows the particle specifications.

Table 6. *Specification of particles mixed into the coffee pre-foaming.*

Specification	Manufacturer	Size	Fluorescence
Hydrophobic, Latex beads, carboxylate-modified polystyrene, fluorescent yellow-green	Sigma Aldrich	0.9-1.1 µm	λ_{ex} ~470 nm λ_{em} ~505 nm
Hydrophobic, Latex beads, carboxylate-modified polystyrene	Sigma Aldrich	0.9 µm	-

Chapter 5 – Results and Discussion

5.1 Growth of Average Bubble Area in Coffee Foam

Average bubble area was measured at 8 points in time over an interval of 21 minutes, starting at minute 4 after initial foam creation. As previously discussed, in *Section 2.3.2.1*, larger bubbles correspond to weaker foam. Therefore, the slower the growth and the smaller the initial bubble size, the more stable and persistent the foam is. Persistency often being defined as one of the, if not the, most important parameter of quality[9]. The impacts of pre-foaming adjustment of the pH, filtering, addition of hydrophobic PS beads and combinations of the filtering and bead addition were analyzed. Raw data from all analyses can be found in *Appendix 2*.

5.1.1 Effect of pH on Average Bubble Area in Coffee Foam

Figure 13 below shows the effect on average bubble growth rate of all tested pH values compared to the standard, including three CLSM images taken from one of the replicates of the time-lapse series on coffee foam with pH 6.3. *Figure 14* further shows the individual pH values compared to the standard, including standard deviations.

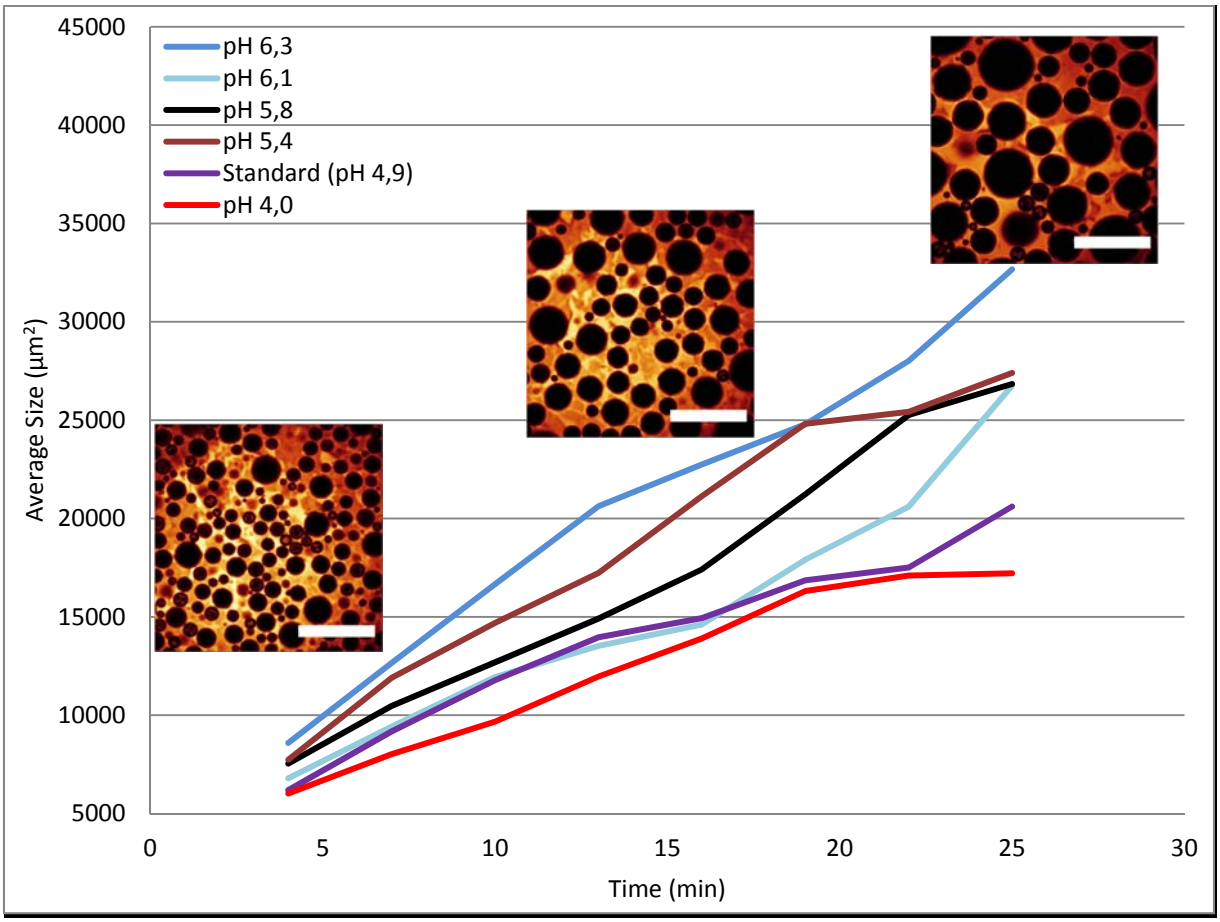

Figure 13. *Growth of average bubble area in coffee foam at 6 different pH values. The pH was adjusted pre-foaming with NaOH (0.5 M) or HCl (0.5 M). The images are from one of the sample replicates adjusted to pH 6.3 and were taken at minute 4, 15 and 25 respectively. The white scale bars in the pictures represent 500 µm.*

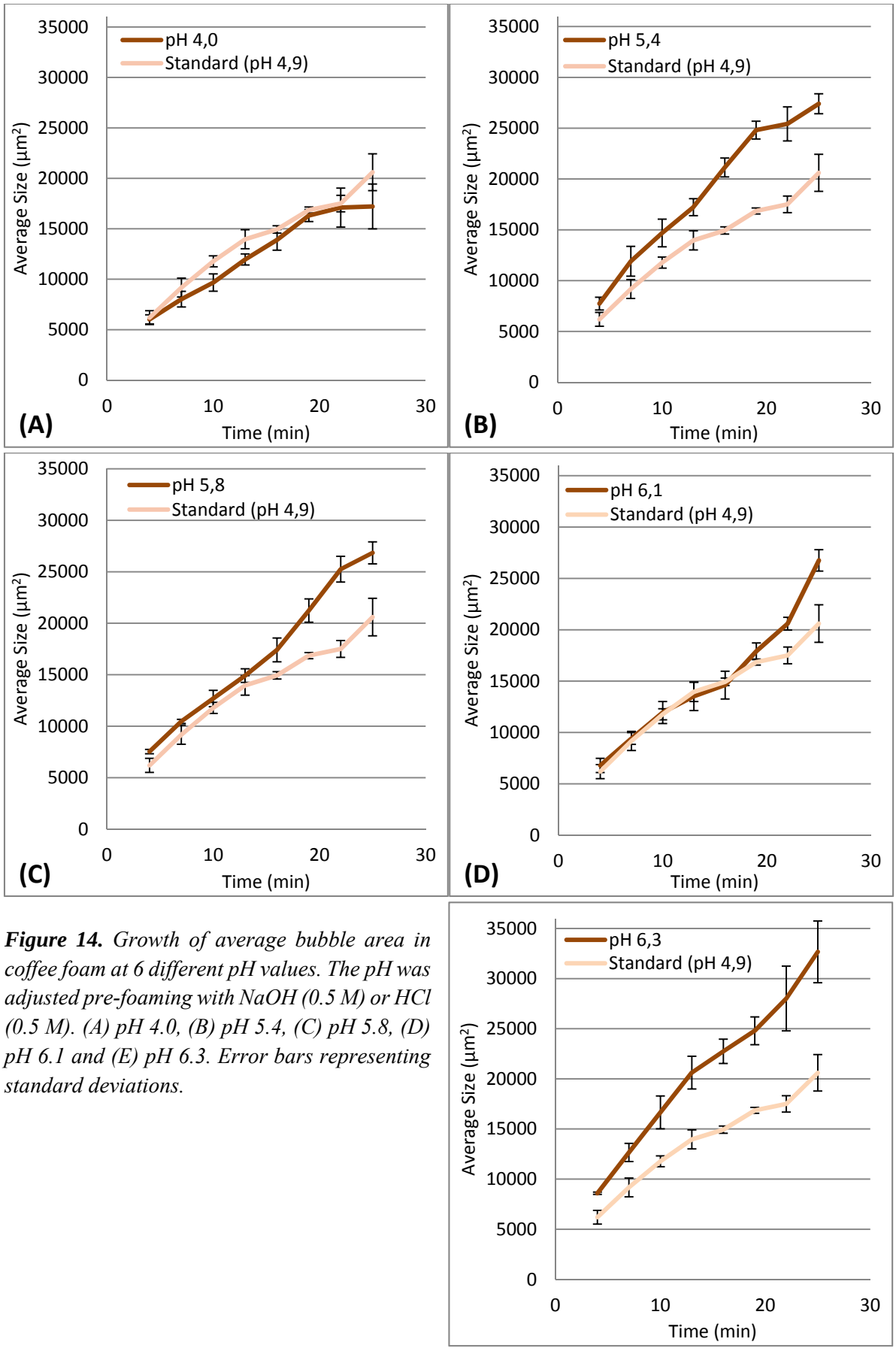

Figure 14. *Growth of average bubble area in coffee foam at 6 different pH values. The pH was adjusted pre-foaming with NaOH (0.5 M) or HCl (0.5 M). (A) pH 4.0, (B) pH 5.4, (C) pH 5.8, (D) pH 6.1 and (E) pH 6.3. Error bars representing standard deviations.*

As can be seen above in *Figure 13* and *Figure 14 (B-E)*, there is a trend of increased pH values destabilizing the foam compared to the standard in the studied time frame. The growth rate of bubbles in all samples was also shown to be overall linear (R^2-values ~0.95), the average growth rate (μm^2/min) under the studied time could thus straightforwardly be defined as the slope of the line. Using the first few points in each curve, the initial bubble area (min 0) could be extrapolated as measure of foamability. *Table 7* below shows growth rates, extrapolated initial bubble area and corresponding standard deviations for the foams with different pH values.

Table 7. *Growth rates of average bubble area and extrapolated initial average bubble area in coffee foams adjusted to different pH values, including standard deviations.*

pH	Growth of average bubble size (μm^2/min)	SD - Growth rate	Initial average bubble size (μm^2)	SD - Initial bubble size
4.0	1733	212	4117	145
4.9 (Standard)	1890	174	4517	331
5.4	2851	110	4625	576
5.8	2824	116	5112	738
6.1	2555	56	4008	628
6.3	3236	495	4158	384

Following the finding by Nunes et al [12], that increased foamability of coffee is correlated to the isoelectric points of green coffee proteins, most of which are in the pH 5.7-6.3 range [18], adjusting the pH to be in this span was expected to decrease initial bubble size and possibly decrease rate of bubble growth as well. The general trend that can be seen in *Table 7* above, of increased pH values destabilizing the foam by increasing initial average bubble area up until pH 6.1, where it drops again, agrees well with this. However, pH 5.8 having the highest extrapolated initial bubble area points towards the span of isoelectric points being slightly narrower or focused more in the upper part of the range (>pH 6.0) for this particular coffee.

The expected effect of pH in the 5.7-6.3 range also decreasing growth rate could however not be seen, the effect was instead the opposite as the standard showed a slower rate of growth compared to all four of the foams with higher pH values, *Table 7*.

Decreasing the pH from 4.9 to 4.0 did however show a tendency of stabilizing the foam, *Figure 14 (A)*, both by slowing down the growth from 1890 μm^2/min to 1733 μm^2/min and by showing a decrease in the extrapolated average bubble size, from 4517 μm^2 to 4117 μm^2.

Other compounds with isoelectric points, such as carbohydrates and lipids, in the tested pH ranges will of course affect the foam as well, but to what extent compared to the proteins is not known. However, since the exact number of different proteins and their relative abundance in coffee is unknown anyway, this does not really matter for the observed results. Isoelectric focusing of other compounds found in coffee besides the proteins, might however be interesting and could possibly be used to identify an optimal pH for foamability. On the other hand, even for the pH value that resulted in the best foamability the foam stability was still significantly reduced. If foam persistency up until a certain point in time is to be maximized this will of course have to be taken into account.

5.1.2 Effect of Filtration on Average Bubble Area in Coffee Foam

Figure 15 below shows the increase in average bubble area with time in the foams from the two pre-filtered coffees. Coffee filtered through the 0.45 µm filter is not included due to the measurements having too high standard deviations to be relevant and time for retesting could not be afforded, a reason for the large errors could not be identified. *Table 8* below further shows bubble growth rates (which once again were proved to be linear), extrapolated initial bubble area and corresponding standard deviations for the foams.

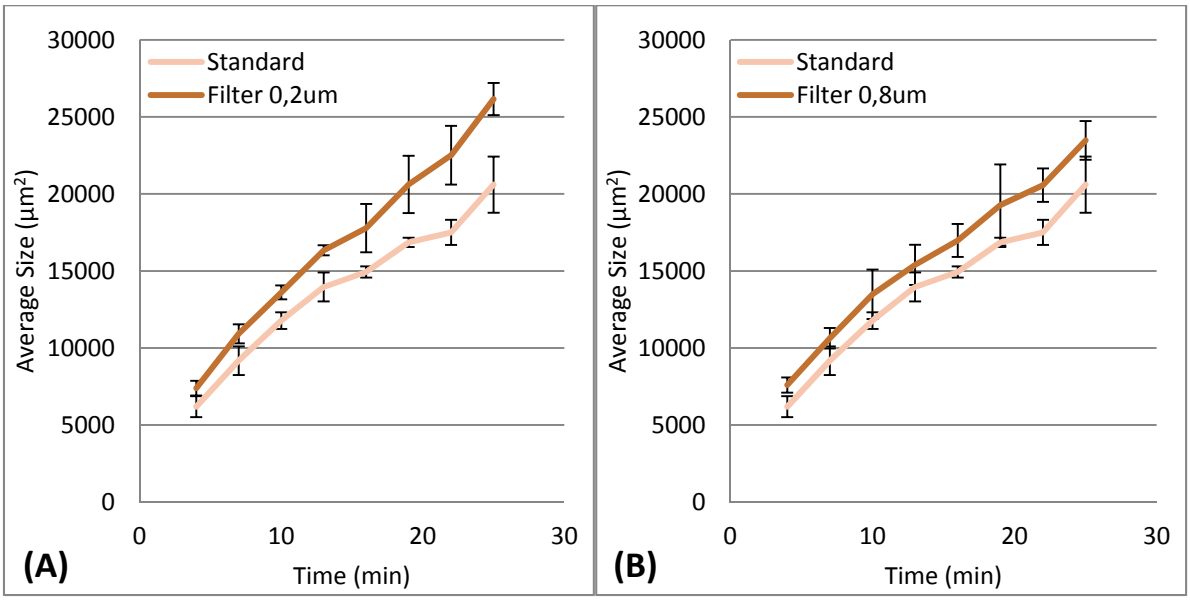

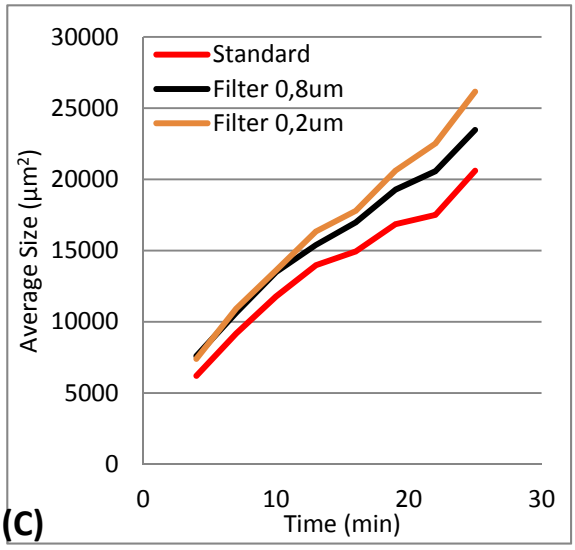

Figure 15. *Growth of average bubble area in coffee foam after pre-foaming filtration through filters with different pore sizes. (A) Filtered through 0.2µm, (B) filtered through 0.8 µm and (C) showing both, not including standard deviations.*

Table 8. *Growth rates of average bubble area and extrapolated initial average bubble area in coffee foams filtered pre-foaming, including standard deviations.*

Filter pore size	Growth of average bubble size (µm²/min)	SD - Growth rate	Initial average bubble size (µm²)	SD - Initial bubble size
Unfiltered (Standard)	1890	174	4517	331
0.8 µm	2121	152	4315	55
0.2 µm	2521	270	5302	825

Filtering the coffee pre-foaming proved to destabilize the foam by increasing the growth rate of the average bubble area, as can be seen in *Table 8* above. The finer filter, *Figure 15 (A)*, showed indications towards destabilized the foam to a greater extent by increasing the growth rate from 1890 μm^2/min to 2521 μm^2/min, the initial average bubble size was also significantly increased, from 4517 μm^2 to 5302 μm^2. The 0.8 µm filter did increase the growth rate, although to a lesser extent than the 0.2 µm filter, but the initial average bubble size was essentially unaffected.

The effects of filtering the coffee could also be observed visually by employing different sample stains, as filtration proved able to remove particles moving freely in the lamellae. All filters made a difference, signifying that a large fraction of the particles visible in the CLSM were >0.8 µm. Staining these particles with BODIPY proved the most efficient, indicating that they are at least partly lipid-like in nature. *Figure 16* below shows foam stained with Texas red and BODIPY, unfiltered (1) and filtered through a filter with a pore size of 0.2 µm (2). Note the absence of particles in picture (2). The surface of the bubble in picture (2) being stained green is due to it being at a different depth compared to the bubbles in picture (1), as described in *Section 3.4*, in reality there is no difference in the staining of surface active compounds between the two.

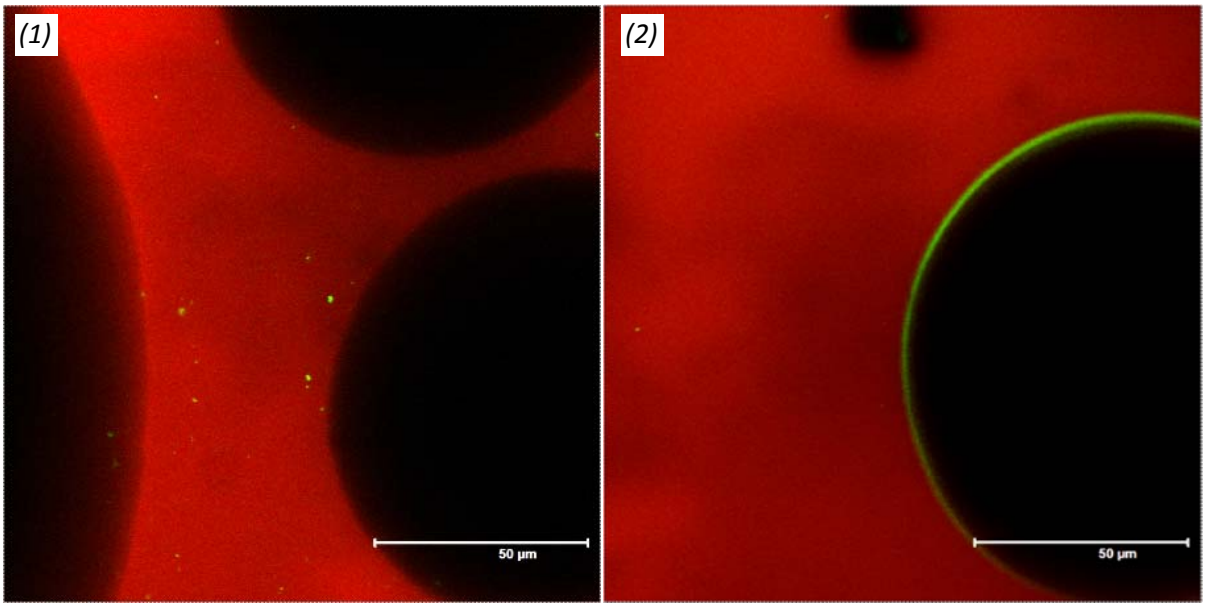

Figure 16. *Foam stained with Texas red, red in the picture and BODIPY, green in the picture, (1) unfiltered coffee and (2) filtered through a filter with a pore size of 0.2 µm.*

Acridine orange also stained particles moving freely in the lamellae, which again could be removed by filtration. These are in all likelihood the same particles as those stained by BODIPY, pointing towards them being complexes of different compounds as they can be stained by dyes having affinity for different functional groups. Pictures produced by staining with Acridine orange did however have a tendency to produce a lot of artefacts which may be interpreted as particles, but these were unaffected by filters and not very consistent in their appearance, in some samples not being observable at all. Most likely they are the result of Acridine orange having some solubility issues in the coffee. *Figure 17* below shows foam stained with Acridine orange and Nile blue before and after filtering (0.2 µm), the small bright green specks in the first picture (1) are the aforementioned particles, not seen in the second picture (2).

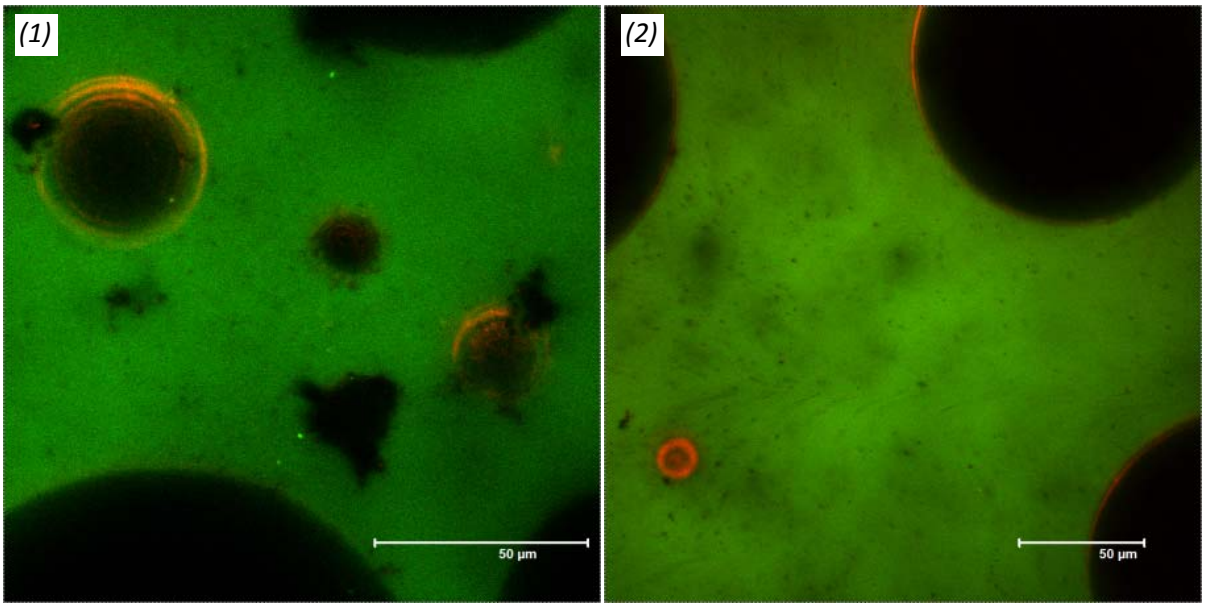

Figure 17. *Foam stained with Nile blue, red in the picture and Acridine orange, green in the picture, (1) unfiltered coffee and (2) filtered through a filter with a pore size of 0.2 µm.*

5.1.3 Effect of Adding Hydrophobic Particles on Average Bubble Area in Coffee Foam

Hydrophobic, ~1 µm large, fluorescent, carboxylate modified polystyrene beads were added to the coffee pre-foaming to further study the impact of particles on the foam. *Figure 18* below shows average bubble area of foam with PS beads compared to the standard and *Figure 19* shows the distribution of beads in the foam. *Table 9* further shows the bubble growth rate, extrapolated initial bubble area and corresponding standard deviations for the foam with added PS beads.

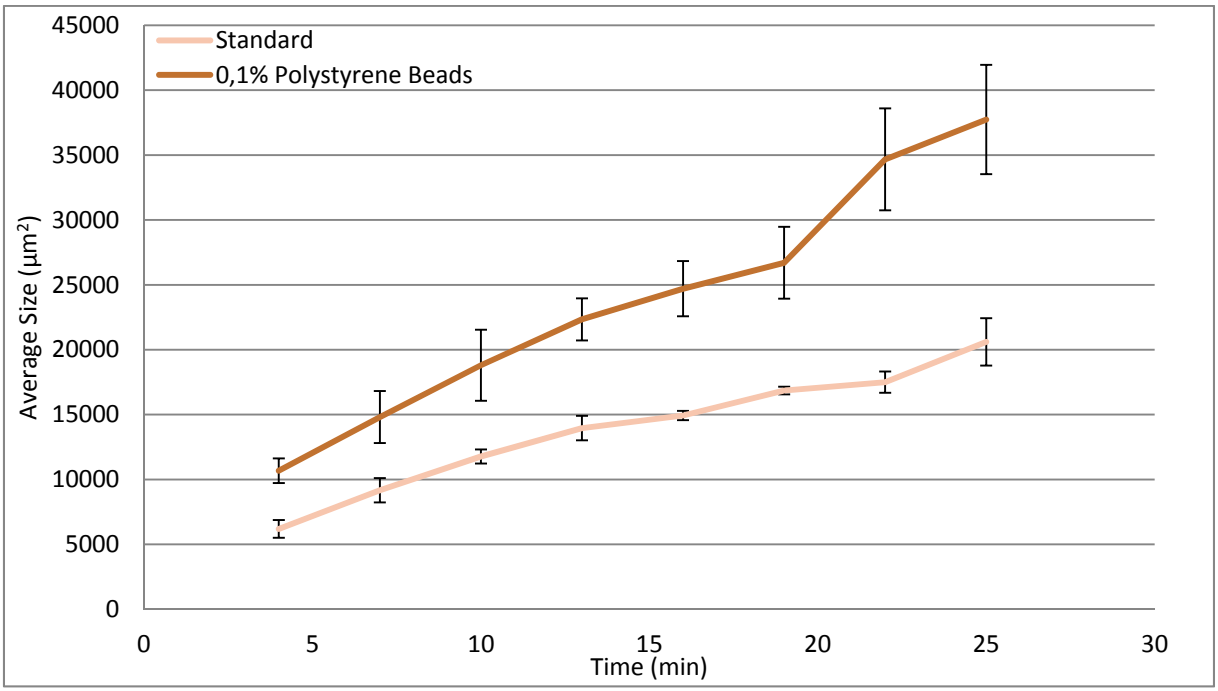

Figure 18. *Growth of average bubble area with time after addition of PS beads (total amount 0.1 % w/w) compared to foam from the coffee standard. Error bars representing standard deviations.*

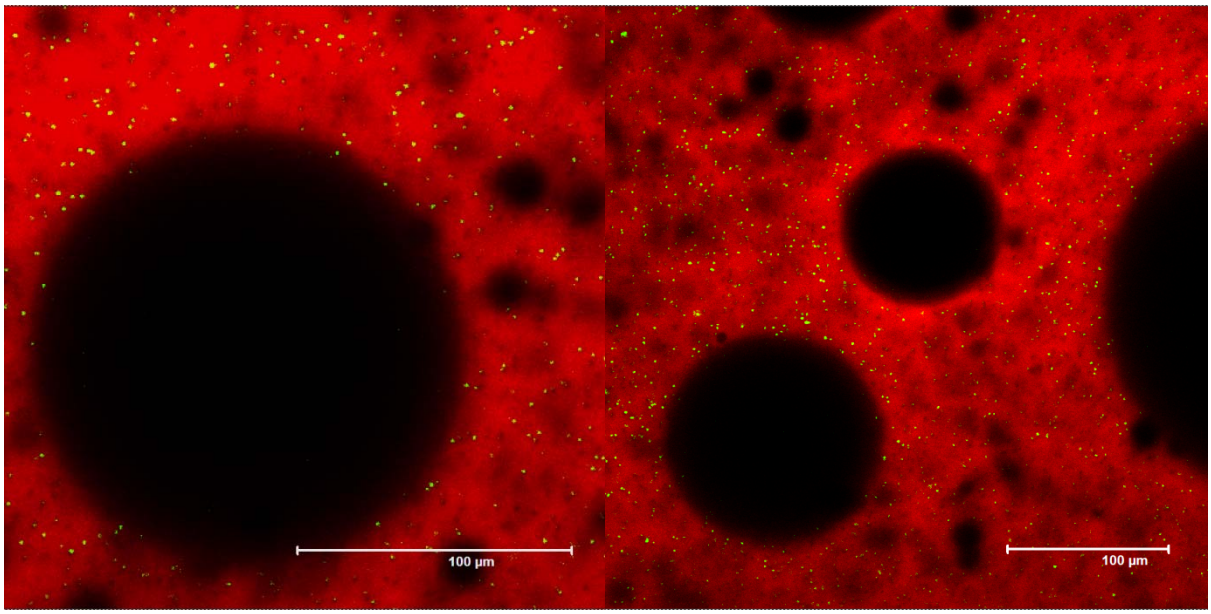

Figure 19. *Foam stained with Texas red (red in the picture) containing the fluorescent PS beads (green in the picture). The beads are distributed throughout the foam, no aggregation at the bubble interface can be observed.*

Table 9. *Growth rates of average bubble area and extrapolated initial average bubble area in coffee foam with PS particles (0.1 % w/w), including standard deviations.*

Concentration of particles (w/w)	Growth of average bubble size (µm²/min)	SD - growth rate	Initial average bubble size (µm²)	SD - initial bubble size
0.0% (Standard)	1890	174	4517	331
0.1 % PS Beads	3746	902	6150	1020

The PS beads heavily destabilized the foam, both the initial and final bubble area was impacted more than by any other of the studied sample treatments. The beads were also shown to distribute throughout the entire liquid phase of the foam despite their hydrophobic nature, as can be seen in *Figure 19*. The initial theory of the beads possibly aggregating in the liquid/air bubble interface and stabilizing the foam as a Pickering emulsion could not be observed.

In reality hydrophobic particles have not only been used to stabilize foams, they are also commonly used as means to control foaming in industrial tanks and reactors, since they have the capability of inducing film-bridging between two bubbles by interacting with the surfaces of both simultaneously. However, this mechanism is dependent on the thickness of the foam lamellae relative to the particles, consequently larger particles have been shown to be more efficient for this purpose, with diameters of 500 µm - 6 mm frequently being reported in literature as being the most effective [56-58]. Although smaller ones, 1-10 µm, have been suggested to be able work like this as well if the foam structure permits its [59]. Though the fact that the PS beads used in this study did not interact with the bubble surfaces at all and that they are smaller than particles typically used for foam destruction purposes points towards the increase in average bubble area and drainage being due to some other mechanism(s).

Because of this, the initial intention of increasing the bead concentration was abandoned; combining the filter operation and particle addition was instead investigated, see *Section 5.1.4* and *5.2.4*.

5.1.4 Combined Effect of Particle Addition and Filtering on Average Bubble Area in Coffee Foam

A theory, possibly related as to why the hydrophobic beads did not migrate to the bubble surfaces, was purposed by Gmoser [4] when discussing how larger particles in coffee in general related to foam rheology. The purposed theory was that the larger particles behave as competing surfaces, absorbing other compounds that would otherwise help to stabilize the foam by collecting on the bubble surfaces, feasibly changing their own solubility in the process. As the PS beads used were carboxylate modified and thus provided binding sites for various compounds this may be applicable in this instance as well. To further investigate this, coffee was first filtered (0.2 µm) before adding particles and foaming, as to remove some of the compounds which would otherwise interact with the beads. Thus possibly freeing up binding sites on the PS beads and preserving their hydrophobicity to a greater extent, possibly also increasing their chance of migrating to the surface of bubbles by also removing compounds interfering through other mechanisms.

Figure 20 below shows results from the average bubble area measurement on the foam with beads added post-filtering. However, results from this sample treatment ended up having very high standard deviations (11-25 %), similar to the 0.45 µm filtration, making comparisons to the other filter and particle addition treatments impossible. Again, no apparent reason for the large error could be identified and due to time constraints no retests were done. The post-filter addition of PS beads did however clearly destabilize the foam compared to the standard. Confocal imaging could also show that the distribution of the beads in the foam was visually unchanged, as can be seen in *Figure 21* below, compare *Figure 20* above.

In conclusion, the PS beads interaction with other particles present in the coffee is most likely part of the reason behind these results. Further tests on these sample treatments are done from the point of view of drainage in *Section 5.2.4* as that was proven to be more time efficient. Adding fully inert hydrophobic particles to the coffee as a comparison might however be interesting for future studies but the relevancy when comparing to particles actually found in coffee is questionable.

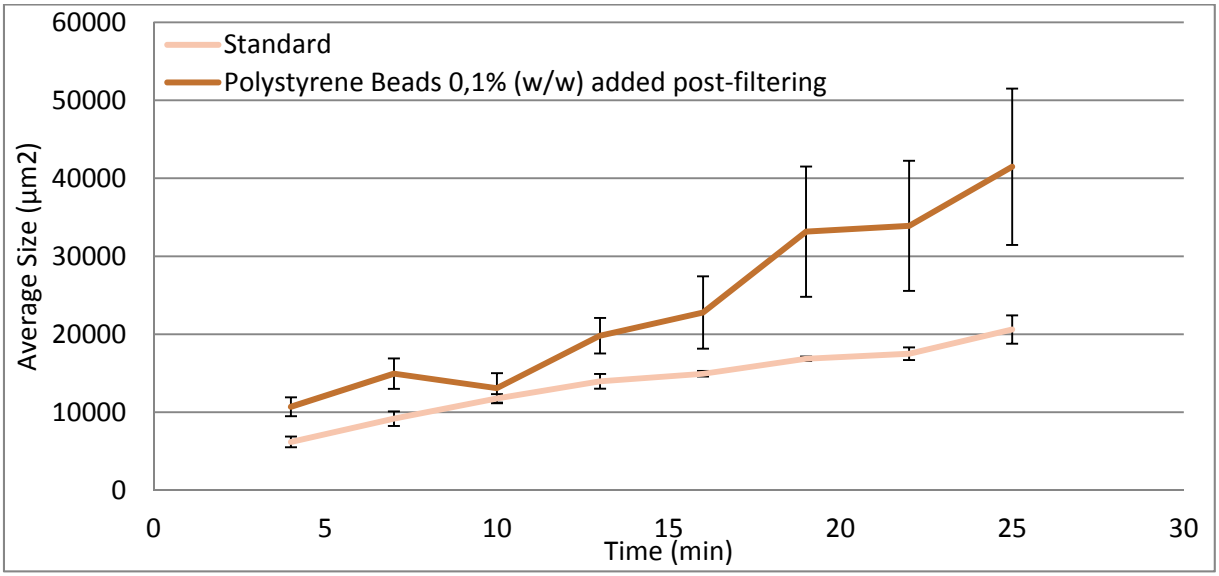

Figure 20. *Growth of average bubble area with time after addition of PS beads (total amount 0.1 % w/w) post-filtering (0.2 µm), compared to foam from the coffee standard. Error bars representing standard deviations.*

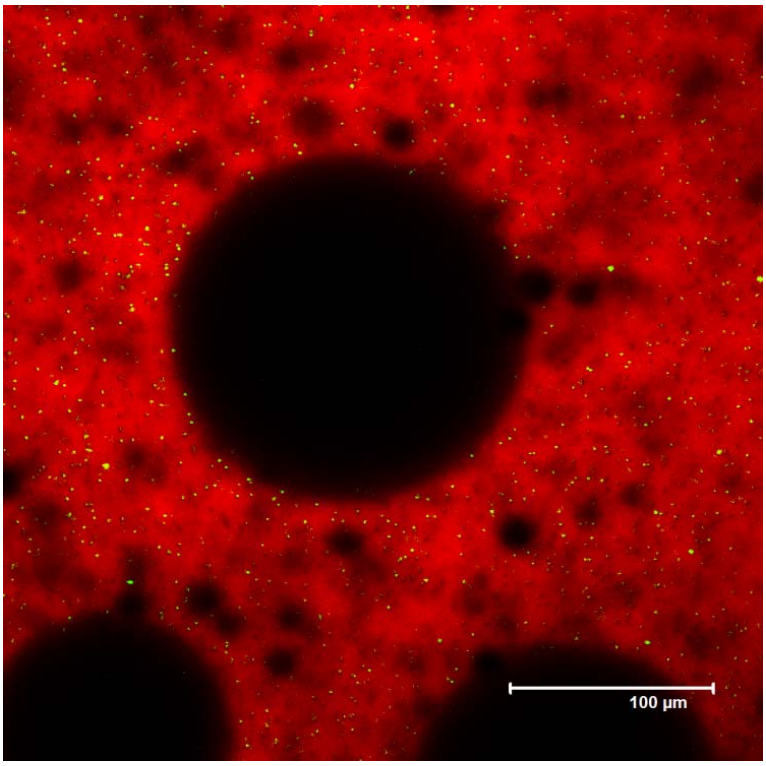

Figure 21. *Foam stained with Texas red (red in the picture) containing the fluorescent PS beads (green in the picture). PS beads (total amount 0.1 % w/w) added post-filtering (0.2 µm). The beads are distributed throughout the foam, no aggregation at the bubble interface can be observed.*

5.1.5 General Growth Functions of Average Bubble Area in Foams Applied to Coffee

The simple relationship for general foam growth in 2D described in literature, $G \sim t^{2/3}$ [22], was shown to be inaccurate when applied to coffee foam as all the average bubble areas in all foams grew linearly in the studied time frame of 0-25 minutes. An initial time-lapse series of 60 min (no replicates) did however point towards the growth rate eventually becoming exponential (data not shown). Exponential growth does nevertheless fit the relationships described in literature even worse. The long term degradation of foam was also not further investigated as it was deemed irrelevant based on actual coffee consumption time, the initially chosen timespan thus remained the focus of the study. Studying coffee foam for longer than 40-50 minutes by the method in question also had the problem of bubble count in the monitored area dropping too low. The average area measurements became considerably impacted by bubbles migrating in and out of the window and the precision consequently decreased. Lowering the magnification at some point during the analysis will probably have to be done to produce adequate data if this is to be studied in the future.

Trying to apply the general formulas for average growth rate of single bubbles in foams publicized in literature, shown in *Section 2.3.2.1*, proved problematic. The formulas are all dependent on number of sides (2D) or faces (3D) a bubble has i.e. the number of bubbles the bubble in question is in contact with. This proved hard to determine as the lamellae in coffee foam appears to be rather thick and bubbles are always at different depth relative to each other. As can be seen in the foam pictures throughout this report there are large areas of liquid in all foams. The difference between a small bubble at a distance or the top of a large bubble close by is e.g. hard to differentiate between.

5.2 Drainage in Coffee Foam

The amount and rate of which liquid drains from a foam heavily impacts its stability, as discussed in *Section 2.3.2.2*, a quickly draining foam will deteriorate faster than a foam capable of retaining more of its initial liquid. To measure drainage, the bottom of a centrifuge tube used for foaming was photographed with a digital microscope over a period of 21 minutes, starting at minute 4 after foaming, capturing 8 images in total. Using the scale on the tube and image analysis software, the amount of drained coffee was measured as a function of time. The impacts of adjusting the pH, filtering the coffee pre-foaming, adding hydrophobic PS beads to the coffee pre-foaming as well as combining particle addition and filtering were analyzed. Raw data from all analyses can be found in *Appendix 3*.

5.2.1 Effect of pH on Drainage in Coffee Foam

Figure 22 below shows volume (ml) of coffee drained over the studied time period for all pH-adjusted samples. As can be seen in the graph, the effect of pH on drainage correlated relatively well to the increase in average bubble size (*Figure 13, Section 5.1.1*) as increased pH values led to destabilization in all foams. Lowering the pH to 4.0 once again resulted in a foam very close to the standard, an increase in initial drainage could however be observed.

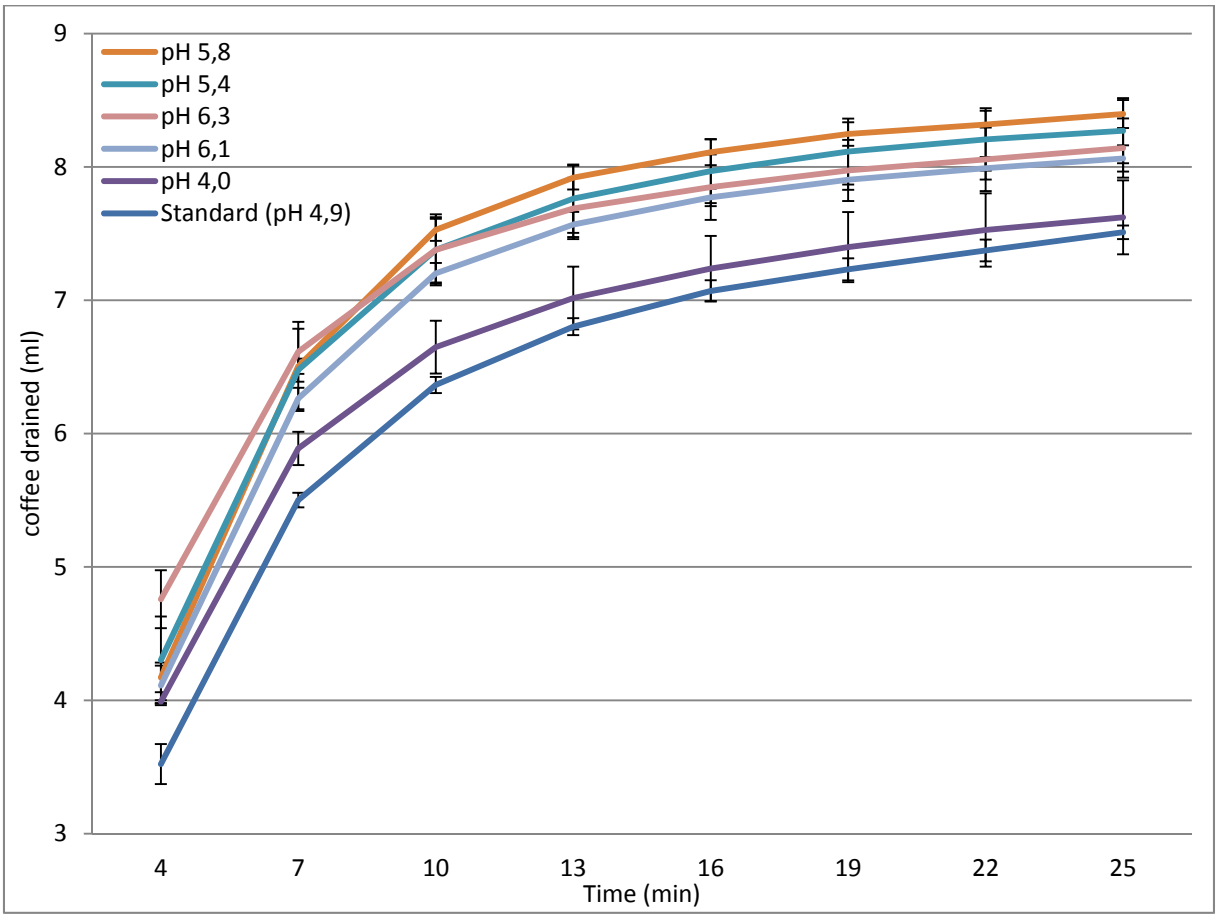

Figure 22. *Liquid (ml) drained from the foam with time (4-25 min) for pH 4.0, 5.4, 5.8, 6.1, 6.3 and the standard coffee (pH 4.9). Error bars representing standard deviations.*

5.2.2 Effect of Filtration on Drainage in Coffee Foam

Figure 23 below shows volume (ml) of coffee drained over the studied time period for coffee filtered through filters with pore sizes of 0.2, 0.45 and 0.8 µm. As oppose to the effect on the growth rate of bubbles, filtration marginally stabilized the foam from the point of view of drainage. However, the differences were rather small and initially not significant when comparing between filters or to the standard. No real correlation between filter pore size and reduced drainage could be observed, possibly pointing towards larger particles, removed by all filters, having the largest effect on the drainage.

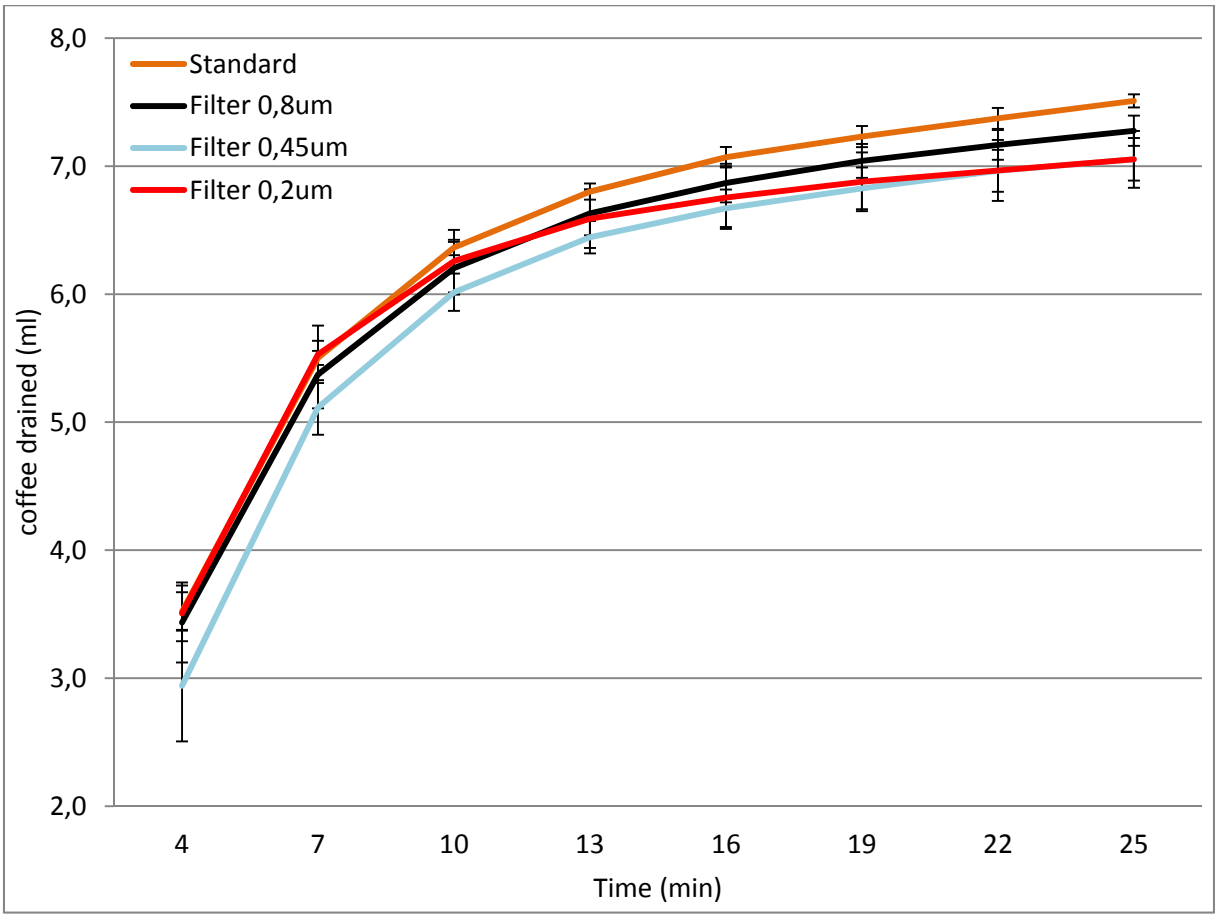

Figure 23. *Liquid (ml) drained from the foam with time after filtration through filters with different pore sizes. Error bars representing standard deviations.*

The tendency of foam from filtered coffees to drain less does also agree with a conclusion by Gmoser [4]. By looking at foamability under aeration i.e. when a stream of air flows out at the bottom of flask of coffee, she observed that foamability was increased and drainage reduced after filtering the coffee. Her hypothesis being that when the foam can only be formed from a single point in the solution, i.e. at the air stream, the rate at which surface active compounds can migrate there impacts the foamability. Thus if large particles, being in the way and behaving as competing surfaces, as previously discussed (*Section 5.1.4*), are removed, smaller surface active particles can migrate to the foaming point faster and increase the amount and stability of foam formed. The fact that foam forms from multiple sites during high-shear mixing might impact the results a bit, but the core principal still stands.

5.2.3 Effect of Adding Hydrophobic Particles on Drainage in Coffee Foam

Figure 24 below shows amount (ml) of coffee drained over the studied time period for foam containing PS beads compared to the standard foam. Adding the PS beads (0.1 % w/w) increased the drainage significantly, volume of drained coffee proved to be were very similar to when pH was adjusted to 5.4 (one of the least drainage resistant foams), see *Figure 22*. As bubble size is one of the two major factors affecting the rate of drainage and bubble size was heavily increased by the addition of the PS beads, the increased drainage correlates well to the CLSM bubble size measurement. It is however not clear if increased drainage lead to larger bubbles or vice versa, the beads affecting both factors simultaneously to some extent is although probably most likely.

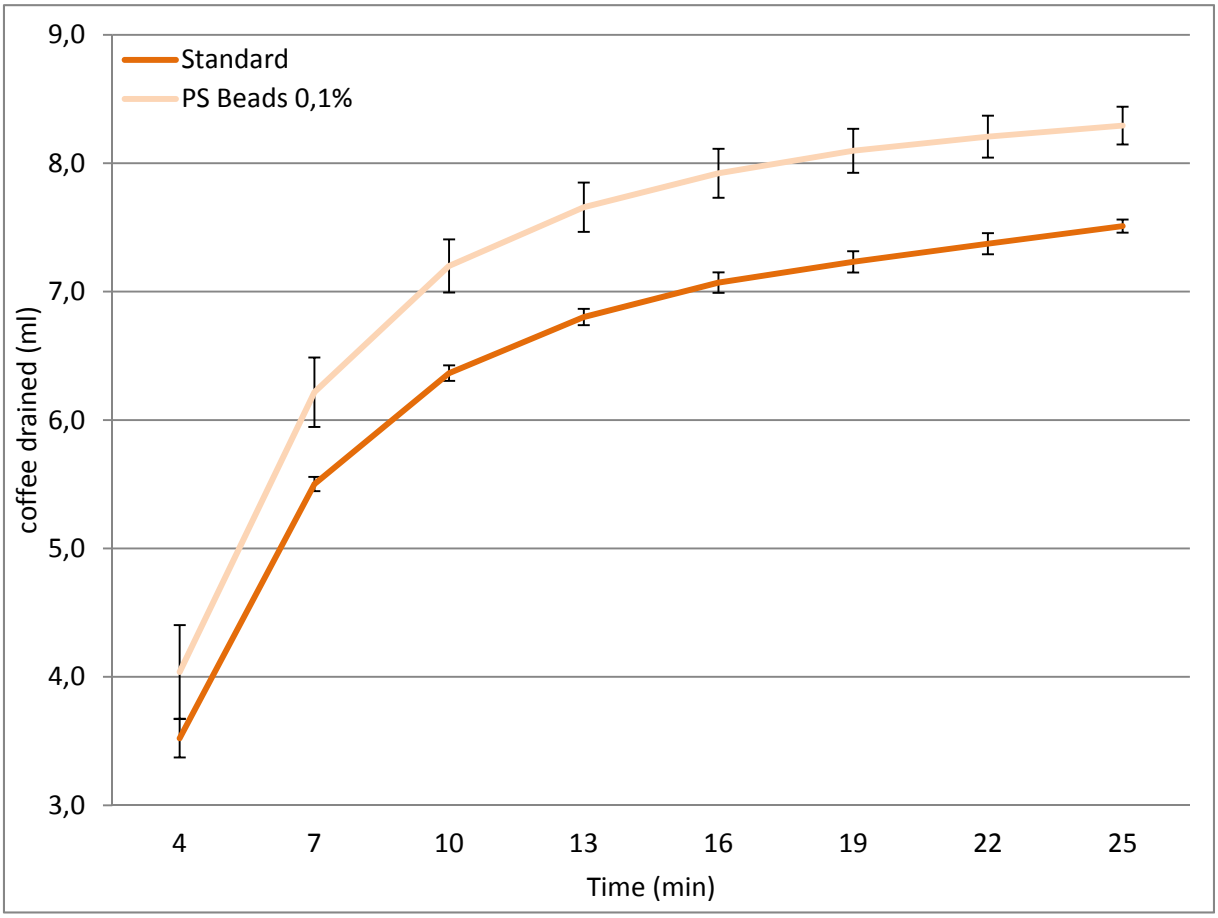

Figure 24. *Liquid (ml) drained from the foam with time after addition of polystyrene beads (0.1% w/w) compared to standard coffee foam. Error bars representing standard deviations.*

5.2.4 Combined Effect of Particle Addition and Filtering on Drainage in Coffee Foam

The theory of particles and beads interacting with each other in the liquid, as discussed in *Section 5.1.4*, was examined from the perspective of drainage as well. Addition of particles both pre- and post-filtering was studied. With the reasoning behind the pre-filter addition being that the beads are allowed to bind to smaller particles and thus removing those when the beads are later filtered away i.e. soaking up and removing small particles pre-foaming. The beads were added to the coffee 45 minutes before filtering (0.20 µm) and were regularly (every 5 minutes) stirred by hand by swirling the flask. *Figure 25* below shows amount (ml) of coffee drained over the studied time period for the foams compared to the standard. *Figure 26* further shows the pre- and post-filtering bead additions compared to only adding beads and only filtering the coffee pre-foaming.

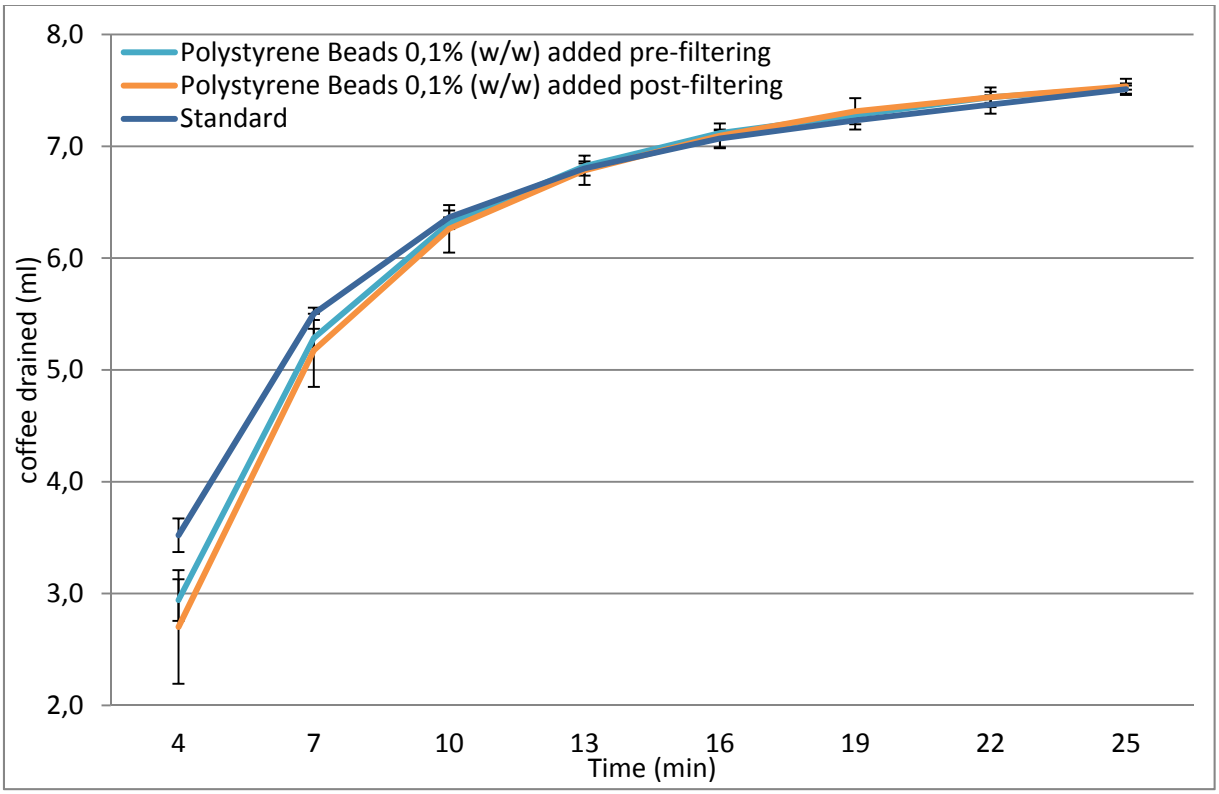

Figure 25. *Liquid (ml) drained from the foam with time after addition of polystyrene beads (0.1 % w/w) before and after filtering (0.20µm) compared to standard coffee foam. Error bars representing standard deviations.*

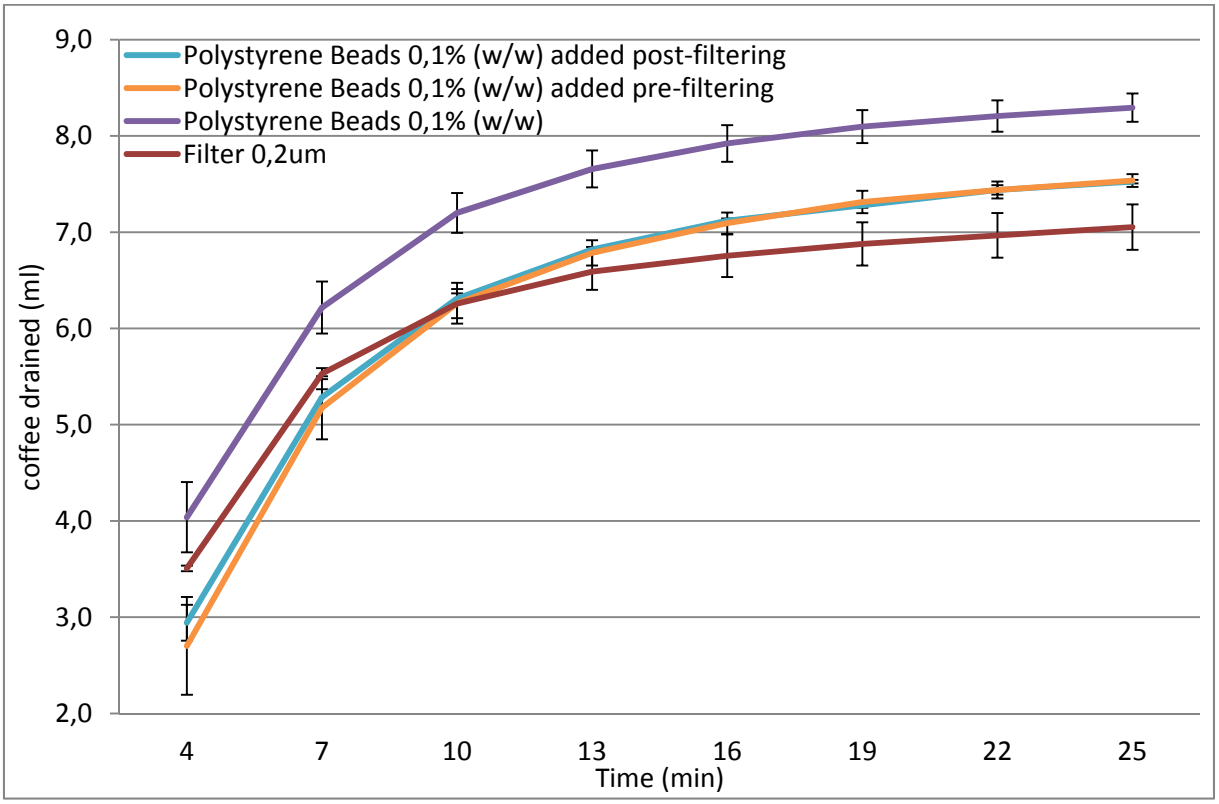

Figure 26. *Liquid (ml) drained from the foam with time after addition of polystyrene beads (0.1 % w/w) before and after filtering (0.20 µm) compared to only adding PS beads and only filtering.*

As can be seen in the graph above (*Figure 25*), both the pre- and post-filtering addition of PS beads resulted in almost identical foams, which also very closely resembled the standard, apart from the initial drainage being slightly reduced.

Comparing the pre- and post-filtering addition of PS beads to just filtering or just adding PS beads (*Figure 26*), a few things can be observed. Since the PS bead addition on its own heavily destabilized the foam while just filtering the coffee stabilized the foam, first filtering and then adding beads essentially working against each other, with the final drained volume ending up in between the two, seems reasonable. However, as the destabilizing effect of only adding beads was significantly greater than the stabilizing effect of only filtering, it stands to reason that there is some interaction between the beads and other compounds in the coffee affecting the properties of the beads, seeing as their destabilizing effect was reduced. Initially (minute 4-10) even stabilizing the foam compared to when the coffee was only filtered.

The same conclusion i.e. that the beads interact with other particles in the coffee, can be drawn from the second experiment as well. As first adding beads and then filtering them away resulted in a different foam compared to just filtering, indicating that compounds affecting the foam stability do interact with the beads and leave the coffee with them.

Also noteworthy is the fact that the pre- and post-filtering addition of beads both resulted in a foam initially more resistant to drainage. A reason for this may be that the foamability is increased, as smaller average initial bubble volumes would help to reduce the drainage especially early on.

5.3 Visual Analysis of CLSM Images and 3D Modeling of Instant Coffee Foam

5.3.1 Visual Analysis of Coffee Foam in 2D

Visual comparisons between images of foams from coffee that had gone through the different sample treatments were performed, the dyes that were chosen in the method development, see *Table 3,* S*ection 3.6*, were all used. *Figure 27* below shows images taken of standard coffee, using combinations of the five dyes: (1) Texas red and Sirius red, (2) Acridine orange and Nile blue and (3) Texas red and BODIPY.

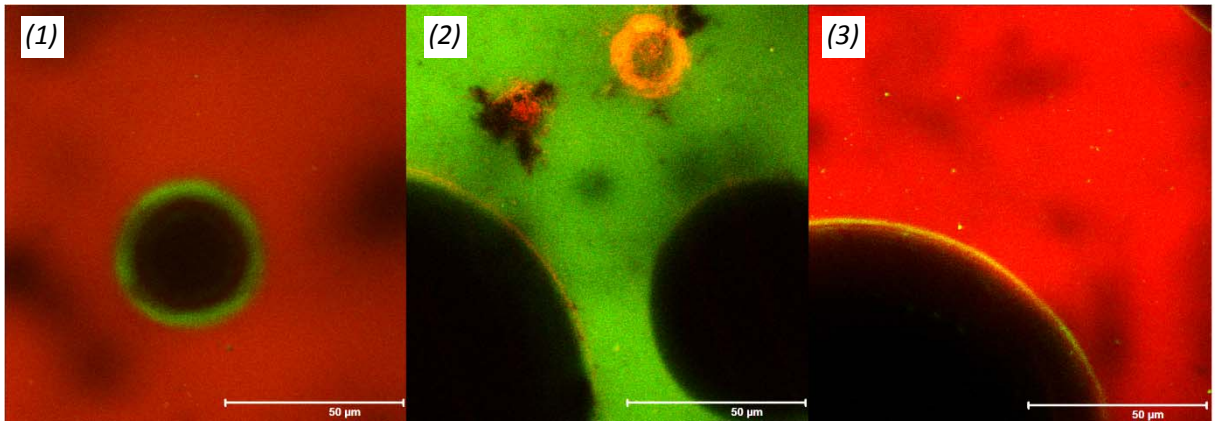

Figure 27. *CLSM images of standard coffee, using combinations of the five dyes determined to be the best for studying the foam. (1) Texas red, appearing as red and Sirius red, appearing as green, (2) Acridine orange, appearing as green and Nile blue, appearing as red and (3) Texas red, appearing as red and BODIPY, appearing as green.*

No differences in overall structure could be noted between the different treatments at a single point in time except for when using quantitative measures such as the bubble area determination. The ability to stain and observe surface active compounds was also visually unaffected by all sample treatments. The fact that the capability of observing these surface active compounds was, as previously described, heavily impacted by instrument setup, the focal plane depth relative to the bubbles in question, diffusion of the dyes etc. made comparisons other than "present in the foam or not" impossible. Lipophilic dyes, Nile blue and BODIPY, as well as Sirius red, with affinity for protein, could stain the compounds aggregating on the bubble surfaces i.e. the surface active compound, confirming that both proteins and lipids are present.

As previously stated, confocal imaging confirms that hydrophilic particles with at least partly lipid-like properties are present in the foam, as they can be stained by BODIPY, see the small green specks in the liquid phase in *Figure 27 (3)* above. Particles being stained by Acridine orange, possibly being the same ones, are also present. Time-lapse imagining confirms that these particles are moving freely in the lamellae with the liquid flow. The flow itself being very irregular and impacted by bubbles growing, shrinking and bursting all throughout the foam, thus no clear direction or velocity of the liquid could be determined.

As previously mentioned, coffee foam does also seem to have relatively thick lamellae, as can be seen in all the images throughout this report, there are areas of the foam with significant amounts of liquid and few bubbles. Data from the image analysis used for average bubble area determination shows the relative area of bubbles in the monitored window to be ~50 % during the entire studied time, in the studied focal plane. This is however a little bit misguiding due to the fact that bubbles not fully inside

the studied windows are ignored and thus counted as liquid, making the actual value slightly higher. But the fact that the average area of bubbles relative to the area of the liquid remains essentially the same from foaming and up to 25 minutes is nonetheless interesting.

5.3.2 Visual Analysis of Coffee Foam in 3D

Figure 28 below shows 6 images of coffee foam modeled in Avizo after stacks (z-axis) of images taken in the CLSM. The small structures appearing almost as pillars sticking out of the foam, seen clearly in the first three images (1-3), are artefacts, resulting from light being blocked by nondissolved dye still on the cover slip. The irregularity and uneven surface of the bubbles, seen very clearly in (3), where some bubbles appear almost as unaligned stacks of round plates, are due to the movement in the foam during the imaging. All image stacks are slightly realigned prior to 3D modeling as a means to compensate for this movement. All images are also edited pre-modeling as to remove the previously discussed reflections appearing in the foam, see *Section 3.5*.

When trying to create a 3D model of coffee foam by means of CLSM two specific problems were encountered, the movement in the foam being the first one. As can be seen in *Figure 28* below, structures could be modeled, but quality was significantly reduced for the sake of speed. Reducing the resolution from 1024x1024 to 512x512, increasing the scan speed from 400 mHz to 800 mHz and increasing the depth to ~10 µm between every image (compare 1-2 µm usually used for more stable samples), resulted in the best models. However, as a bubble is of a very distinct shape and even though motion can be seen as artefacts in the foam, the overall structure can still be observed quite easily due to the fact that every bubble is known to in reality be spherical.

The second problem was simply the depth limitations of the technique, the quality of the images drops as the focal plane is moved further into the foam. The depth limit turned out to be somewhere between 100-150 µm for the acquisition of reasonably good images, dependent on dye and time given for diffusion. As can be seen in *Figure 28*, this meant that essentially only one "layer" of bubbles could be modeled. Instantly starting to capture an image stack while the bubbles were still small meant that the dye had not had the chance to diffuse to its optimal depth, waiting for diffusion meant that the bubbles had time to grow. This made the result almost exactly the same in the end regardless i.e. imaging small bubbles at a reduced depth or larger bubbles at an increased depth.

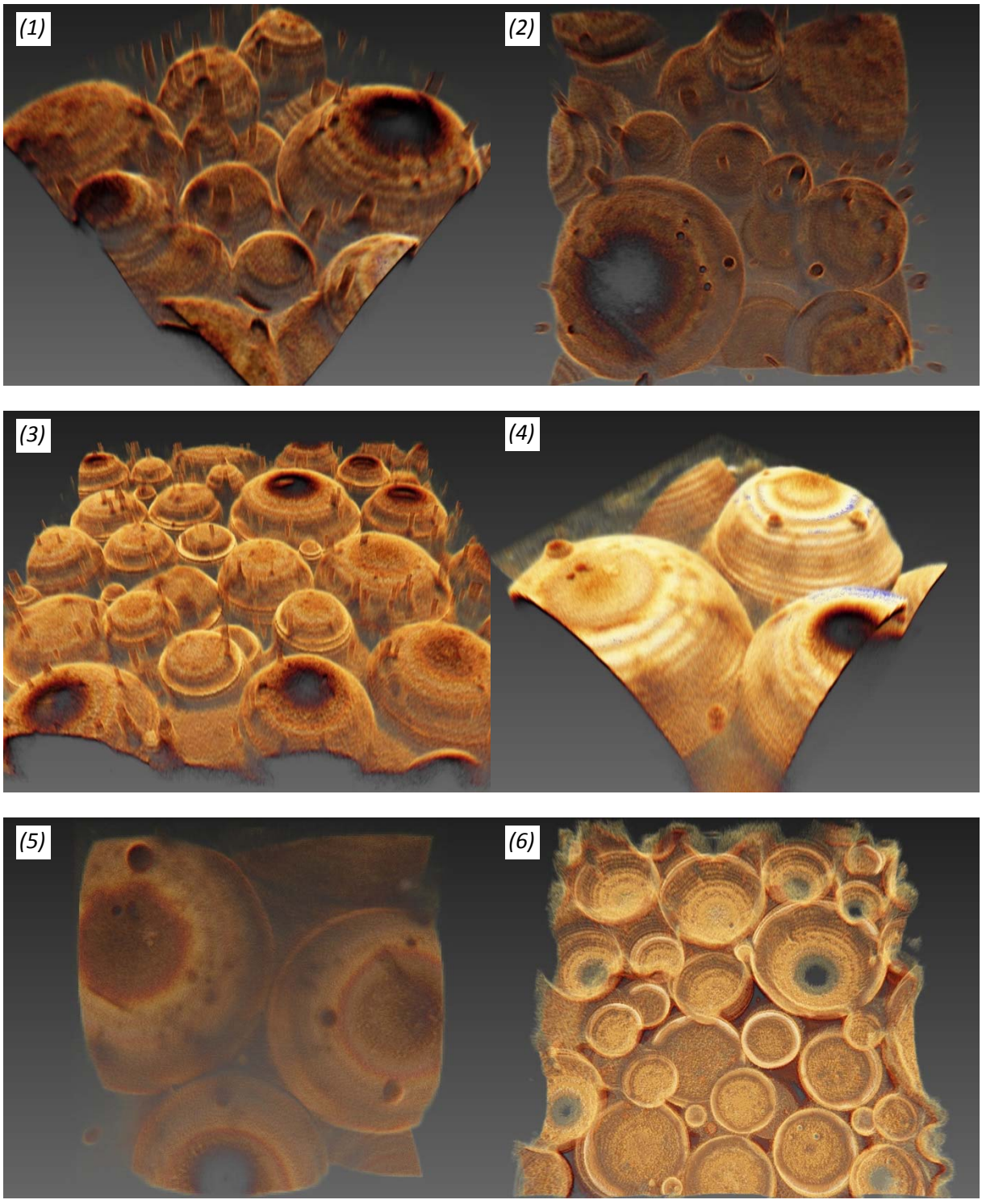

Figure 28. *Coffee foam modeled in Avizo using stacks of CLSM images of standard coffee. (1-5) Foam viewed from the "outside" i.e. convex bubbles. (6) Foam viewed from the "inside" i.e. concave bubbles.*

Conclusions

Confocal laser scanning microscopy and image analysis were powerful tools for measuring the average bubble area as a function of time, observing the distribution and movement of particles in the lamellae and specifically staining and detecting surface active lipids and proteins. Additional advantages involve the small foam volume used (<0.20 ml per run), removing the need for efficient high-volume foam production. Limitations mainly involved the ability to study the foam structure in 3D as the method was negatively impacted by the large differences in refractive index between the air and the foam structure and the dynamic nature of the coffee foam itself. Thus no clear foam model showing multiple bubble layers could be created. In addition no specific dye for carbohydrate staining could be identified.

Drainage could be easily and accurately measured using the developed USB-microscope and image analysis method.

Growth rate of average bubble area in coffee foam was shown to be virtually linear for at least the first 25 minutes, as oppose to what was described in literature for dynamic liquid foams in general, where growth was described as logarithmic. Extrapolating the growth of average bubble area to minute zero as a measure of foamability proved viable.

Higher pH values of 6.1-6.3, compared to pH 4.9 of the standard, increased the foamability of coffee. Higher pH values in the 5.4-6.3 range also proved to destabilize the foam over time, increasing both growth rate of average bubble area and drainage. A lower pH of 4.0 showed a slight tendency of stabilizing the foam and increasing foamability.

Filtering the coffee through filters with pore sizes of 0.20, 0.45 and 0.80 μm increased the growth rate of average bubble area but reduced the drainage in the foam. Furthermore, addition of hydrophobic carboxylate-modified polystyrene beads (~1 μm) proved to significantly destabilize the foam, no stabilizing Pickering effect could be induced. Combinations of filtering and particle addition confirmed that particle interaction in the coffee is a significant parameter for foamability and stability. The results indicates that particles binding to each other both affects the properties of the particle aggregates themselves as well as reduces the amount of particles available for aggregation on, and stabilization of, the foam bubbles.

Coffee foam was shown to have fairly thick lamellae in relation to the size of its bubbles and thus contain a relatively large amount of liquid, making application of known growth formulas of foam bubbles in 2D hard to apply.

Future Work

Isoelectric focusing of coffee constituents in immobilized pH gradient gels to identify possible maxima of foamability could perhaps be done. Previous articles have focused on the proteins from unroasted, unfermented coffee beans i.e. green coffee beans. Not only focusing on proteins, but focusing on all particles with isoelectric points found in ready coffee would give the most relevant data. By identifying peaks of isoelectric points and taking the destabilization of foams over time by increased pH into account, optimizing the foam properties over a certain time period could possibly be done.

The addition of hydrophobic particles to create stable Pickering foams can be further studied as the beads used in this study proved unable to aggregate in the bubble interface. Fully inert beads, beads of different sizes and polarities as well as particles actually able to be used as additives in coffee, perhaps made from discarded parts of the coffee bean itself, could all be examined. Fluorescently labeled particles would however probably be able to provide the best data as their migration to the bubble interfaces could be followed by CLSM while the growth of the average bubble area is simultaneously monitored.

To additionally examine the particles present in the coffee, low vacuum scanning electron microscopy (SEM) could possibly be employed as it allows for greater magnification. Drying the coffee will however probably have to be done to fix the particles as looking at them in solution involves numerous problems. Using filters of different sizes as cutoffs and looking both at material caught in the filter and found in the filtrate might be able to provide good data of the sizes, shapes and relative distributions.

Evaporation is another potentially very relevant factor that is not very well studied. Further developing the described method for drainage measurements to take evaporation into account by e.g. performing the analysis on a scale and thus weighing the evaporated liquid might provide relevant data. Testing the same sample treatments as those used in this study as well as different temperatures, both of the coffee and the surrounding environment could perhaps be done to evaluate how the cooling rate affects the foam and what impact the evaporation has relative to the drainage. Using various containers as to evaluate the impact of the foam surface should probably also be done as that is most definitely heavily impacting evaporation.

As the developed CLSM method only requires small foam samples, different foaming processes can more easily be studied. Even naturally formed coffee foam could probably be sampled straight from the surface of a cup of coffee. Thus allowing for further tuning of the standardized coffee foam creation process as to produce foam identical to what is naturally created on the specific type of coffee in question.

References

1. Solange I. Muatto, E.M.S.M., Silvia Martins, José A. Teixeira, *Production, Composition, and Application of Coffee and its Industrial Residues.* Food Bioprocess Technology, 2011. **4**: p. 661-672.

2. D. Barron, N.P., W. Matthey-Doret, S. Ali, J. Sudre, J. C. Germain, E. Kolodziejczyk, P. Pollien, D. Labbe, C. Jarisch, V. Dugas, C. Hartmanna, B. Folmerb, *Impact of crema on the aroma release and the in-mouth sensory perception of espresso coffee.* Food & Function, 2012. **3**: p. 923-930.

3. International, E. *Instant Coffee: Veratility and Convenience Drive Growth*. 2014 [cited 2015 22-01]; Available from: http://blog.euromonitor.com/2014/07/instant-coffee-versatility-and-convenience-drive-growth.html.

4. Gmoser, R., *Instant coffee foam stability: Bulk and surface rheology approach*, in *Division of Food Technology, Engineering and Nutrition*. 2014, Lund University. MSc Thesis.

5. Romain Briandet, E.K.K., Reginald H. Wilson, *Discrimination of Arabica and Robusta in Instant Coffee by Fourier Transform Infrared Spectroscopy and Chemometrics.* J. Agric. Food Chem, 1996. **44**: p. 170-174.

6. K. Fujioka, T.S., *Chlorogenic acid and caffeine contents in various commercial brewed coffee.* Food Chemitry, 2008. **106**: p. 217-221.

7. Luciano Navarinia, M.F., Furio Suggi Liverani, Libero Liggierib, Francesca Raverab, *Dynamic tensiometric characterization of espresso coffee beverage.* Food Hydrocolloids, 2004. **18**: p. 387-393.

8. Economist, T. *Brewed awakening - Plenty of coffee, too few drinkers*. 2013 [cited 2015 01-28]; Available from: http://www.economist.com/news/finance-and-economics/21581727-plenty-coffee-too-few-drinkers-brewed-awakening.

9. Ernesto Illy, L.N., *Neglected Food Bubbles: The Espresso Coffee Foam.* Food Biophysics, 2011. **6**: p. 335-348.

10. Farah, A., *Coffee: Emerging Health Effects and Disease Prevention,*. First ed, ed. Y.-F. Chu. 2012: John Wiley & Sons, Inc. Blackwell Publishing Ltd.

11. Phillipe Montavon, E.D., GILBERT RUMO, GUDRUN PRATZ, *Evolution of Green Coffee Protein Profiles with Maturation and Relationship to Coffee Cup Quality.* Journal of agricultural and food chemistry, 2003. **51**: p. 2328-2334.

12. Fernando M. Nunes, M.A.C., Armando C. Duarte, Ivonne Delgadillo, *Foamability, Foam Stability, and Chemical Composition of Espresso Coffee As Affected by the Degree of Roast.* J. Agric. Food Chem, 1997. **45**: p. 3238-3243.

13. Hall, L. *Instant Coffee*. How Products are Made 2006 [cited 2015 01-30]; Volume 3:[Available from: http://www.madehow.com/Volume-3/Instant-Coffee.html.

14. P. Capeka, M.M., L. Navarinib, F. Suggi-Liveranib, *Molecular heterogeneity of arabinogalactan-protein from Coffea arabica instant coffee.* International Journal of Biological Macromolecules, 2013. **59**: p. 402-407.

15. Susanne Dold, C.L., Eric Kolodziejczyk, Philippe Pollien, Santo Ali, Juan Carlos Germain, Sonia Garcia Perin, Nicolas Pineau, Britta Folmer, Karl-Heinz Engel, Denis Barron, Christoph Hartmann, *Influence of Foam Structure on the Release Kinetics of Volatiles from Espresso Coffee Prior to Consumption.* journal of agricultural and food chemistry 2011. **59**: p. 11196-111203.

16. Fernando M. Nunes, M.A.C., *Influence of polysaccharide composition in foam stability of espresso coffee.* Carbohydrate Polymers, 1998. **37**: p. 283-285.

17. L. Piazza, J.G., A. Bulbarello, *Interfacial rheology study of espresso coffee foam structure and properties.* Journal of Food Engineering, 2008. **84**: p. 420-429.

18. Macrae R, C.R.J., *Nitrogenous components In Coffee: Vol. 1, Chemistry*, E.E.A. Science, Editor. 1985: London. p. 115-152.

19. Ali J. Green, K.A.L., Paul Hooley, Philip W. Cox, *Formation and stability of food foams and aerated emulsions: Hydrophobins as novel functional ingredients.* Current Opinion in Colloid & Interface Science, 2013. **18**: p. 292-301.

20. Wilde P. J, H.F.A., COOPER D, RIDOUT M. J, MULLER R. E, MILLS E. N. C., *Destabilization of beer foam by lipids: Structural and interfacial effects.* Journal of the American Society of Brewing Chemists, 2003. **61**: p. 196-202.

21. Sabrina Rami-shojaei, C.V., Christophe Schmitt, *Automatic analysis of 2D foam sequences: Application to the characterization of aqueous proteins foams stability.* Image and Vision Computing 2009. **27**: p. 609-622.

22. Ji San Lee, B.M.W., Jung Ho Je, *X-ray phase-contrast imaging of dynamics of complex fluids.* JOURNAL OF PHYSICS D: APPLIED PHYSICS, 2013. **46**.

23. Krzan, M., *RHEOLOGY OF THE WET SURFACTANT FOAMS AND BIOFOMAS – A REVIEW*. 2013, Haber Institute of Catalysis and Surface Chemistry: Polish Academy of Science.

24. Lambert, J., et al., *Experimental Growth Law for Bubbles in a Moderately ``Wet'' 3D Liquid Foam.* Physical Review Letters, 2007. **99**(5): p. 058304.

25. Robert D. MacPherson, D.J.S., *The von Neumann relation generalized to coarsening of three-dimensional microstructures.* nature, 2007. **446**: p. 1053-1055.

26. S. SAUERBREI, E.C.H., P. J. PLATH, *THE APOLLONIAN DECAY OF BEER FOAM BUBBLE SIZE DISTRIBUTION AND THE LATTICES OF YOUNG DIAGRAMS AND THEIR CORRELATED MIXING FUNCTIONS.* Discrete Dynamics in Nature and Society, 2005. **2006**: p. 1-35.

27. Xin Yang, E.A.F., *The stability and physical properties of egg white and whey protein foams explained based on microstructure and interfacial properties.* Food Hydrocolloids, 2011. **25**: p. 1687-1701.

28. NASA. *Wet Foam and Drainage*. 2007 [cited 2015 02-26]; Available from: http://www.esa.int/spaceinimages/Images/2007/11/Wet_Foam_and_Drainage.

29. Sascha Hilgenfeldt, S.A.K., Howard A. Stone, *Dynamics of Coarsening Foams: Accelerated and Self-Limiting Drainage.* Physical Review Letters, 2001. **86**: p. 4704-4707.

30. Nikolai D. Denkov, K.G.M., *Antifoam effects of solid particles, oil drops and oil-solid compounds in aqueous foams*. Colloidal Particles at Liquid interfaces, ed. E. B.P. Binks & T.S. Horozov. 2006, Cambridge University Press, Cambridge, UK.

31. Abbott, P.S. *Foam Drainage*. 2014 [cited 2015 02-17]; Available from: http://www.stevenabbott.co.uk/PracticalSurfactants/FoamDrainage.html.

32. Plateau, J., *STATIQUE EXPÉRIMENTALE ET THÉORIQUE DES LIQUIDES SOUMIS AUX SEULES FORCES MOLÉCULAIRES,*. Vol. 1. 1873, PARIS, LONDON: GAUTHIER-VILLARS, TRÜBNER and Co, English translation°c 2005 Kenneth A. Brakke

33. Hartmut A. Wege, S.K., Vesselin N. Paunov, Qixin Zhong, Orlin D. Velev, *Long-Term Stabilization of Foams and Emulsions with In-Situ Formed Microparticles from Hydrophobic Cellulose.* Langmuir, 2008. **24**: p. 9245-9253.

34. Urs T. Gonzenbach, A.R.S., Elena Tervoort, Ludwig J. Gauckler, *Ultrastable Particle-Stabilized Foams.* Angew. Chem. Int. Ed., 2006. **45**: p. 3526-3530.

35. Paddock, S.W., *Confocal Laser Scanning Microscopy.* BioTechniques, 1999. **27**(5): p. 992-1004.

36. Hoyt, C., *Liquid crystal tunable filters clear the way for imaging multiprobe fluorescence.* Biophotonics International 1996. **July/August**.

37. Z. DARiYNKIEWICZ, F.T., T. SHARPLESS, M. R. MELAMED, *CONFORMATION OF RNA IN SITU AS STUDIED BY ACRIDINE ORANGE STAINING AND AUTOMATED CYTOFLUOROMETRY.* Experimental Cell Research, 1975. **95**: p. 143-153.

38. McMaster, G.K. and G.G. Carmichael, *Analysis of single- and double-stranded nucleic acids on polyacrylamide and agarose gels by using glyoxal and acridine orange.* Proceedings of the National Academy of Sciences, 1977. **74**(11): p. 4835-4838.

39. Ichimura, S., et al., *The nature of strong binding between acridine orange and deoxyribonucleic acid as revealed by equilibrium dialysis and thermal renaturation.* Biochimica et Biophysica Acta (BBA) - Nucleic Acids and Protein Synthesis, 1969. **190**(1): p. 116-125.

40. Diboll, A.G., *Histochemistry and Fine Structure of the Pollen Tube Residue in the Megagametophyte of Zea Mays.* Caryologia, 1968. **21**(1): p. 91-95.

41. G. S. JOHAR, U.-I.A., H. S. SODHI, *New methods for the detection of carboxylic acid groups in organic compounds, with acriflavine.* Talanta, 1971. **18**: p. 1051-1055.

42. Martin Goetz, M.V., Stephan Kanzler, Peter R. Galle, Peter Delaney, Markus F. Neurath, Ralf Kiesslich, *In vivo confocal laser laparoscopy allows real time subsurface microscopy in animal models of liver disease.* Journal of Hepatology, 2008. **48**: p. 91-97.

43. Ralf Kiesslich, M.G., Michael Vieth, Peter R. Galle, Markus F. Neurath, *Confocal Laser Endomicroscopy.* Gastrointest Endoscopy Clin N Am, 2005. **15**: p. 715-731.

44. S. El Hallani, C.F.P., C.E. Macaulay, M. Follen, M. Guillaud, P. Lane, *Ex vivo confocal imaging with contrast agents for the detection of oral potentially malignant lesions.* Oral Oncology, 2013. **49**: p. 582-590.

45. Fred van de Velde, F.W., , Marijke W. Edelman, Erik van der Linden, R. Hans Tromp *Visualisation of biopolymer mixtures using confocal scanning laser microscopy (CSLM) and covalent labelling techniques.* Colloids and Surfaces B: Biointerfaces, 2003. **31**: p. 159-168.

46. Jenna Lamb, T.L., *Seeing red: the use of Congo Red dye to identify cooked and damaged starch grains in archaeological residues.* Journal of Archaeological Science, 2005. **32**: p. 1433-1440.

47. Fred van de Velde, J.v.R., R Hans Tromp, *Visualisation of starch granule morphologies using confocal scanning laser microscopy (CSLM).* Journal of the Science of Food and Agriculture, 2002. **82**: p. 1528-1536.

48. J. C. G. Blonk, H.v.A., *Confbcal scanning light microscopy in food research.* Food Research International, 1993. **26**: p. 297-311.

49. Tajalli, H., et al., *The photophysical properties of Nile red and Nile blue in ordered anisotropic media.* Dyes and Pigments, 2008. **78**(1): p. 15-24.

50. Vesselinovitch, D. and K. Fischer-Dzoga, *Techniques in Pathology in Atherosclerosis Research1*, in *Advances in Lipid Research*, P. Rodolfo and K. David, Editors. 1981, Elsevier. p. 1-63.

51. Sandy Schuster, R., Gisela Guthausen, Jascha Zapp, Alexandra M.Greiner, and H.P.S. Karsten Köhler, *Analysis of W1/O/W2 double emulsions with CLSM: Statisticalimage processing for droplet size distribution.* Chemical Engineering Science, 2012. **81**: p. 84-90.

52. Piérard, G.E., *Sirius Red Polarization Method is Useful to Visualize the Organization of Connective Tissues but not the Molecular Composition of their Fibrous Polymers.* Matrix, 1989. **9**(1): p. 68-71.

53. Junqueira, L.C.U., G. Bignolas, and R.R. Brentani, *A simple and sensitive method for the quantitative estimation of collagen.* Analytical Biochemistry, 1979. **94**(1): p. 96-99.

54. Titus, J.A., et al., *Texas red, a hydrophilic, red-emitting flourophore for use with flourescein in dual parameter flow microfluorometric and fluorescence microscopic studies.* Journal of Immunological Methods, 1982. **50**(2): p. 193-204.

55. Technologies, L. *Texas Red® (and Texas Red®-X) Dye*. 2015 [cited 2015 03-02]; Available from: http://www.lifetechnologies.com/se/en/home/life-science/cell-analysis/fluorophores/texas-red.html.

56. E. R. Armstrong, C.G.J.B., M. A. Bergougnou, *Effects of Solids Wettability on the Characteristics of Three-phase Fluidization.* Fluidization Technology, 1976. **127**: p. 405.

57. Tsutsumi A, A.G.D., L. Fan, *Characteristics of Gas-Liquid-Solid Fluidization with Nonwettable Particles.* AIChE Journal, 1991. **37**(6): p. 951-952.

58. Clara Mata, D.D.J., *Foam Control using a Fluidized Bed of Hydrophobic Particles*. 1997: University of Minnesota AEM, 107 Akerman Hall, 110 Union Street Minneapolis, MN 55455.

59. Robert Aveyard, P.C., Paul D. I. Fletcher, Christine E. Rutherford, *Foam Breakdown by Hydrophobic Particles and Nonpolar Oil.* Langmuir, 1993. **9**: p. 604-613.

Appendix 1

Lambda scans of unstained coffee foam using five different wave lengths, emitted light picked up from the excitation wavelength and up to 700nm.

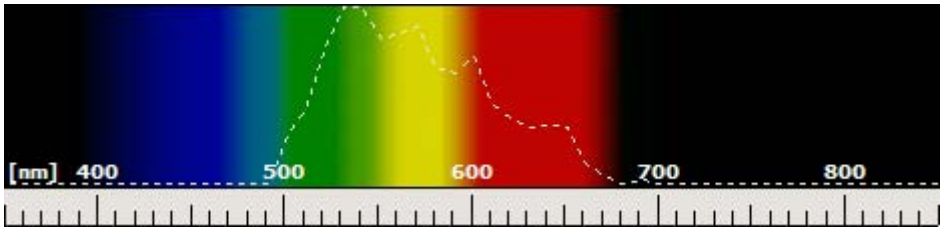

Figure 1. *488nm excitation*

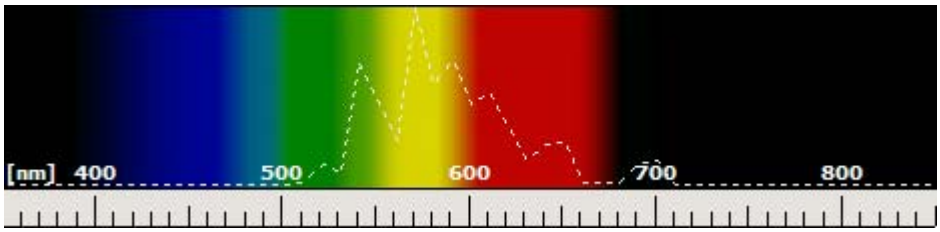

Figure 2. *496nm excitation*

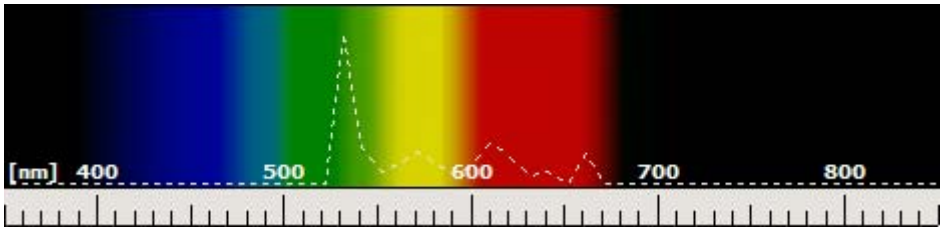

Figure 3. *514 nm excitation*

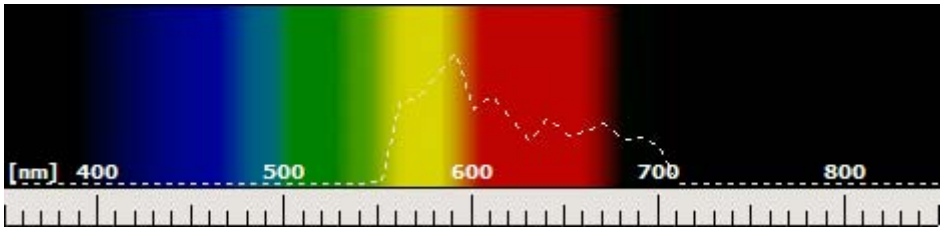

Figure 4. *543 nm excitation*

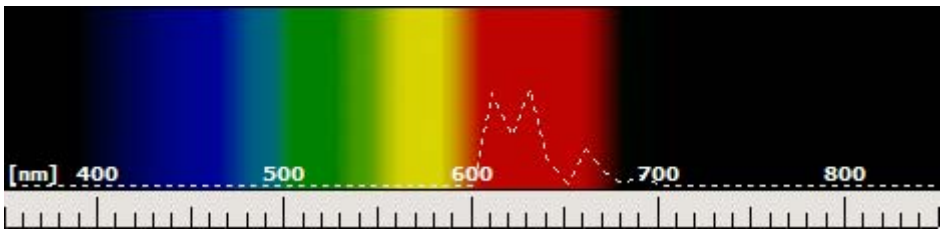

Figure 5. *594 nm excitation*

Appendix 2

Table 1. *Raw data, SD and RSD% from the time-lapse measurements of average bubble size.*

Standard								
Replicate	**Minute**	**Sample**	**Count**	**Total Area**	**Avg.Size**	**SD Avg.Size**	**RSD% Avg.Size**	**%Area**
1	4	1.1	220,00	1251142,58	5687,01	-	-	56,55
	7	1.2	136,00	1209270,02	8891,69	-	-	54,65
	10	1.3	106,00	1173225,10	11068,16	-	-	53,02
	13	1.4	80,00	1136528,32	14206,60	-	-	51,37
	16	1.5	70,00	1064770,50	15211,01	-	-	48,12
	19	1.6	70,00	1151743,16	16453,47	-	-	52,05
	22	1.7	63,00	1173894,04	18633,24	-	-	53,05
	25	1.8	63,00	1187985,84	18856,92	-	-	53,69
2	4	2.1	149,00	1066804,20	7159,76	-	-	48,21
	7	2.2	79,00	824174,81	10432,59	-	-	37,25
	10	2.3	66,00	817043,46	12379,45	-	-	36,93
	13	2.4	68,00	1018256,84	14974,37	-	-	46,02
	16	2.5	64,00	970773,93	15168,34	-	-	43,87
	19	2.6	59,00	1012395,02	17159,24	-	-	45,76
	22	2.7	57,00	977111,81	17142,31	-	-	44,16
	25	2.8	48,00	982070,31	20459,80	-	-	44,38
3	4	3.1	227,00	1300576,17	5729,41	-	-	58,78
	7	3.2	152,00	1246452,64	8200,35	-	-	56,33
	10	3.3	105,00	1247192,38	11878,02	-	-	56,37
	13	3.4	95,00	1206838,38	12703,56	-	-	54,54
	16	3.5	83,00	1197480,47	14427,48	-	-	54,12
	19	3.6	73,00	1237978,51	16958,61	-	-	55,95
	22	3.7	68,00	1137863,77	16733,29	-	-	51,43
	25	3.8	56,00	1259665,52	22494,03	-	-	56,93
AVG	4	AVG 1	198,67	1206174,32	6192,06	**684,49**	**11,05%**	54,51
	7	AVG 2	122,33	1093299,15	9174,88	**933,05**	**10,17%**	49,41
	10	AVG 3	92,33	1079153,65	11775,21	**540,24**	**4,59%**	48,77
	13	AVG 4	81,00	1120541,18	13961,51	**943,11**	**6,76%**	50,64
	16	AVG 5	72,33	1077674,97	14935,61	**359,73**	**2,41%**	48,71
	19	AVG 6	67,33	1134038,90	16857,11	**296,93**	**1,76%**	51,25
	22	AVG 7	62,67	1096289,88	17502,95	**816,49**	**4,66%**	49,55
	25	AVG 8	55,67	1143240,56	20603,58	**1822,81**	**8,85%**	51,67

pH 4,0								
Replicate	**Minute**	**Sample**	**Count**	**Total Area**	**Avg.Size**	**SD Avg.Size**	**RSD% Avg.Size**	**%Area**
1	4	1.1	193,00	1063659,67	5511,19	-	-	48,07
	7	1.2	160,00	1113354,49	6958,47	-	-	50,32
	10	1.3	136,00	1165334,47	8568,64	-	-	52,67
	13	1.4	103,00	1160161,13	11263,70	-	-	52,43
	16	1.5	90,00	1120388,18	12448,76	-	-	50,64
	19	1.6	76,00	1191379,40	15676,05	-	-	53,84
	22	1.7	76,00	1150375,98	15136,53	-	-	51,99
	25	1.8	80,00	1156325,68	14454,07	-	-	52,26
2	4	2.1	170,00	1122500,00	6602,94	-	-	50,73
	7	2.2	127,00	1116318,36	8789,91	-	-	50,45
	10	2.3	116,00	1235510,25	10650,95	-	-	55,84
	13	2.4	97,00	1221914,06	12597,05	-	-	55,22
	16	2.5	88,00	1290329,59	14662,84	-	-	58,32
	19	2.6	80,00	1368022,46	17100,28	-	-	61,83
	22	2.7	68,00	1340830,08	19718,09	-	-	60,60
	25	2.8	67,00	1333532,71	19903,47	-	-	60,27
3	4	3.1	207,00	1231394,04	5948,76	-	-	55,65
	7	3.2	138,00	1146838,38	8310,42	-	-	51,83
	10	3.3	119,00	1164882,81	9788,93	-	-	52,65
	13	3.4	90,00	1082363,28	12026,26	-	-	48,92
	16	3.5	85,00	1240202,64	14590,62	-	-	56,05
	19	3.6	68,00	1098869,63	16159,85	-	-	49,66
	22	3.7	61,00	1003051,76	16443,47	-	-	45,33
	25	3.8	59,00	1019370,12	17277,46	-	-	46,07
AVG	4	AVG 1	190,00	1139184,57	6020,96	**448,62**	**7,45%**	51,49
	7	AVG 2	141,67	1125503,74	8019,60	**775,45**	**9,67%**	50,87
	10	AVG 3	123,67	1188575,85	9669,51	**854,29**	**8,83%**	53,72
	13	AVG 4	96,67	1154812,83	11962,34	**546,21**	**4,57%**	52,19
	16	AVG 5	87,67	1216973,47	13900,74	**1027,13**	**7,39%**	55,00
	19	AVG 6	74,67	1219423,83	16312,06	**591,32**	**3,63%**	55,11
	22	AVG 7	68,33	1164752,60	17099,36	**1927,06**	**11,27%**	52,64
	25	AVG 8	68,67	1169742,84	17211,67	**2225,20**	**12,93%**	52,87

pH 5,4								
Replicate	**Minute**	**Sample**	**Count**	**Total Area**	**Avg.Size**	**SD Avg.Size**	**RSD% Avg.Size**	**%Area**
1	4	1.1	119,00	880148,93	7396,21	-	-	39,78
	7	1.2	89,00	1023835,45	11503,77	-	-	46,27
	10	1.3	81,00	1090229,49	13459,62	-	-	49,27
	13	1.4	69,00	1122658,69	16270,42	-	-	50,74
	16	1.5	55,00	1096997,07	19945,40	-	-	49,58
	19	1.6	42,00	1085195,32	25837,98	-	-	49,05
	22	1.7	45,00	1040961,92	23132,49	-	-	47,05
	25	1.8	37,00	1020317,38	27576,15	-	-	46,11
2	4	2.1	114,00	982080,08	8614,74	-	-	44,39
	7	2.2	62,00	859743,65	13866,83	-	-	38,86
	10	2.3	57,00	945385,74	16585,72	-	-	42,73
	13	2.4	52,00	951882,32	18305,43	-	-	43,02
	16	2.5	46,00	976872,56	21236,36	-	-	44,15
	19	2.6	42,00	1046025,39	24905,37	-	-	47,28
	22	2.7	42,00	1092744,14	26017,72	-	-	49,39
	25	2.8	36,00	1026323,24	28508,98	-	-	46,38
3	4	3.1	120,00	864277,34	7202,31	-	-	39,06
	7	3.2	83,00	858232,42	10340,15	-	-	38,79
	10	3.3	71,00	995778,81	14025,05	-	-	45,00
	13	3.4	54,00	924653,32	17123,21	-	-	41,79
	16	3.5	53,00	1177678,22	22220,34	-	-	53,23
	19	3.6	50,00	1184709,47	23694,19	-	-	53,54
	22	3.7	47,00	1274318,84	27113,17	-	-	57,59
	25	3.8	45,00	1175485,84	26121,91	-	-	53,13
AVG	4	AVG 1	117,67	908835,45	7737,75	**625,15**	**8,08%**	41,07
	7	AVG 2	78,00	913937,17	11903,58	**1467,26**	**12,33%**	41,31
	10	AVG 3	69,67	1010464,68	14690,13	**1360,11**	**9,26%**	45,67
	13	AVG 4	58,33	999731,45	17233,02	**834,41**	**4,84%**	45,18
	16	AVG 5	51,33	1083849,29	21134,04	**931,56**	**4,41%**	48,98
	19	AVG 6	44,67	1105310,06	24812,51	**877,66**	**3,54%**	49,95
	22	AVG 7	44,67	1136008,30	25421,12	**1678,97**	**6,60%**	51,34
	25	AVG 8	39,33	1074042,16	27402,34	**982,24**	**3,58%**	48,54

pH 5,8								
Replicate	**Minute**	**Sample**	**Count**	**Total Area**	**Avg.Size**	**SD Avg.Size**	**RSD% Avg.Size**	**%Area**
1	4	1.1	178,00	1328918,46	7465,83	-	-	60,06
	7	1.2	131,00	1334670,41	10188,32	-	-	60,32
	10	1.3	104,00	1240461,43	11927,51	-	-	56,06
	13	1.4	90,00	1280939,94	14232,67	-	-	57,89
	16	1.5	64,00	1183618,17	18494,03	-	-	53,49
	19	1.6	55,00	1242236,33	22586,12	-	-	56,14
	22	1.7	47,00	1242014,16	26425,83	-	-	56,13
	25	1.8	41,00	1118222,66	27273,72	-	-	50,54
2	4	2.1	159,00	1243803,71	7822,67	-	-	56,21
	7	2.2	112,00	1193923,34	10660,03	-	-	53,96
	10	2.3	91,00	1123557,13	12346,78	-	-	50,78
	13	2.4	78,00	1146586,91	14699,83	-	-	51,82
	16	2.5	69,00	1090305,18	15801,52	-	-	49,28
	19	2.6	57,00	1213664,55	21292,36	-	-	54,85
	22	2.7	42,00	1084670,41	25825,49	-	-	49,02
	25	2.8	41,00	1040107,42	25368,47	-	-	47,01
3	4	3.1	175,00	1281457,52	7322,61	-	-	57,92
	7	3.2	115,00	1213859,86	10555,30	-	-	54,86
	10	3.3	87,00	1199777,83	13790,55	-	-	54,22
	13	3.4	74,00	1169365,23	15802,23	-	-	52,85
	16	3.5	63,00	1129621,58	17930,50	-	-	51,05
	19	3.6	52,00	1029953,61	19806,80	-	-	46,55
	22	3.7	49,00	1152663,58	23523,75	-	-	52,09
	25	3.8	43,00	1198662,12	27875,86	-	-	54,17
AVG	4	AVG 1	170,67	1284726,56	7537,04	**210,26**	**2,79%**	58,06
	7	AVG 2	119,33	1247484,54	10467,89	**202,25**	**1,93%**	56,38
	10	AVG 3	94,00	1187932,13	12688,28	**797,99**	**6,29%**	53,69
	13	AVG 4	80,67	1198964,03	14911,58	**658,03**	**4,41%**	54,19
	16	AVG 5	65,33	1134514,98	17408,69	**1159,49**	**6,66%**	51,27
	19	AVG 6	54,67	1161951,50	21228,43	**1135,55**	**5,35%**	52,51
	22	AVG 7	46,00	1159782,71	25258,36	**1250,80**	**4,95%**	52,42
	25	AVG 8	41,67	1118997,40	26839,35	**1068,72**	**3,98%**	50,57

pH 6,1								
Replicate	**Minute**	**Sample**	**Count**	**Total Area**	**Avg.Size**	**SD Avg.Size**	**RSD% Avg.Size**	**%Area**
1	4	1.1	163,00	1063125,00	6522,24	-	-	48,05
	7	1.2	111,00	1004858,40	9052,78	-	-	45,41
	10	1.3	98,00	1140969,24	11642,54	-	-	51,57
	13	1.4	86,00	1062539,06	12355,11	-	-	48,02
	16	1.5	80,00	1055434,57	13192,93	-	-	47,70
	19	1.6	65,00	1095544,44	16854,53	-	-	49,51
	22	1.7	50,00	986125,48	19722,51	-	-	44,57
	25	1.8	33,00	880544,44	26683,17	-	-	39,80
2	4	2.1	151,00	1168027,34	7735,28	-	-	52,79
	7	2.2	117,00	1196191,40	10223,86	-	-	54,06
	10	2.3	85,00	1137133,79	13378,05	-	-	51,39
	13	2.4	77,00	1190021,97	15454,83	-	-	53,78
	16	2.5	71,00	1166599,12	16430,97	-	-	52,72
	19	2.6	63,00	1136066,89	18032,81	-	-	51,34
	22	2.7	55,00	1159902,34	21089,13	-	-	52,42
	25	2.8	42,00	1178784,19	28066,29	-	-	53,28
3	4	3.1	166,00	1016303,71	6122,31	-	-	45,93
	7	3.2	103,00	924497,07	8975,70	-	-	41,78
	10	3.3	91,00	983623,05	10809,04	-	-	44,45
	13	3.4	75,00	955903,32	12745,38	-	-	43,20
	16	3.5	66,00	938186,04	14214,94	-	-	42,40
	19	3.6	52,00	979348,15	18833,62	-	-	44,26
	22	3.7	43,00	901967,77	20976,00	-	-	40,76
	25	3.8	36,00	918315,43	25508,76	-	-	41,50
AVG	4	AVG 1	160,00	1082485,35	6793,28	**685,81**	**10,10%**	48,92
	7	AVG 2	110,33	1041848,96	9417,45	**571,09**	**6,06%**	47,09
	10	AVG 3	91,33	1087242,03	11943,21	**1070,12**	**8,96%**	49,14
	13	AVG 4	79,33	1069488,12	13518,44	**1378,48**	**10,20%**	48,34
	16	AVG 5	72,33	1053406,58	14612,95	**1351,55**	**9,25%**	47,61
	19	AVG 6	60,00	1070319,82	17906,99	**812,84**	**4,54%**	48,37
	22	AVG 7	49,33	1015998,53	20595,88	**619,29**	**3,01%**	45,92
	25	AVG 8	37,00	992548,02	26752,74	**1045,26**	**3,91%**	44,86

pH 6,3								
Replicate	**Minute**	**Sample**	**Count**	**Total Area**	**Avg.Size**	**SD Avg.Size**	**RSD% Avg.Size**	**%Area**
1	4	1.1	146,00	1230371,09	8427,20	-	-	55,61
	7	1.2	86,00	1090075,68	12675,30	-	-	49,27
	10	1.3	61,00	1015922,85	16654,47	-	-	45,91
	13	1.4	50,00	1059348,15	21186,96	-	-	47,88
	16	1.5	49,00	1130817,88	23077,92	-	-	51,11
	19	1.6	50,00	1153918,46	23078,37	-	-	52,15
	22	1.7	45,00	1055664,07	23459,20	-	-	47,71
	25	1.8	43,00	1220581,06	28385,61	-	-	55,16
2	4	2.1	142,00	1229116,21	8655,75	-	-	55,55
	7	2.2	96,00	1320952,15	13759,92	-	-	59,70
	10	2.3	72,00	1344252,93	18670,18	-	-	60,75
	13	2.4	59,00	1314455,57	22278,91	-	-	59,41
	16	2.5	61,00	1465903,32	24031,20	-	-	66,25
	19	2.6	57,00	1509045,41	26474,48	-	-	68,20
	22	2.7	49,00	1501203,60	30636,81	-	-	67,85
	25	2.8	35,00	1195241,70	34149,76	-	-	54,02
3	4	3.1	152,00	1319919,43	8683,68	-	-	59,65
	7	3.2	115,00	1327341,31	11542,10	-	-	59,99
	10	3.3	81,00	1186286,62	14645,51	-	-	53,61
	13	3.4	72,00	1325129,40	18404,58	-	-	59,89
	16	3.5	56,00	1182922,36	21123,61	-	-	53,46
	19	3.6	46,00	1141945,81	24824,91	-	-	51,61
	22	3.7	38,00	1137839,36	29943,14	-	-	51,42
	25	3.8	33,00	1170234,37	35461,65	-	-	52,89
AVG	4	AVG 1	146,67	1259802,25	8588,88	**114,89**	**1,34%**	56,94
	7	AVG 2	99,00	1246123,05	12659,11	**905,49**	**7,15%**	56,32
	10	AVG 3	71,33	1182154,14	16656,72	**1643,06**	**9,86%**	53,43
	13	AVG 4	60,33	1232977,70	20623,48	**1631,10**	**7,91%**	55,72
	16	AVG 5	55,33	1259881,18	22744,24	**1210,24**	**5,32%**	56,94
	19	AVG 6	51,00	1268303,22	24792,59	**1386,65**	**5,59%**	57,32
	22	AVG 7	44,00	1231569,01	28013,05	**3232,49**	**11,54%**	55,66
	25	AVG 8	37,00	1195352,37	32665,67	**3073,49**	**9,41%**	54,02

0,20um Filtration								
Replicate	**Minute**	**Sample**	**Count**	**Total Area**	**Avg.Size**	**SD Avg.Size**	**RSD% Avg.Size**	**%Area**
1	4	**1.1**	183,00	1229350,59	6717,76	-	-	55,56
	7	**1.2**	89,00	1039033,20	11674,53	-	-	46,96
	10	**1.3**	73,00	976330,57	13374,39	-	-	44,13
	13	**1.4**	61,00	1020761,72	16733,80	-	-	46,13
	16	**1.5**	48,00	957998,05	19958,29	-	-	43,30
	19	**1.6**	36,00	836083,99	23224,56	-	-	37,79
	22	**1.7**	32,00	806845,71	25213,93	-	-	36,47
	25	**1.8**	30,00	811447,75	27048,26	-	-	36,67
2	4	**2.1**	126,00	972807,62	7720,70	-	-	43,97
	7	**2.2**	84,00	917709,96	10925,12	-	-	41,48
	10	**2.3**	67,00	885476,07	13216,06	-	-	40,02
	13	**2.4**	60,00	956276,86	15937,95	-	-	43,22
	16	**2.5**	49,00	836403,81	17069,47	-	-	37,80
	19	**2.6**	45,00	856608,89	19035,75	-	-	38,71
	22	**2.7**	44,00	935102,54	21252,33	-	-	42,26
	25	**2.8**	35,00	935668,94	26733,40	-	-	42,29
3	4	**3.1**	172,00	1331909,18	7743,66	-	-	60,20
	7	**3.2**	114,00	1158500,98	10162,29	-	-	52,36
	10	**3.3**	81,00	1153166,50	14236,62	-	-	52,12
	13	**3.4**	68,00	1111789,55	16349,85	-	-	50,25
	16	**3.5**	59,00	962551,27	16314,43	-	-	43,50
	19	**3.6**	44,00	861589,36	19581,58	-	-	38,94
	22	**3.7**	45,00	948422,85	21076,06	-	-	42,86
	25	**3.8**	43,00	1061989,75	24697,44	-	-	48,00
AVG	4	**AVG 1**	160,33	1178022,46	7394,04	**478,29**	**6,47%**	53,24
	7	**AVG 2**	95,67	1038414,71	10920,65	**617,38**	**5,65%**	46,93
	10	**AVG 3**	73,67	1004991,05	13609,03	**448,46**	**3,30%**	45,42
	13	**AVG 4**	63,00	1029609,37	16340,53	**324,97**	**1,99%**	46,53
	16	**AVG 5**	52,00	918984,38	17780,73	**1570,32**	**8,83%**	41,53
	19	**AVG 6**	41,67	851427,41	20613,96	**1859,37**	**9,02%**	38,48
	22	**AVG 7**	40,33	896790,36	22514,11	**1910,42**	**8,49%**	40,53
	25	**AVG 8**	36,00	936368,81	26159,70	**1041,93**	**3,98%**	42,32

0,45um Filtration								
Replicate	**Minute**	**Sample**	**Count**	**Total Area**	**Avg.Size**	**SD Avg.Size**	**RSD% Avg.Size**	**%Area**
1	4	**1.1**	175,00	1214460,45	6939,77	-	-	54,89
	7	**1.2**	122,00	1139624,02	9341,18	-	-	51,51
	10	**1.3**	93,00	1124143,07	12087,56	-	-	50,81
	13	**1.4**	87,00	1158493,65	13316,02	-	-	52,36
	16	**1.5**	68,00	1073881,84	15792,38	-	-	48,53
	19	**1.6**	64,00	1158928,22	18108,25	-	-	52,38
	22	**1.7**	57,00	1151826,16	20207,48	-	-	52,06
	25	**1.8**	54,00	1174858,40	21756,64	-	-	53,10
2	4	**2.1**	200,00	1321154,78	6605,77	-	-	59,71
	7	**2.2**	133,00	1195488,29	8988,63	-	-	54,03
	10	**2.3**	102,00	1090317,38	10689,39	-	-	49,28
	13	**2.4**	78,00	1079052,74	13834,01	-	-	48,77
	16	**2.5**	63,00	1035131,84	16430,66	-	-	46,78
	19	**2.6**	46,00	1151562,50	25033,97	-	-	52,04
	22	**2.7**	40,00	1103803,71	27595,09	-	-	49,89
	25	**2.8**	33,00	1062658,68	32201,78	-	-	48,03
3	4	**3.1**	143,00	1245297,85	8708,38	-	-	56,28
	7	**3.2**	93,00	1071604,00	11522,62	-	-	48,43
	10	**3.3**	61,00	976462,40	16007,58	-	-	44,13
	13	**3.4**	42,00	896542,97	21346,26	-	-	40,52
	16	**3.5**	38,00	1053037,10	27711,50	-	-	47,59
	19	**3.6**	35,00	1001591,81	28616,91	-	-	45,27
	22	**3.7**	30,00	988818,35	32960,61	-	-	44,69
	25	**3.8**	28,00	770822,75	27529,38	-	-	34,84
AVG	4	**AVG 1**	172,67	1260304,36	7417,98	**922,58**	**12,44%**	56,96
	7	**AVG 2**	116,00	1135572,10	9950,81	**1120,72**	**11,26%**	51,32
	10	**AVG 3**	85,33	1063640,95	12928,18	**2251,04**	**17,41%**	48,07
	13	**AVG 4**	69,00	1044696,45	16165,43	**3669,50**	**22,70%**	47,21
	16	**AVG 5**	56,33	1054016,92	19978,18	**5474,49**	**27,40%**	47,64
	19	**AVG 6**	48,33	1104027,51	23919,71	**4361,89**	**18,24%**	49,90
	22	**AVG 7**	42,33	1081482,74	26921,06	**5228,22**	**19,42%**	48,88
	25	**AVG 8**	38,33	1002779,94	27162,60	**4272,09**	**15,73%**	45,32

0,8um Filtration								
Replicate	**Minute**	**Sample**	**Count**	**Total Area**	**Avg.Size**	**SD Avg.Size**	**RSD% Avg.Size**	**%Area**
1	4	**1.1**	168,00	1387583,01	8259,42	-	-	62,71
	7	**1.2**	108,00	1234255,37	11428,29	-	-	55,78
	10	**1.3**	80,00	1260119,63	15751,50	-	-	56,95
	13	**1.4**	74,00	1270339,36	17166,75	-	-	57,41
	16	**1.5**	71,00	1267309,57	17849,43	-	-	57,28
	19	**1.6**	58,00	1321389,16	22782,57	-	-	59,72
	22	**1.7**	57,00	1259768,06	22101,19	-	-	56,94
	25	**1.8**	48,00	1211052,25	25230,26	-	-	54,73
2	4	**2.1**	150,00	1060187,99	7067,92	-	-	47,92
	7	**2.2**	88,00	862966,31	9806,44	-	-	39,00
	10	**2.3**	74,00	922792,97	12470,18	-	-	41,71
	13	**2.4**	67,00	943034,67	14075,14	-	-	42,62
	16	**2.5**	57,00	1004384,77	17620,79	-	-	45,39
	19	**2.6**	57,00	1062146,00	18634,14	-	-	48,00
	22	**2.7**	50,00	994240,72	19884,81	-	-	44,93
	25	**2.8**	46,00	1051125,49	22850,55	-	-	47,51
3	4	**3.1**	155,00	1156289,07	7459,93	-	-	52,26
	7	**3.2**	119,00	1270271,00	10674,55	-	-	57,41
	10	**3.3**	93,00	1137541,50	12231,63	-	-	51,41
	13	**3.4**	78,00	1165358,89	14940,50	-	-	52,67
	16	**3.5**	76,00	1175593,26	15468,33	-	-	53,13
	19	**3.6**	69,00	1133461,91	16426,98	-	-	51,23
	22	**3.7**	62,00	1223081,06	19727,11	-	-	55,28
	25	**3.8**	53,00	1184758,30	22353,93	-	-	53,55
AVG	4	**AVG 1**	157,67	1201353,35	7595,76	**495,82**	**6,53%**	54,29
	7	**AVG 2**	105,00	1122497,56	10636,42	**662,67**	**6,23%**	50,73
	10	**AVG 3**	82,33	1106818,03	13484,43	**1606,01**	**11,91%**	50,02
	13	**AVG 4**	73,00	1126244,30	15394,13	**1302,26**	**8,46%**	50,90
	16	**AVG 5**	68,00	1149095,87	16979,52	**1072,64**	**6,32%**	51,93
	19	**AVG 6**	61,33	1172332,36	19281,23	**2634,69**	**13,66%**	52,98
	22	**AVG 7**	56,33	1159029,95	20571,04	**1083,90**	**5,27%**	52,38
	25	**AVG 8**	49,00	1148978,68	23478,25	**1255,34**	**5,35%**	51,93

Polystyrene Beads 0,1%								
Replicate	**Minute**	**Sample**	**Count**	**Total Area**	**Avg.Size**	**SD Avg.Size**	**RSD% Avg.Size**	**%Area**
1	4	**1.1**	125,00	1174243,16	9393,95	-	-	44,47
	7	**1.2**	91,00	1130288,08	12420,75	-	-	42,81
	10	**1.3**	66,00	1083508,30	16416,79	-	-	41,04
	13	**1.4**	53,00	1067595,21	20143,31	-	-	40,43
	16	**1.5**	36,00	995122,07	27642,28	-	-	37,69
	19	**1.6**	33,00	964912,11	29239,76	-	-	36,55
	22	**1.7**	19,00	752165,53	39587,66	-	-	28,49
	25	**1.8**	19,00	820432,14	43180,64	-	-	31,07
2	4	**2.1**	111,00	1219506,83	10986,55	-	-	46,19
	7	**2.2**	61,00	1056909,18	17326,38	-	-	40,03
	10	**2.3**	44,00	996254,89	22642,16	-	-	37,73
	13	**2.4**	37,00	889321,29	24035,71	-	-	33,68
	16	**2.5**	37,00	879409,18	23767,82	-	-	33,31
	19	**2.6**	26,00	593933,11	22843,58	-	-	22,50
	22	**2.7**	27,00	929548,33	34427,72	-	-	35,21
	25	**2.8**	28,00	921894,52	32924,80	-	-	34,92
3	4	**3.1**	108,00	1259194,34	11659,21	-	-	56,91
	7	**3.2**	85,00	1248581,54	14689,20	-	-	56,43
	10	**3.3**	64,00	1111672,36	17369,88	-	-	50,24
	13	**3.4**	49,00	1118835,45	22833,38	-	-	50,57
	16	**3.5**	47,00	1066706,54	22695,88	-	-	48,21
	19	**3.6**	36,00	1008659,67	28018,32	-	-	45,59
	22	**3.7**	29,00	869272,46	29974,91	-	-	39,29
	25	**3.8**	21,00	779116,21	37100,77	-	-	35,21
AVG	4	**AVG 1**	114,67	1217648,11	10679,90	**949,87**	**8,89%**	49,19
	7	**AVG 2**	79,00	1145259,60	14812,11	**2004,60**	**13,53%**	46,42
	10	**AVG 3**	58,00	1063811,85	18809,61	**2737,81**	**14,56%**	43,00
	13	**AVG 4**	46,33	1025250,65	22337,46	**1627,30**	**7,29%**	41,56
	16	**AVG 5**	40,00	980412,60	24701,99	**2124,65**	**8,60%**	39,74
	19	**AVG 6**	31,67	855834,96	26700,56	**2772,50**	**10,38%**	34,88
	22	**AVG 7**	25,00	850328,77	34663,43	**3927,93**	**11,33%**	34,33
	25	**AVG 8**	22,67	840480,96	37735,41	**4210,91**	**11,16%**	33,73

Polystyrene Beads 0,1% (w/w) added post-filtering								
Replicate	**Minute**	**Sample**	**Count**	**Total Area**	**Avg.Size**	**SD Avg.Size**	**RSD% Avg.Size**	**%Area**
1	4	**1.1**	147,00	1356120,42	9225,31	-	-	54,89
	7	**1.2**	68,00	833388,96	12255,72	-	-	33,73
	10	**1.3**	70,00	830941,37	11870,59	-	-	33,63
	13	**1.4**	46,00	828824,69	18017,93	-	-	33,55
	16	**1.5**	40,00	990787,88	24769,70	-	-	40,10
	19	**1.6**	31,00	821935,89	26514,06	-	-	33,27
	22	**1.7**	25,00	697657,50	27906,30	-	-	28,24
	25	**1.8**	21,00	738229,49	35153,79	-	-	29,88
2	4	**2.1**	155,00	1659079,24	10703,74	-	-	67,16
	7	**2.2**	90,00	1415183,49	15724,26	-	-	57,28
	10	**2.3**	62,00	717450,86	11571,79	-	-	29,04
	13	**2.4**	25,00	460215,18	18408,61	-	-	18,63
	16	**2.5**	23,00	376816,27	16383,32	-	-	15,25
	19	**2.6**	16,00	718916,32	44932,27	-	-	29,10
	22	**2.7**	10,00	456944,43	45694,44	-	-	18,50
	25	**2.8**	6,00	333755,15	55625,86	-	-	22,01
3	4	**3.1**	126,00	1534343,83	12177,33	-	-	62,11
	7	**3.2**	51,00	859868,57	16860,17	-	-	34,81
	10	**3.3**	58,00	916139,87	15795,52	-	-	37,08
	13	**3.4**	45,00	1035887,36	23019,72	-	-	41,93
	16	**3.5**	37,00	1006415,58	27200,42	-	-	40,74
	19	**3.6**	30,00	839896,26	27996,54	-	-	34,00
	22	**3.7**	17,00	477565,33	28092,08	-	-	19,33
	25	**3.8**	11,00	370174,89	33652,26	-	-	14,98
AVG	4	**AVG 1**	142,67	1516514,50	10702,13	**1205,16**	**11,26%**	61,38
	7	**AVG 2**	69,67	1036147,01	14946,72	**1958,51**	**13,10%**	41,94
	10	**AVG 3**	63,33	821510,70	13079,30	**1924,53**	**14,71%**	33,25
	13	**AVG 4**	38,67	774975,74	19815,42	**2271,39**	**11,46%**	31,37
	16	**AVG 5**	33,33	791339,91	22784,48	**4633,81**	**20,34%**	32,03
	19	**AVG 6**	25,67	793582,82	33147,62	**8354,95**	**25,21%**	32,12
	22	**AVG 7**	17,33	544055,75	33897,61	**8341,97**	**24,61%**	22,02
	25	**AVG 8**	12,67	480719,84	41477,30	**10023,30**	**24,17%**	22,29

Appendix 3

Table 1. *Raw data, SD and RSD% from the time-lapse measurements of foam drainage.*

Standard						
Time (min)	**Replicate 1 (ml)**	**Replicate 2 (ml)**	**Replicate 3 (ml)**	**AVG (ml)**	**SD**	**RSD%**
4	3,72	3,35	3,50	3,5	0,15	4,25%
7	5,57	5,50	5,44	5,5	0,06	1,00%
10	6,40	6,42	6,28	6,4	0,06	0,95%
13	6,81	6,88	6,72	6,8	0,06	0,93%
16	7,08	7,17	6,97	7,1	0,08	1,13%
19	7,20	7,35	7,15	7,2	0,08	1,14%
22	7,35	7,49	7,29	7,4	0,08	1,11%
25	7,51	7,58	7,45	7,5	0,05	0,68%
Filter 0,2um						
Time (min)	**Replicate 1 (ml)**	**Replicate 2 (ml)**	**Replicate 3 (ml)**	**AVG (ml)**	**SD**	**RSD%**
4	3,5	3,5	3,5	3,5	0,03	0,83%
7	5,6	5,5	5,6	5,5	0,06	1,03%
10	6,4	6,0	6,4	6,3	0,15	2,42%
13	6,7	6,3	6,8	6,6	0,19	2,87%
16	6,8	6,5	7,0	6,8	0,22	3,28%
19	7,0	6,6	7,1	6,9	0,22	3,26%
22	7,1	6,7	7,2	7,0	0,23	3,33%
25	7,1	6,7	7,3	7,1	0,24	3,35%
Filter 0,45um						
Time (min)	**Replicate 1 (ml)**	**Replicate 2 (ml)**	**Replicate 3 (ml)**	**AVG (ml)**	**SD**	**RSD%**
4	3,3	2,3	3,3	2,9	0,44	14,82%
7	5,2	4,8	5,4	5,1	0,21	4,16%
10	5,9	5,9	6,2	6,0	0,15	2,42%
13	6,3	6,4	6,6	6,4	0,13	1,97%
16	6,5	6,7	6,8	6,7	0,15	2,19%
19	6,6	6,9	7,0	6,8	0,16	2,38%
22	6,7	7,0	7,1	7,0	0,16	2,35%
25	6,8	7,1	7,2	7,1	0,17	2,36%
Filter 0,8um						
Time (min)	**Replicate 1 (ml)**	**Replicate 2 (ml)**	**Replicate 3 (ml)**	**AVG (ml)**	**SD**	**RSD%**
4	3,1	3,4	3,8	3,4	0,31	9,09%
7	5,1	5,4	5,7	5,4	0,26	4,91%
10	5,9	6,2	6,4	6,2	0,21	3,32%
13	6,4	6,7	6,8	6,6	0,17	2,59%
16	6,7	6,9	7,0	6,9	0,15	2,19%
19	6,9	7,1	7,2	7,0	0,13	1,89%
22	7,0	7,2	7,3	7,2	0,12	1,63%
25	7,1	7,4	7,4	7,3	0,12	1,62%

pH 4,0						
Time (min)	**Replicate 1 (ml)**	**Replicate 2 (ml)**	**Replicate 3 (ml)**	**AVG (ml)**	**SD**	**RSD%**
4	4,0	4,0	4,0	4,0	0,01	0,27%
7	5,7	6,0	5,9	5,9	0,12	2,12%
10	6,4	6,9	6,6	6,6	0,20	2,98%
13	6,8	7,3	7,0	7,0	0,24	3,35%
16	7,0	7,6	7,2	7,2	0,24	3,37%
19	7,1	7,8	7,3	7,4	0,26	3,55%
22	7,2	7,9	7,5	7,5	0,27	3,65%
25	7,3	8,0	7,5	7,6	0,28	3,63%
pH 5,4						
Time (min)	**Replicate 1 (ml)**	**Replicate 2 (ml)**	**Replicate 3 (ml)**	**AVG (ml)**	**SD**	**RSD%**
4	3,9	4,6	4,4	4,3	0,33	7,59%
7	6,0	6,7	6,7	6,5	0,31	4,76%
10	7,0	7,6	7,5	7,4	0,27	3,61%
13	7,4	8,0	7,9	7,8	0,26	3,31%
16	7,6	8,2	8,1	8,0	0,24	3,02%
19	7,8	8,3	8,2	8,1	0,25	3,05%
22	7,9	8,4	8,3	8,2	0,23	2,85%
25	7,9	8,5	8,4	8,3	0,24	2,95%
pH 5,8						
Time (min)	**Replicate 1 (ml)**	**Replicate 2 (ml)**	**Replicate 3 (ml)**	**AVG (ml)**	**SD**	**RSD%**
4	4,3	4,2	4,0	4,2	0,11	2,66%
7	6,5	6,6	6,4	6,5	0,06	0,88%
10	7,5	7,6	7,5	7,5	0,08	1,10%
13	7,9	8,0	7,8	7,9	0,09	1,13%
16	8,1	8,2	8,0	8,1	0,10	1,19%
19	8,2	8,4	8,1	8,2	0,09	1,07%
22	8,3	8,5	8,2	8,3	0,10	1,23%
25	8,4	8,5	8,3	8,4	0,11	1,25%
pH 6,1						
Time (min)	**Replicate 1 (ml)**	**Replicate 2 (ml)**	**Replicate 3 (ml)**	**AVG (ml)**	**SD**	**RSD%**
4	4,3	4,1	3,9	4,1	0,15	3,60%
7	6,3	6,3	6,2	6,3	0,08	1,29%
10	7,1	7,3	7,2	7,2	0,08	1,08%
13	7,5	7,7	7,5	7,6	0,09	1,24%
16	7,7	7,9	7,8	7,8	0,07	0,85%
19	7,8	8,0	7,9	7,9	0,08	0,95%
22	7,9	8,1	7,9	8,0	0,08	1,06%
25	8,0	8,2	8,0	8,1	0,10	1,22%

pH 6,3						
Time (min)	**Replicate 1 (ml)**	**Replicate 2 (ml)**	**Replicate 3 (ml)**	**AVG (ml)**	**SD**	**RSD%**
4	4,5	5,0	4,9	4,8	0,22	4,57%
7	6,3	6,8	6,7	6,6	0,22	3,39%
10	7,0	7,6	7,5	7,4	0,24	3,32%
13	7,4	7,9	7,8	7,7	0,23	2,98%
16	7,5	8,1	7,9	7,8	0,25	3,13%
19	7,7	8,2	8,0	8,0	0,23	2,88%
22	7,7	8,3	8,1	8,1	0,24	2,96%
25	7,8	8,4	8,2	8,1	0,22	2,73%
Polystyrene Beads 0,1% (w/w)						
Time (min)	**Replicate 1 (ml)**	**Replicate 2 (ml)**	**Replicate 3 (ml)**	**AVG (ml)**	**SD**	**RSD%**
4	3,56	4,45	4,11	4,0	0,36	9,03%
7	5,84	6,43	6,39	6,2	0,27	4,35%
10	6,91	7,31	7,38	7,2	0,21	2,88%
13	7,40	7,73	7,85	7,7	0,19	2,51%
16	7,68	7,95	8,14	7,9	0,19	2,41%
19	7,88	8,11	8,30	8,1	0,17	2,12%
22	8,01	8,21	8,41	8,2	0,16	1,99%
25	8,11	8,30	8,47	8,3	0,15	1,77%
Polystyrene Beads 0,1% (w/w) added post-filtering						
Time (min)	**Replicate 1 (ml)**	**Replicate 2 (ml)**	**Replicate 3 (ml)**	**AVG (ml)**	**SD**	**RSD%**
4	2,69	3,14	3,00	2,9	0,19	6,33%
7	5,21	5,40	5,25	5,3	0,08	1,58%
10	6,26	6,38	6,30	6,3	0,05	0,82%
13	6,79	6,83	6,85	6,8	0,02	0,36%
16	7,11	7,10	7,15	7,1	0,02	0,33%
19	7,31	7,28	7,25	7,3	0,02	0,34%
22	7,44	7,38	7,50	7,4	0,05	0,66%
25	7,52	7,51	7,55	7,5	0,02	0,25%
Polystyrene Beads 0,1% (w/w) added pre-filtering						
Time (min)	**Replicate 1 (ml)**	**Replicate 2 (ml)**	**Replicate 3 (ml)**	**AVG (ml)**	**SD**	**RSD%**
4	2,37	3,42	2,32	2,7	0,51	18,82%
7	4,90	5,64	4,99	5,2	0,33	6,33%
10	6,03	6,54	6,22	6,3	0,21	3,39%
13	6,63	6,95	6,78	6,8	0,13	1,93%
16	6,95	7,22	7,11	7,1	0,11	1,56%
19	7,17	7,45	7,33	7,3	0,12	1,59%
22	7,33	7,54	7,45	7,4	0,09	1,19%
25	7,45	7,61	7,55	7,5	0,07	0,88%

Appendix 4

Raw data (*Table 1*) and t-tests (*Table 2*) comparing average bubble area measurements on standard coffee foam. Foam made in triplicate from 2.5ml and 10ml of coffee. The foam was measured at minute 4, 13 and 25, proving that sample volume does not significantly affect average bubble area.

Table 1. *Raw data (μm^2) from the comparison of average bubble size of foams made from 2.5ml and 10ml of coffee.*

Minute 4		**Minute 13**		**Minute 25**	
10 ml	**2,5 ml**	**10 ml**	**2,5 ml**	**10 ml**	**2,5 ml**
5687,01	8044,361	14206,60	14482,91	18856,92	21775,635
7159,76	7873,029	14974,37	14419,738	20459,80	26040,907
5729,41	7280,728	12703,56	12644,616	22494,03	17360,882

Table 2*. T-tests from the comparison of average bubble size of foams made from 2.5ml and 10ml of coffee.*

Minute 4 t-Test: Two-Sample Assuming Unequal Variances		
	Variable 1	*Variable 2*
Mean	6192,061	7732,706
Variance	702780,9	160551,748
Observations	3	3
Hypothesized Mean Difference	0	
df	3	
t Stat	-2,87193	
P(T<=t) one-tail	0,031975	
t Critical one-tail	2,353363	
P(T<=t) two-tail	0,063949	
t Critical two-tail	3,182446	

Minute 13 t-Test: Two-Sample Assuming Unequal Variances		
	Variable 1	*Variable 2*
Mean	13961,51	13849,088
Variance	1334190	1089062,27
Observations	3	3
Hypothesized Mean Difference	0	
df	4	
t Stat	0,125088	
P(T<=t) one-tail	0,453244	
t Critical one-tail	2,131847	
P(T<=t) two-tail	0,906489	
t Critical two-tail	2,776445	

Minute 25		
t-Test: Two-Sample Assuming Unequal Variances		
	Variable 1	*Variable 2*
Mean	20603,58	21725,808
Variance	3322646	18837570,5
Observations	3	3
Hypothesized Mean Difference	0	
df	3	
t Stat	-0,41291	
P(T<=t) one-tail	0,353705	
t Critical one-tail	2,353363	
P(T<=t) two-tail	0,70741	
t Critical two-tail	3,182446	